NASA-CR-201925

Contract No. NASW-4698
MCR-95-1312

6883⊔

Final Technology Report   **December, 1995**

Mars Aqueous Chemistry Experiment (MACE)

LOCKHEED MARTIN

PUBLICLY AVAILABLE

Contract No. NASW-4698
MCR-95-1312

Final Technology Report   December, 1995

Mars Aqueous Chemistry Experiment (MACE)

Approved by:

Benton C. Clark
MACE Program Manager
Lockheed Martin Astronautics

Prepared for:

NASA Headquarters

LOCKHEED MARTIN
ASTRONAUTICS
P.O. Box 179
Denver, Colorado 80201

FOREWORD

This work was conducted at Lockheed Martin Astronautics (formerly, Martin Marietta Astronautics) in Denver, Colorado. It resulted from in-house studies of the initial feasibility and importance of a chemical reaction investigation for future Mars missions, conducted in the Payloads, Sensors, and Instruments (PS&I) Section.

The Project Manager was Benton Clark. The majority of this work was performed by three primary contributors, each with different specialties.

Pat Thompson did detail design, fabrication, and laboratory testing of the fluids handling system, and was responsible for many of the design improvements and features which evolved during the course of this work. He also made primary contributions to instrument overall design to improve its feasibility and manufacturability.

Larry Mason did sensor evaluation, conducted chemical experiments with actual samples, and wrote all the instrument control software and performed analysis of results. He also collaborated on the sensor development effort, accomplished related in-house sensor tests and evaluations, and contributed to the chemistry approaches for this concept.

Mike Thornton did detail design of the final integrated instrument concept, fabricated many of the parts, and assembled a demonstration model which included many functional mechanisms. He prepared samples and documented their chemistry with x-ray fluorescence. He also developed the soil delivery metering concept and the shaped memory metal actuator mechanism.

Several other people made important contributions, including Jan Thornton (thermal modeling; general design), Don Thielman (conductivity; general design), Scot Anderson (electronics).

TABLE OF CONTENTS

A. INTRODUCTION

The Mars Aqueous Chemistry Experiment (MACE) is designed to fill a gap in investigation of the Martian surface materials and their composition. It is specifically optimized for small samples, but these can include soils, soil aggregates (e.g., duricrust), and rock fragments. What MACE can accomplish that has not been accomplished since Viking is the ability to react Martian surface materials chemically, especially with water. This is a fundamental area of investigation which will not be addressed in the initial return to the red planet.

This work was conducted under NASA Contract NASW-4698 for its applicability to future Mars lander missions.

B. SCIENCE OVERVIEW

MACE is of importance to many planetary science disciplines.

Scientific Goals and Objectives. The scientific objectives of MACE are manifold, but include the following important investigations:
  (1) determine the reactions between Martian surface materials and liquid water
  (2) explore for microenvironmental factors that would have favored or mitigated against survival of biotic forms
  (3) investigate the unusual oxidation capabilities of Martian soil that were discovered during the Viking mission
  (4) explore for evidence of chemical and physical modifications of the surface to understand the weathering processes operating on Mars
  (5) determine the extent to which the regolith is a sink and possible also a buffer of atmospheric gas inventory and stability of chemical species
  (6) better understand the physical chemistry of the ambient environment

It might be argued that these are all measurements that could be accomplished on returned samples. This is true with respect to several measurement aspects, but not all, and many landings will take place at sites from which sample returns will not be performed.

Measurements which may be compromised by the return process include the search for oxidant capacity, unless the samples can be properly preserved against loss of labile elements. If, for example, the oxidant is in some kind of equilibrium with the atmosphere or the oxidizing specie is labile, this property of the sample may be lost during the return.

More important, sample returns are extremely expensive missions and will be performed very judiciously. MACE can be used to characterize regions of Mars prior to sample return, as a screening tool for selection of which samples to bring back, and even for subsequent missions where the instrument reagents and operating protocols are optimized to exploit the knowledge gained from laboratory analyses of selected samples here on Earth.

Sample Accommodation. MACE can accommodate soil particulates, duricrust clods/peds, small rocks, lithic fragments, and the products of sub-sampling (core drill segments, solid drill cuttings, grinding dust, sawdust, etc.).

Mineralogic Determinations. For example, the carbonate detection capabilities of a Differential Scanning Calorimeter / Evolved Gas Analyzer (DSC/EGA) are at a significant level. However, the intertwined complexity of physical and chemical effects on such an instrument will make unlikely the clear determination of the types of major carbonates. And, it will certainly not be capable of detecting trace accessory elements in the carbonates. With MACE, however, it will not only be possible to address these fundamental questions, but also to determine the redox potential (Eh) and hydrogen activity (pH) of the chemical environment. From this and measures of the chemical constituents, the reactivity of the surface and pathways of interaction can be understood and predicted for future events.

B-1

C. OBJECTIVES OF DEVELOPMENT

The development program for MACE addressed several issues recognized once the initial concept was originated. These included

- the problems of handling and managing fluids under Martian conditions of very low pressure and a cold, dusty environment.

- micro-sensors and ancillary equipment which could perform the required measurements under instrument operating conditions

- development of a final flight-configuration for an Instrument Concept

- experiments with real samples, simulating Mars, to validate the ability of the concept to obtain meaningful scientific data

In the succeeding sections of this report, each of these issues is addressed to the level of detail that was possible within the resources available to conduct this study.

D. FLUIDS HANDLING

The MACE breadboard development has produced three units for demonstration of fluid handling. The first two units were constructed with manual valves and were primarily used for conceptual investigations at Earth nominal atmospheric pressure. The first unit was used as a visual aid to demonstrate the experiment concept and fluid handling. The second had electrodes installed for testing the resistivity of a simulated soil sample, an upgraded valve configuration, and a fluid cell constructed into the lower portion of the Reaction Chamber for testing the electrical conductivity of the leachate (presumably to contain electrolytes, such as $MgSO_4$, Na_2SO_4, $NaCl$ and other putative Martian salts). The electronics to drive the conductivity sensor was breadboarded and testing was initiated. A third unit was constructed to prove the fluids manipulation concept under nominal Mars atmospheric pressure (6 millibar). It was further determined that this unit should also be functional on a lab bench, $i.e.$, within one earth atmosphere (one bar) pressure. This additional requirement made development of working concepts difficult, because a high level of ambient pressure poses significant problems in fluid manipulation in small sealed systems. Figures D-1 through 5 detail the Fluids Handling Breadboard and associated MACE test setup.
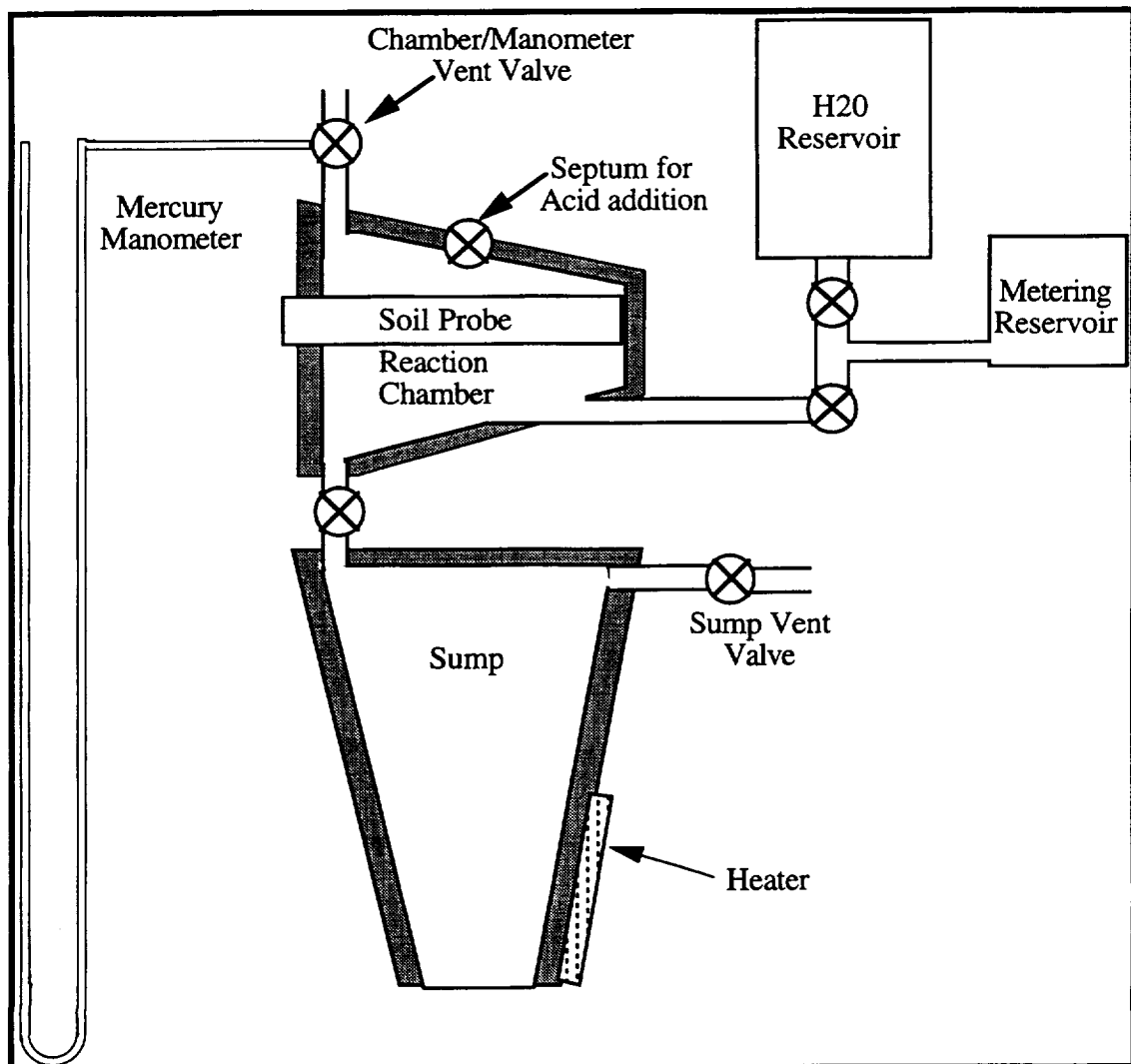

Figure D-1.   MACE Fluids Test Unit #3 Schematic

At Earth nominal pressure most small systems are either vented to atmosphere or use high pressure to overcome trapped air bubbles and allow fluid movement. In the MACE concept both the Reaction Chamber and the Sump are small fixed volume enclosures. Forcing fluid into and between these volumes increases the internal chamber pressure until the pressures of the delivery system and the internal volume are equal and fluid no longer flows. Using only the pressure head provided by gravity as a driving force in such systems was found to be not practical. The pressure provided by one foot in height of water (pressure head) is equivalent to about one half pound per square inch (0.43 psi). Earth atmospheric pressure is ~13.1 psi in Denver. Since the chamber volume was small and fixed (~7 ml) the pressure increases as fluid begins to flow into the chamber. If the fluid movement is driven by an inch or so of pressure head, after a few drops of fluid have entered the chamber at earth normal pressure the internal pressure has been raised enough for flow to cease (as occurred in the original concept). Since the inlet tube opening was very small (0.032" diameter), there was no way for the trapped air to escape, creating a "vapor lock" condition; fluid flow into the chamber was stopped.

To overcome this problem in a sealed system requires a higher delivery pressure from the Reservoir Volume to Metered Volume, and somewhat lower pressure to transfer fluid to the Reaction Chamber. This was accomplished by designing a weighted plunger system that displaced water in the reservoir as it was delivered to the Reaction Chamber. Both the Reservoir Volume and the Metered Volume in the third development unit use this principle.
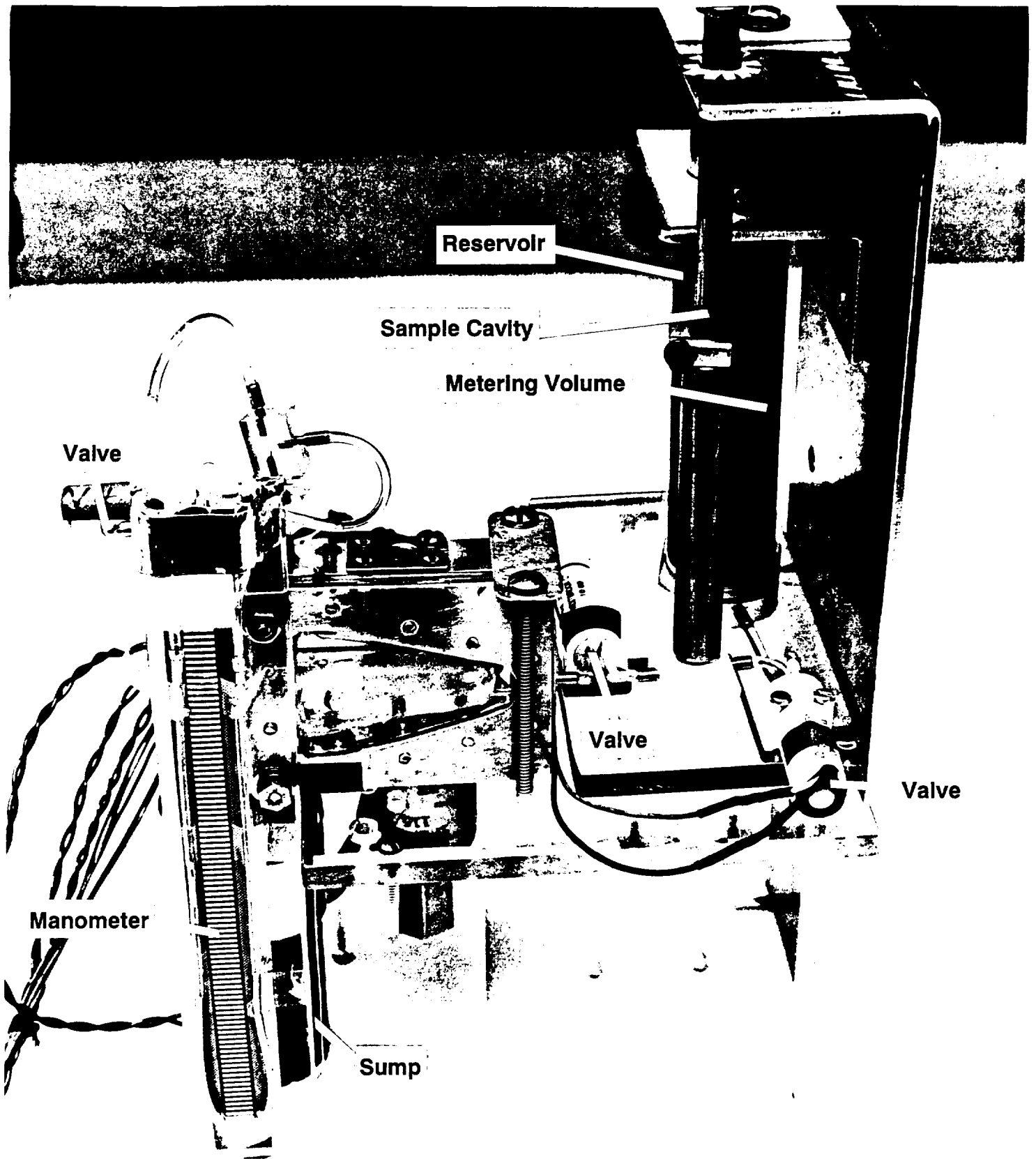
Reservoir

Sample Cavity

Metering Volume

Valve

Valve

Valve

Manometer

Sump

Figure D-2.   MACE Fluids Handling Breadboard Unit #3

The Reservoir Volume used a plunger 0.705 inches in diameter, and a weight of 1.82 lbs. The Metered Volume had a plunger 0.250 inches in diameter, and a weight of 0.185 lbs. The pressure provided by these weights was 4.5 psi from the Reservoir Volume, and 3.3 psi from the Metered Volume. This is independent of whatever background atmospheric pressure exists around and within the unit. These are low pressures from a fluids handling sense, but are high enough to overcome the atmospheric problems encountered when operating on the lab bench. The fluid-handling valves are miniature solenoid valves (Lee #LFAA1201618H), similar to flight-like units, and can be enabled for remote operation, as required when testing under Mars conditions in a modified vacuum chamber. The breadboard construction in the third unit was modular to allow for changes, modifications, and additions to the system without a complete rebuild, as was necessary with the first two units.
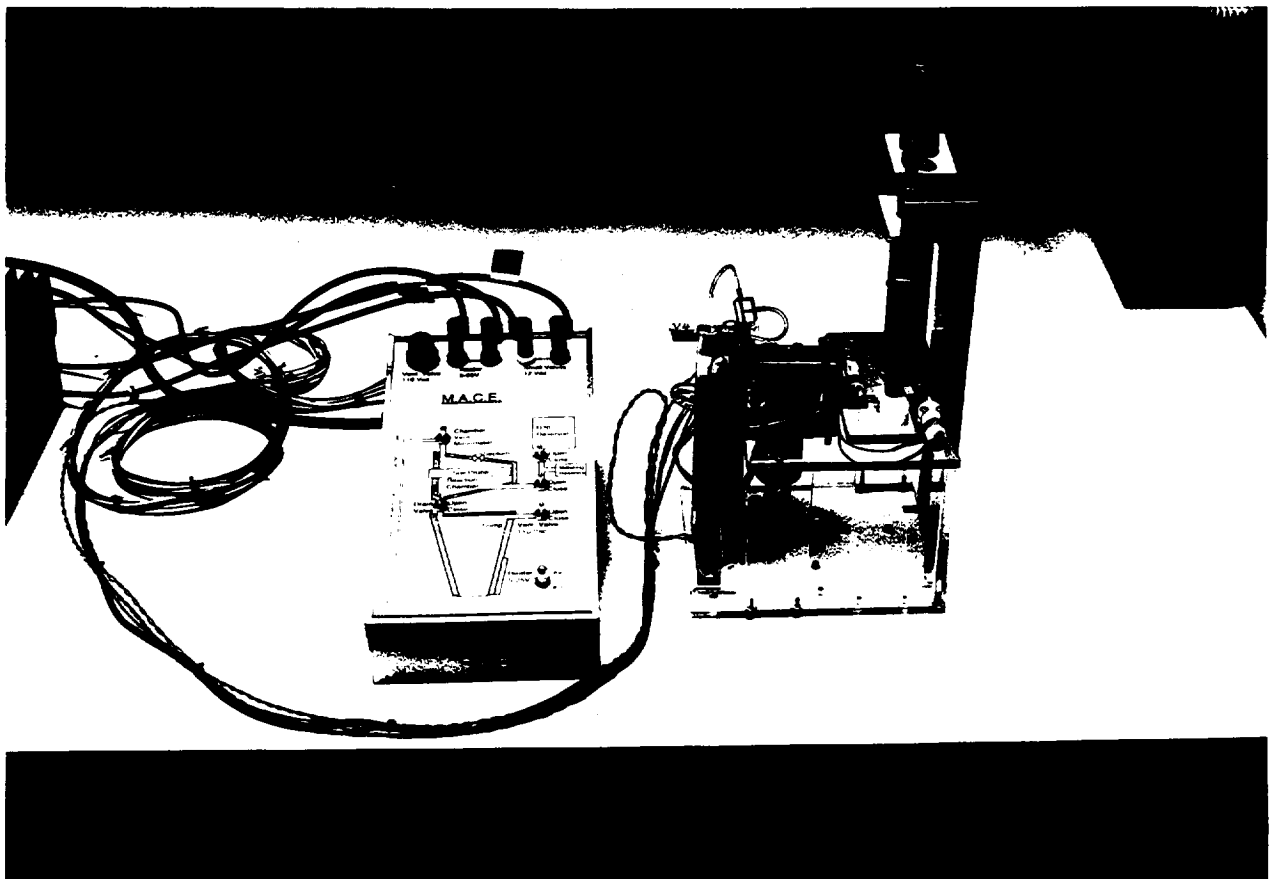

Figure D- 3.   Control Unit for Remote Operation of MACE Fluids Handling Breadboard

An alternative design was conceived to avoid the problems of friction between sealing surfaces of plunger and reservoir wall, which detracts from the total pressure applied to water in the system. The Reservoir Volume and the Metered Volume are both constructed using tubular elastomer membranes contained within separate cylinders, and each plunger acts to deform its respective membrane while providing pressure to the fluid. The membrane simply rolls from cylinder wall to plunger wall as the plunger

descends. In operation this provides for a nearly frictionless method of hermetically sealing the reservoir as each plunger moves within its containing cylinder.
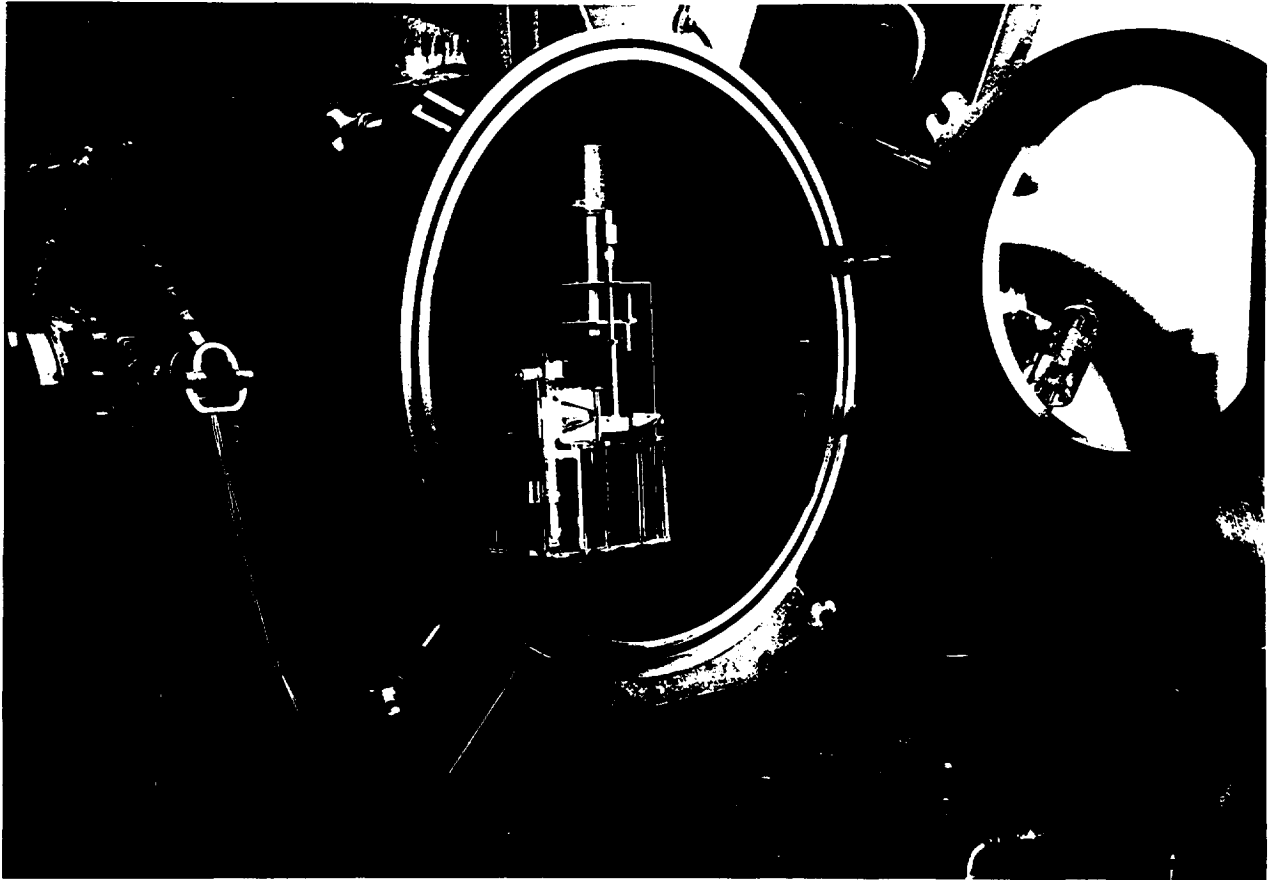

Figure D-4. *Mars Simulation Chamber Used for Low Atmospheric Pressure Testing*

This design simplifies the operation, allows accurate calculation of applied pressure, and does not require any factors for unknown fictional constants such as static, sliding, or compression set. A similar mechanism may be used on an actual flight instrument, but more suitable materials will be necessary than used in this proof of concept model, (*i.e.*, flight approved elastomer, Teflon coated phosphor bronze bellows, or other mechanisms and material currently under consideration).

The MACE unit #3 functions well in both atmospheric and simulated Martian pressures. Fluid was delivered first to the Metering Volume then to the Reaction Chamber. The time required to fill the Metered Volume from the Reservoir Volume was less than 5 seconds. The time to dispense this volume to the Reaction Chamber is between 1.5 and 2 seconds. There is an adjustment capability to change the volume dispensed through the Metering Volume, presently set at 2.08 ml. The time is

approximately the same for bench top (1 atmosphere) or vacuum chamber (6 mbar) ambient pressure operation. On the lab bench, however, if the reaction chamber already contains the first injected aliquot of water, the internal pressure equalizes to the 3.3 psi of the Metered Volume before the second injection has finished flowing into the Reaction Chamber. There is no problem draining the Reaction Chamber at 6 mbar, because what little gas is left dissolves in the water and the partial pressure provided by the water itself (after being degassed by boiling) is adequate to allow the flow of water into the sump. There is enough background pressure in the reaction Chamber to drain the fluid into the sump once the sump is vented to ambient atmosphere.
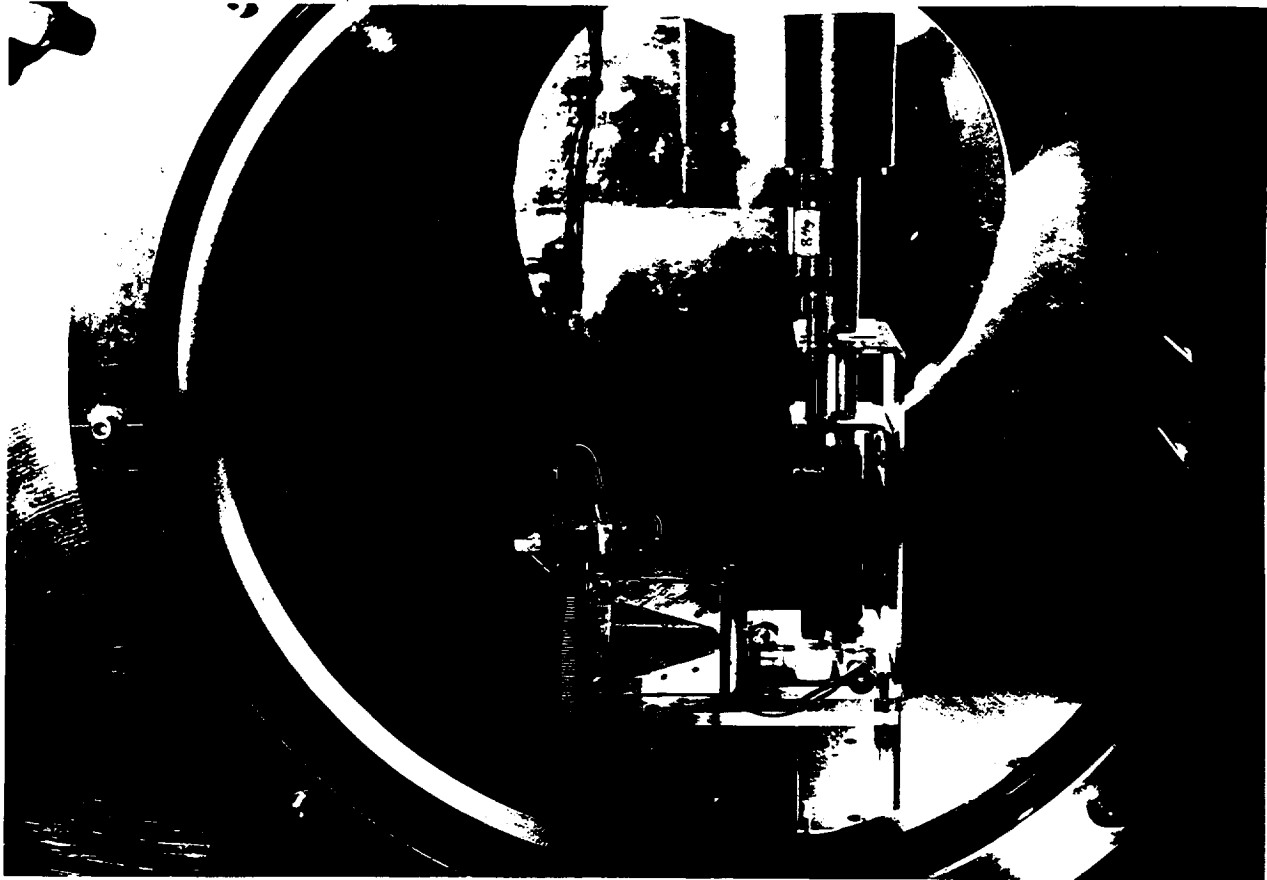

Figure D-5. MACE Fluids Breadboard Operational in Mars Simulation Chamber

The sump vent valve was used to vent the sump to atmosphere in order to evaporate the water and allow XRF analysis of the water soluble regolith components. This valve is solenoid driven, but is a commercial pneumatic type solenoid valve, chosen for its availability and for the fact that it has a large ports and valve orifice. The large diameter tubing and orifice help speed up the evaporation of water for XRF analysis. On the lab bench the sump is simply removed and drained to discard or analyze the collected water.

The test unit #3 currently had a mercury manometer connected to the Reaction Chamber through a tee and valve. This allows pressure measurements to be acquired when gases are released or evolved from the soil samples under analysis. The valve also allows the Reaction Chamber and manometer to be vented as the system is evacuated during pump down in the vacuum chamber. The unit has been bench tested in one atmosphere, and also tested under Martian ambient pressures. The initial verification and operation of the fluid management system was very successful. Fluid flow was under excellent control; the sample chamber could be filled in small increments, and be held constant at any level. No back-pressures occurred under simulated Mars pressure; and chamber clean-up via evaporation/sublimation was very efficient and rapid. These tests also revealed additional areas that require attention, especially the generation of gas bubbles, which could act to prematurely wet the sample in the early humidification phase of sample analysis.

The final method of fluid transport utilizes reservoir ullage to create a pressure head, but with the bladder diaphragm concept avoid dissolving gas into the liquid, which would then be partially released when exposed to low Martian pressures in the analysis and sample chambers.

E. SENSORS SELECTION

Aqueous Chemistry

Three areas of activity are reported in this section: (1) wet chemical analysis specifications, (2) test strip technology, and (3) Ion Selective Electrode (ISE) characteristics.

Wet Chemical Analyses -- Test kits were acquired for wet chemical (spectrophotometric) analysis of the ions Calcium, Chloride, Iron, Nitrate, and Sulfate. The analysis procedures were characterized in terms of sensitivity, error, complexity, analysis time, and colorimetric wavelength, as shown in Table E-1. The chemistry associated with each of these analyses in based upon reacting the ion of interest with appropriate molecules to create a soluble complex that adsorbs light, i.e. creates a colored solution. The adsorption of light at a particular wavelength is then proportional to the concentration of the ion of interest by Beers law of optical absorption. Solutions of known ionic concentration are prepared and analyzed in parallel with the samples to calibrate the procedure, establish a linear range, and verify proper response.

Table E-1. Wet Chemical Ion Analysis Protocol Characterizations

Ion	Sensitivity range (ppm)	Analysis error (%)	Number of reagents/steps	Analysis time (min)	Colorimetric wavelength (nm)
Ca^{++}	5 - 300	4	3	10	540
Cl^-	0.4 - 40	3	2	1	450
Fe^{++}	0.04 - 4.0	0.1	1	3	565
NO_3^-	5 - 90	5	3	10	515
SO_4^{--}	10 - 600	5	5	12*	515

*incubate @ 40C

The concentration range for each of these analyses spans at most two orders of magnitude before becoming non-linear. If the linear range is exceeded appropriate dilutions of the sample must be performed and the analysis repeated. Each analysis is also dependent on temperature to varying degrees, and interference effects from other ions may be present. The wavelengths listed in Table E-1 represents the adsorption maximum for the particular color complex formed, and thus the maximum sensitivity for each analysis. The adsorption peaks are fairly broad, spanning about 100 nm. As a result, a single wavelength intermediate to all analyses may be chosen for commonality with some loss of sensitivity.

Ion Test Strips -- Test strips were acquired to evaluate the technology applicability for autonomous determination of ions in aqueous solution. This type of test is inherently semi-quantitative, relatively sensitive, quick, and spans a concentration range from 1 - 250 ppm. The principle of operation is similar to wet chemical methods, and is based on a chemical reaction that either oxidizes or reduces a dye indicator that is chemically bound to the test strip. The result is a change in color that is proportional to the concentration of the ion of interest in the aqueous solution. The color produced by the reaction is compared to a scale of colors for rough determination of ionic concentration. The resolution obtainable using test strips is within an error margin of ±25%, depending on the age and storage history of the test strips, presence of interfering ions, temperature of the solution, skill of the analyst in comparing colors, and prior knowledge of the test solution. These test strips are most applicable for a quick test to determine a rough order of magnitude for concentration of ions in solution.

<u>Ion Selective Electrodes</u> --When an ISE and a reference electrode are placed in an aqueous solution, a potentiometric cell is formed. The sensing half of the electrochemical cell (half cell) responds to ion activity (concentration) in a relationship described by the Nernst equation (1):

$$E = E_0 + 2.3\frac{RT}{nF}(\log_{10} C)$$ (1)

where   E = developed electrochemical potential (V)
        E_0 = standard potential of the system (V)
        R = ideal gas constant (8.314 V•coulombs•mol/K)
        T = absolute solution temperature (°K)
        F = Faraday's constant (96493 coulombs)
        n = number of electrons in the electrochemical reaction
        C = concentration of ions in solution (M)

The 2.3RT/nF term can be reduced to a single slope factor at constant temperature for each electrode and reference electrochemical cell. The reference half cell also behaves according to the Nernst equation, but does not change potential with respect to the sensed ion. At constant temperature, each overall galvanic (ISE + reference) cell can be described using an equation in which the cell potential varies directly with the log of ion concentration in a straight-line manner, as shown in Equation (2).

$$E = V_o + S * \log_{10}(C)$$ (2)

where   E = developed galvanic cell voltage (V)
        V_o = voltage offset (V)
        S = slope (V/decade of ion concentration)
        C = concentration of ions in solution (M)

<u>Comparison of Ion Quantitation Methods</u> -- The three methods for measurement of ions in solution considered for use in MACE have been evaluated, as summarized in Table E-2.

Table E-2.   *Ion Measurement Methods Applicability Study*

Method	Dynamic Range	Resolution	Type of Analysis Output	Relative Complexity
Ion Selective Electrodes	10^5	±5%	voltage	simple
Test Strips	10^2	±25%	color comparison	intermediate
Wet Chemistry	10^2	±5%	colorimetric	complex

The method of choice for ion analysis is Ion Selective Electrodes, due to the large dynamic range, resolution, electrical signal output, and simplicity. The other two methods both require a spectrophotometer to measure developed color and convert the ion concentration to an electrical signal. This involves a substantial increase in instrument complexity relative to that required for Ion Selective Electrodes.

Ion Selective Electrode (ISE) survey
A relationship was established with the Stanford Research Institute International (SRI International, Menlo Park, CA) to begin development activities associated with miniaturized

aqueous ion sensors. The Physical Electronics Laboratory (PEL) at SRI routinely fabricates miniaturized devices with micrometer to nanometer dimensions. The personnel at SRI have a high degree of expertise and direct experience in fabrication of a wide variety of microsensors.

A subcontract to SRI was initiated, using MACE PIDDP funds, to perform a survey of current technology appropriate for use in sensing ions in aqueous solution consistent with the goals of MACE. Dr. Jose P. Joseph (Microsensors Program Director at PEL) performed the technology survey and reported the results. The survey report included mostly solid state electrolyte ISE's, but also addressed other technologies where appropriate. The survey considered the state of current technology, interference and selectivity estimates, recommendations for Ionic Strength Adjustment solutions, and estimates of the development effort required to miniaturize the sensors for use in MACE. The ions/sensors of interest for the purposes of the survey included: Ca^{2+}, Mg^{2+}, Na^+, K^+, H^+, Fe^{2+}, Fe^{3+}, SO_4^{2-}, PO_4^{2-}, HCO_3^-, NO_2^-, Cl^-, Br^-, oxidation reduction potential, conductivity, and solid electrolyte reference electrodes. SRI was provided with estimates of nominal and extreme case ion concentrations for each of the ions of interest. Table E-3 lists the ISE's considered in the survey, the sensing material, theoretical detection limit, and major interfering ionic species.

Table E-3. Summary of Ion Selective Electrode Technology Survey for MACE

Ion of Interest (ISE)	Sensing Material	Detection Sensitivity (µM)	Potential Interfering Ions
Potassium (K^+)	valinomycin	16	Li, Na, Mg, Ca
Calcium (Ca^{++})	(R,R)-N,N'-[Bis(11-ethoxycarbonyl)undecyl]-N,N',4,5-tetramethyl-3,6-dioxaoctnediamide	0.04	Na, K, Mg
Hydrogen (pH)	IrO_2	pH 1 to pH 13	Na, K, Ca
Sodium (Na^+)	Bis[12-crown-4-methyl]dodecylmethyl malonate	20	K, Mg, Ca, Li
Magnesium (Mg^{++})	N-heptyl-N',N'-bis {8-[[3(heptylmethylamino)-1.3-dioxoproply]amino] octyl}-N-methyl-propanediamide	10	H, Na, K, Ca
Iron (Fe^{++}, Fe^{+++})	dithia-12-crown-4	10	alkaline earth metal ions
Bromide (Br^-)	bis(diethyldithio carbamato)mercury (II)	10	SO_4, NO_3, Cl
Carbonate (CO_3^-)	Aliquat 336 dissolved in trifluoroacetyl-p-butylbenzene	10	Cl, SO_4, NO_3
Chloride (Cl^-)	quaternary chloride salt	10	Br, NO_3, SO_4
Nitrate ($NO3^-$)	Orion 92-07 nitrate selective membrane	10	Cl, $SO4$, $CO3$, Br
Sulfate (SO_4^{--})	$PbSO_4/PbS/Ag_2S$	50	CO_3, NO_3, Cl
Phosphate (PO_4^{--})	dibenzyltin chloride derivative	80	Cl, Br, NO_3
reference electrode (Fl- or H+)	solid state electrolyte	n/a	n/a
Oxidation - Reduction (redox)	platinum electrodes	n/a	n/a

A wide variety of chemical sensor was considered in the survey, and the conclusion stated that Ion Selective Electrodes (ISE) have sufficient selectivity for the measurement objectives in the MACE instrument. The ISE's listed in Table E-3 represents the best candidate sensor based on survey results, with the problematic interfering ions are shown in bold typeface. In most cases the selectivity of the ISE listed was high enough that even in the presence of moderate amounts of potentially interfering ions, the measurement could be performed with an accuracy better than 2%, and precision less than 6%. The main exception to this was the sulfate ISE, where the carbonate ion represents a major interference with measurement of the sulfate ion. This interference may be reduced if pre-treatment of the sample is performed, or if multiple sensors for the same ion are used. The sensors for a particular ion would be fabricated using different sensing materials, and thus have different selectivity patterns. This multiple sensor technique allows independent estimates to be generated for ionic activities based on pattern recognition technology, or neural network analysis. Figure E-1 shows a schematic representation of a hybrid sensor structure that may be used in the MACE ISE array. The structure includes high impedance electronics to process the raw signals generated by the sensors directly on the array silicon substrate, minimizing both mass and power.
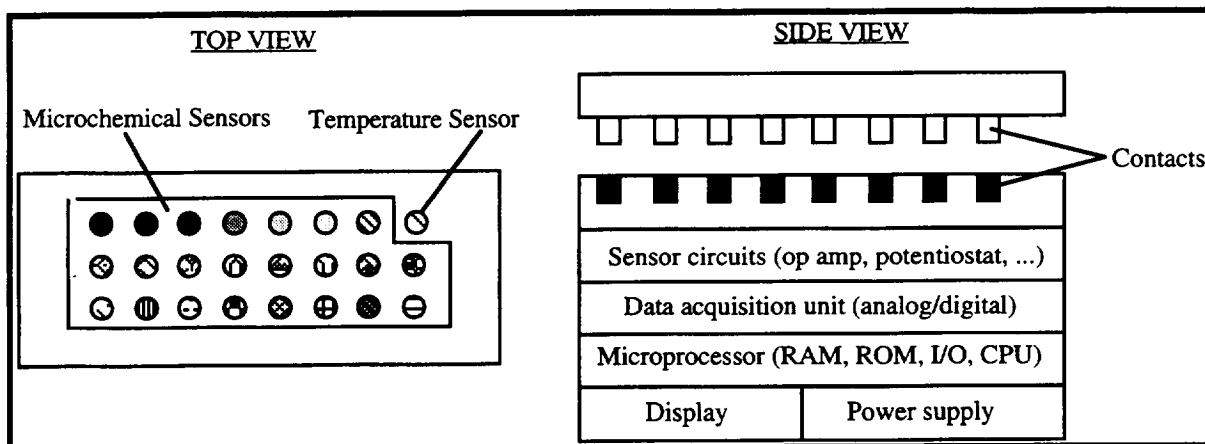

Figure E-1. Schematic diagram of Hybrid ISE Structure

An additional task in the survey included a Rough Order of Magnitude (ROM) estimate for development and fabrication of an array of micro-sensors on a single structure. For the purposes of estimation it was assumed that the array included electrodes for each of the ions of interest to MACE, with spacing between adjacent electrodes (center to center) on the order of 300 μm. The sensor area and configuration in each case were determined by the ease of manufacture and maturity of technology. It is difficult to estimate exact development costs without further definition regarding membrane materials, multiple sensing strategies for particular ions, and sensor redundancy issues. The development cost estimate is in the range from $400 to $600 k for an array of sensors that includes capabilities for measuring each of the ions of interest to MACE.

It is possible to utilize the ISE sensors in a dual capacity in the MACE instrument. The physical layout of the sensors on the ISE array will permit the sensors to also be used as water level sensors. When water is introduced into the analysis chamber, contact with each electrode sensor produces a distinct change in the electrical signal produced by that sensor. Aligning the sensors in a linear array in the analysis chamber will enable the water level to be sensed directly in the chamber. The reference electrode must be at the chamber bottom, and the first electrode to be contacted by the water. As the water level rises in the analysis chamber, contact with each ISE completes an electrochemical cell, and allows ion measurement and level sensing operations to commence.

Evolved Gas Sensors

Work has begun on development of miniaturized solid state sensors for gases of interest to MACE. Gas may primarily be evolved from superoxide and carbonate mineral decomposition, but other reactions may also evolve gases of interest. The two major gases of interest are oxygen and carbon dioxide. The following sections describe the development activities associates with the gas sensing technologies appropriate for the MACE application. The sensors described utilize solid state electrolyte materials, and are readily amenable to miniaturization. The major problem associated with sensors of this type in the MACE application is the high operational temperature requirement ($\approx$500°C), however a miniaturized array of sensors should require minimal power to operate.

CO2 Sensor Development, Testing, and Apparatus

A prototype solid electrolyte potentiometric CO_2 sensor of miniature size was developed for proof of concept studies. The sensor is configured in a planar geometry, with solid state reference and measuring electrodes co-located on one side of a beta alumina electrolyte substrate. A thick film platinum heater on the opposite side of the alumina allows operation at high temperatures.

<u>Experimental Apparatus</u>

Figure E-2 shows the laboratory setup used to evaluate the sensor performance at reduced pressures. The vacuum sensor chamber has a volume of about one liter. It is connected to various test gas cylinders at the inlet, and to a large vacuum chamber capable of attaining sub-millitorr pressures on the outlet. Gas flow metering valves on the inlet and outlet ports allow the gas composition and total pressure in the sensor chamber to be varied over a wide range during the experiments. Data regarding the chamber pressure is monitored using an electrical strain-gauge pressure transducer interfaced to the data acquisition computer. Calibration and verification of the electrical pressure gauge were performed using a mechanical absolute pressure gauge that is traceable to a NIST standard. The sensor and heater temperatures were determined by measuring the resistance through the platinum heater element. Prior to these experiments the heater element resistance was correlated to the melting points of various pure materials. The experiments consisted of systematically varying the total pressure, gas composition, and sensor heater voltage and current while acquiring voltage data from the sensor electrochemical potential. The total pressure in the sensor chamber ranged from 50 to 130 mbar, and covered a variety of gas compositions using Argon, Oxygen, and Carbon Dioxide. The post test data analysis involved correlation of the sensor output data to the gas composition, thermal, and total pressure environments. Figure E-3 shows a schematic diagram of the sensor, including dimensions, measurement interfaces, and environmental influences on the sensor output.
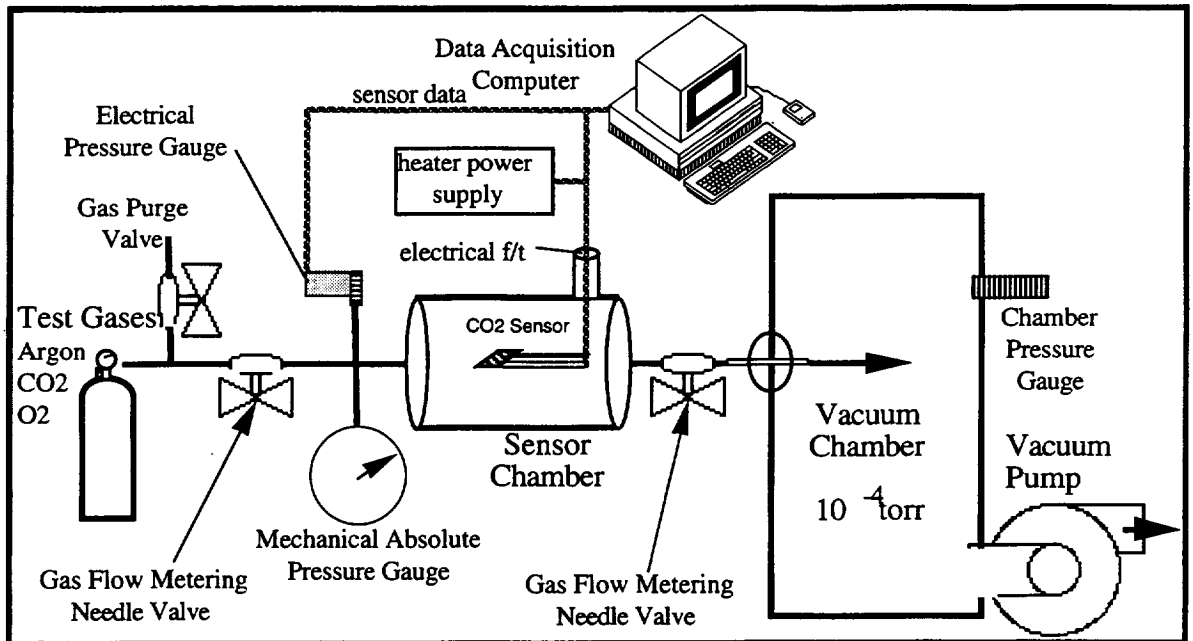
Figure E-2. *Experimental Setup for Solid State CO2 Electrochemical Gas Sensor Reduced Pressure Tests*

Carbon Dioxide Sensor Test Results

The sensor response was found to be a complex function of the total pressure, sensor temperature, gas composition, and CO_2 partial pressure. Analysis of the data has shown that the thermal and gas composition environments influence the output sensor electrochemical potential through separate mechanisms. Figure E-3 shows the **Thermal Influences** in bold, and the *electrochemical influences* in italic.
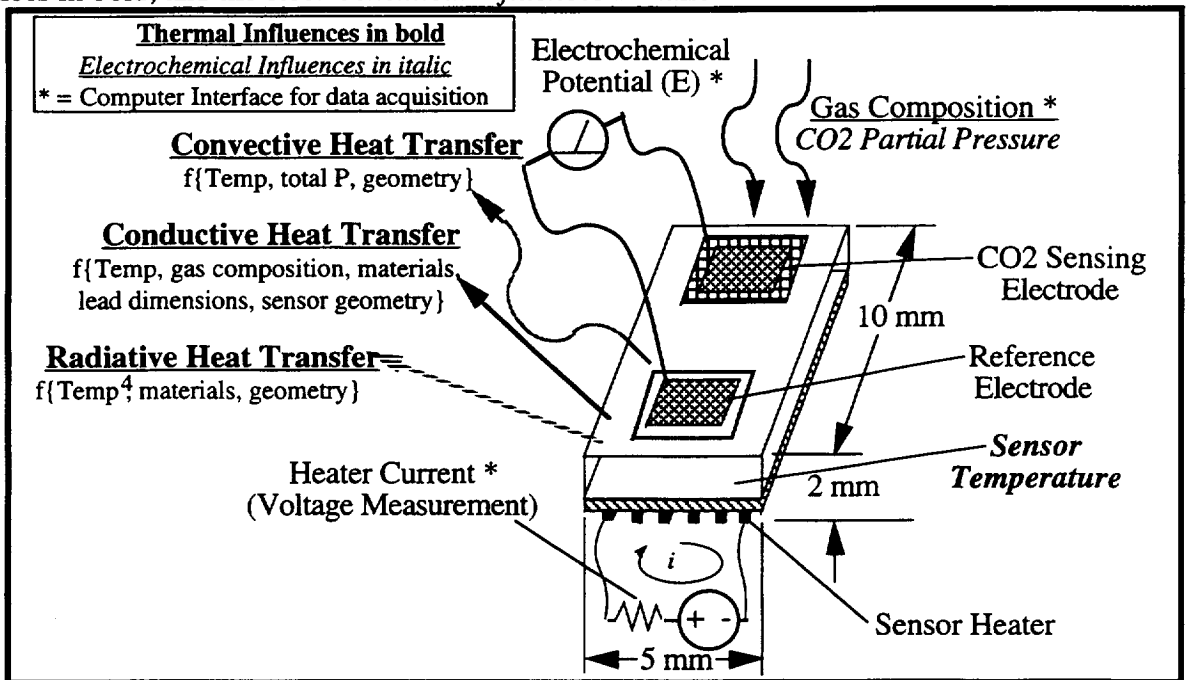
Figure E-3. *CO2 Solid State Electrochemical Gas Sensor Schematic Showing Measurement and Environmental Interfaces*

E-6

The parameters and mechanisms that correlated with the thermal performance of the sensor include heater temperature, sensor materials (emissivity, conductivity), sensor geometry (surface area, view factors, lead dimensions), total pressure (convective heat transfer), and gas composition (gas conduction heat transfer). These factors will change upon further sensor miniaturization. The electrochemical factors associated with the sensor performance include the sensor temperature, gas composition (CO_2 partial pressure), and the total pressure. The electrochemical effects are essentially independent of the sensor size.

Figure E-4 shows results for the reduced pressure Nernst response for a family of sensor temperatures. The minimum detectable limit of CO_2 under the test conditions (50 mbar Ar and 1 mbar O_2) is shown to be less than 1 mbar CO_2 partial pressure, determined from the Nernst plot intercept with the 0 mbar CO_2 partial pressure condition. The figure also shows the variation of Nernst slope with temperature.
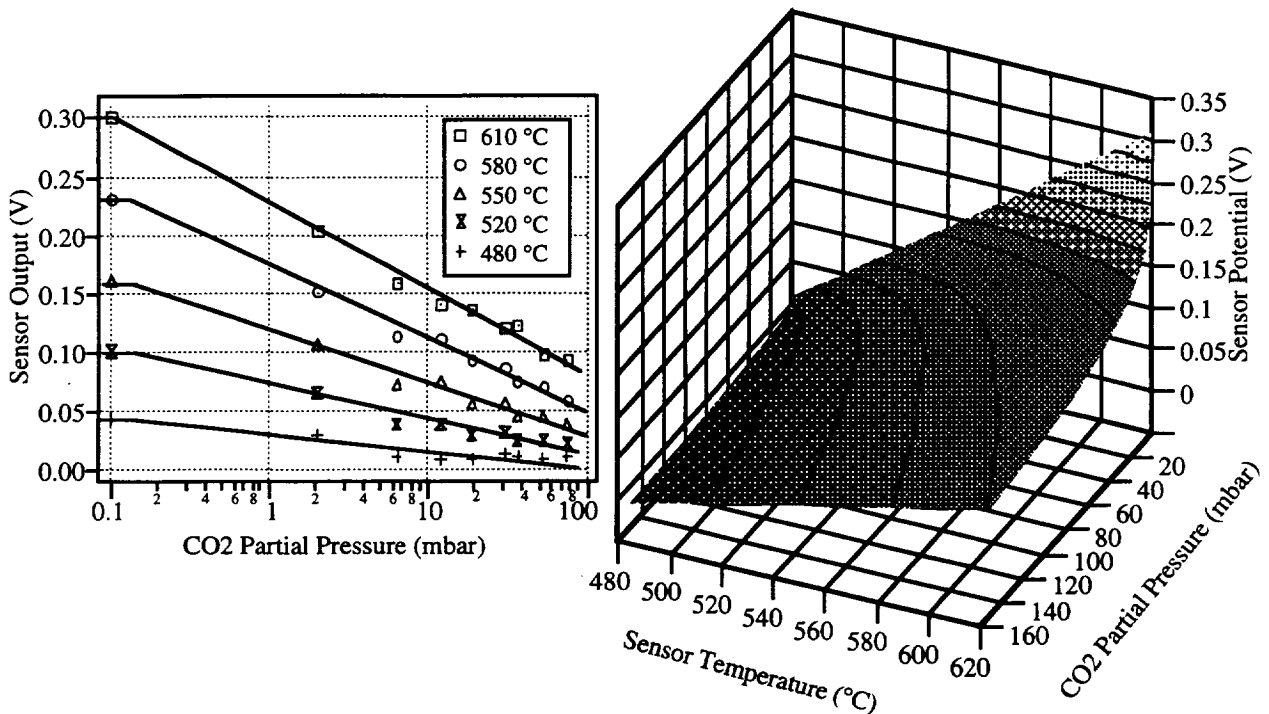

Figure E-4. Reduced Pressure Nernst Response for Sensor Temperature Family of Curves

Sensor selectivity studies were also performed using variable oxygen partial pressure in reduced pressure environments of constant CO_2 and Argon gas compositions. The results show that the Nernst slope for oxygen response passes through zero, and that selection of an appropriate sensor temperature will result in sensor operation that is completely independent of the oxygen partial pressure. The Nernst slope coefficients for O_2 and CO_2 were seen to follow similar functions of temperature, with the O_2 coefficients of much lower magnitude than the CO_2 coefficients.

CO2 Sensor Experiment Summary and Conclusions

The solid state electrochemical gas sensor concept has been proven for operation in reduced pressure environments. The sensor thermal performance was found to be a function of materials, geometry, and pressure environment, and nearly independent of gas composition. Further miniaturization of the sensor will improve the thermal performance while preserving the CO_2 selective electrochemical response. Gas sensors of this type are ideal candidates for use in planetary and space flight instruments. Their rugged nature, small size, low mass and power consumption, and demonstrated reduced pressure performance satisfy the rigorous MACE instrument performance requirements.

Solution Electrical Conductivity Sensor

The salts likely to be present within a Martian regolith sample will alter the electrical conductivity of the analysis water during aqueous dissolution. Measurement of the kinetics of the solution electrical conductivity will yield insight into the total ionic content, while the ISE's will measure specific ion content. The nature of the measurement requires that electrical current be passed through the solution, but the quantity should be minimal to avoid any unintentional electrochemistry from occurring. The total ionic content of the aqueous solution could be quite high, and the measurement should be able to cover several orders of magnitude to provide functionality over the full dissolution range from deionized water to saturated salt solutions. A measurement concept was developed using a single constant current (DC) pulse of short duration. Integration of the voltage waveform required to maintain the constant current pulse yields information regarding the solution resistivity and conductivity. A prototype sensor and electronics assembly has been fabricated, and preliminary tests performed.

A parallel wire conductivity cell was fabricated from 0.020 inch diameter platinum wire, inert epoxy and acrylic plastic. The two electrode wires in the cell are each 5 mm long, spaced 5 mm apart and set into a ~7 mm dia acrylic puck that is about 15 mm long. This configuration allows readings to be taken from standard solutions in test tubes, rather than dispensing the standard solutions and rinsing with deionized water in a full MACE like arrangement. The sensor was couped to the electronic conductivity measurement circuit that to supplies a 20 msec constant current DC pulse. The circuit includes a switched bank of resistors set at multiples of 10 x so that the current pulse between the electrodes can be adjusted between 1μA and 10 mA in factors of 10. An operational amplifier drives the DC pulse, and the conductivity is read as the voltage waveform integrated over the pulse duration. It was observed that after the current pulse was applied, the ground reference showed a voltage offset for tens of seconds, an effect analogous to the charging of a battery. To minimize this problem the pulse duration was reduced to 2 msec. Circuitry was also installed to allow the circuit to be read automatically with a computer rather than through the oscilloscope that had been used during development. Work has been started on the next generation system that will utilize a constant voltage - variable current operation mode to minimize the electrochemical effects and simplify the data acquisition interface.

Aqueous Solution Stirring Mechanisms

A mechanism is required to agitate the analysis chamber during dissolution experiments. The stirring facilitates the distribution of ions throughout the aqueous solution, impedes the formation of an ion depletion layer around the ISE's, and allows measurement of a homogeneous solution. If stirring were not used the ISE array measurements would be subject to uncertainties associated with differential ion diffusivities and solubilities, and depletion boundary layer formation. Additionally, the particle settling experiment requires that particles be initially suspended in solution to enable the kinetics of particle settling to be measured. Three methods were investigated for agitating the soil sample and analysis water in the MACE instrument analysis chamber. These methods include a magnetic

stirring bar (Teflon coated), a vibrating whip, and a piezoelectric transducer, each of which is described in the following paragraphs.

A mixing mechanism that utilized a sonic transducer was fabricated and evaluated, also made of piezoelectric Kynar. The mechanism was driven by a signal generator through an amplifier circuit to supply a voltage to the transducer of about 90 volts. Again, since the transducer was in intimate contact with a conductive solution, it was coated with a thin layer insulating silicone rubber. Agitation from this unit was observed to be even less effective than the vibrating paddle. It may be that the amount of power required for effective agitation was beyond what the transducer can couple to the solution, or that the amplifier output rolls off before an appropriate frequency is reached. Further tests and mechanisms are planned to devise a mechanism to enable stirring and agitation within the MACE analysis chamber.

The second option evaluated consisted of an oscillating paddle mechanism, constructed using Kynar piezoelectric material. The paddle was constructed from a "bimorph", that is, a laminated composite of two piezoelectric layers bonded together. The paddle measures 8 mm wide at the base, tapers to 3 mm width at the tip, and is 25 mm long. To mechanically drive the "bimorph" paddle requires a voltage source of about 260 volts to be alternately applied to each layered surface. Since this paddle will be in contact with the conductive aqueous solution, it was coated with a thin layer of insulating silicone rubber to keep from shorting the power supply. The vibration at the paddle tip was measured to be about 15 mm in air when driven at its resonant frequency, and about 6 mm maximum when not at resonance. In water, the mechanical action was damped to about 4 mm. The larger degree of motion at resonance was not observed when in the water. The stirring action that resulted from the paddle movement in water was minimal. If the frequency of motion was set too high, the paddle action went into a harmonic mode where the agitation produced was not very effective. The advantage to this method is the low power consumption (≈ 200 mW), but the stirring action produced was not very effective.

The magnetic stirring bar method is commonly used in analytical laboratories, and is available as a commercial unit. The mechanism is easily made and effective as long as the material being stirred isn't too thick, or contains any magnetically affected particles. In a laboratory setting power, mass, and space are not usually a consideration. This is not the case in the MACE instrument, and special mechanisms must be designed to minimize the mass and power associated with the stirring mechanism. There is also a high probability that the soil sample will have particles that are magnetically affected, such as iron oxides in the clay fines. Therefore, we limit the magnetic stirrer to the analysis chamber, which is isolated from particulates by the soil sample filter.

Gas Sensing Electrodes

We have established relationships with two companies experienced in custom fabrication of aqueous ion microsensors, Teknekron Inc. (Menlo Park, CA), and Stanford Research Institute (SRI) International (Stanford, CA). Over the last year we have begun preliminary discussions concerning the goals of the MACE project, and possible sensor implementations. In a related Martin Marietta project, a micro-scale CO_2 solid state electrochemical gas sensor in a planar configuration is being developed. This sensor is directly applicable to the MACE project, and will be capable of sensing the partial pressure of CO_2 over a range of from .01 to 100 mbar, using less than 80 mW of power. Figure E-5 shows a schematic representation of a candidate sensor design. The response time is

expected to be on the order of 0.5 seconds, with an expected operational and shelf lifetime of at least 4 years.
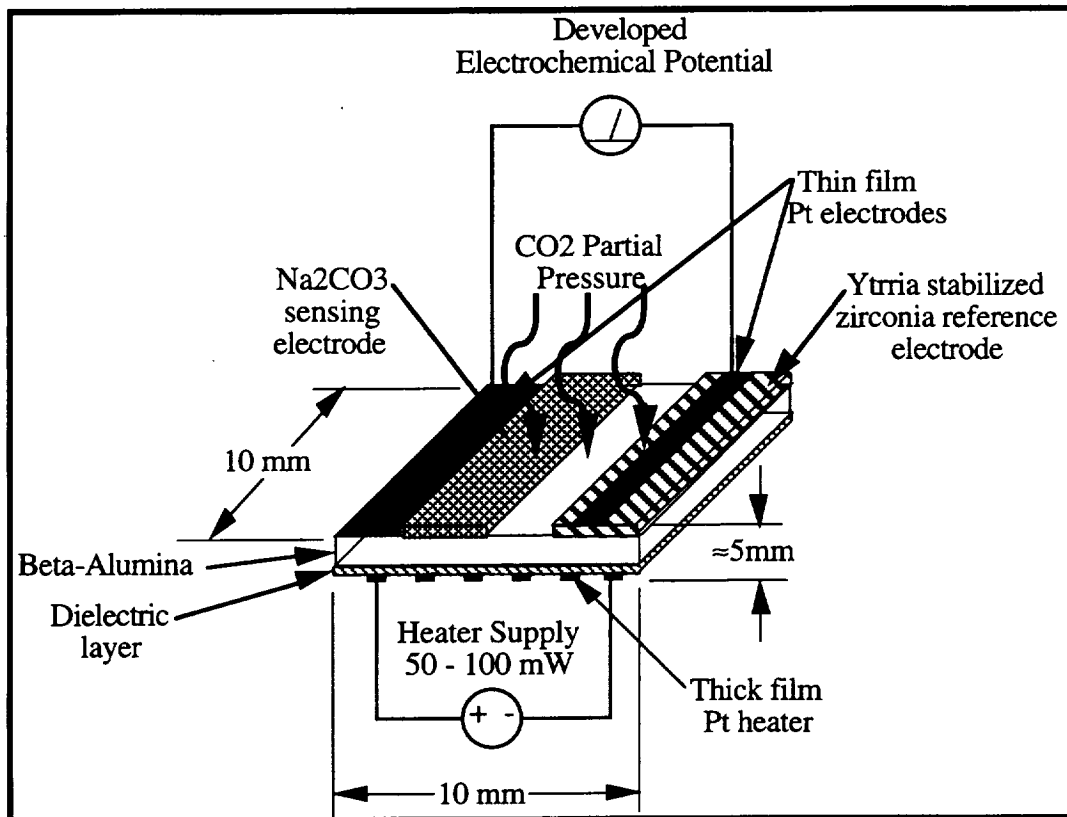
Developed
Electrochemical Potential

Figure E-5.   Martin Marietta/SRI International Micro-scale CO₂ Gas Sensor

The electrode functions by producing a voltage that is proportional to the partial pressure of CO_2 according to the Nernst equation (1). CO_2 gas dissolves into the $NaCO_3$ layer, and changes the half cell potential at the $NaCO_3$ | beta alumina interface. The zirconia reference half cell potential remains constant, and the overall galvanic cell potential changes in proportion to the logarithm of the CO_2 partial pressure.

Larry Mason, a MACE Co-I, visited SRI International in mid April '93, for discussions concerning this sensor. During this visit, additional topics concerning custom fabrication of micro-scale ISE's for measurement of pH, Ca^{++}, Cl^-, K^+, Na^+, and Mg^{++} ions in aqueous solution were also discussed. These ions represent important constituents in the Martian regolith. These sensors are not all available commercially, and none are available in the micro-scale. Other topics of discussion at SRI included sensor repeatability, lifetime, electrolyte materials suitability for MESUR/MACE, and selectivity and interference issues.

SRI International developed the oxygen sensor that is currently used in the pollution control systems on automobiles manufactured in the US. This sensor is also applicable to MACE, particularly for measurement of the liberated oxygen superoxide decomposition. The relative amount of effort involved in customizing this relatively mature sensor for use in MACE was also discussed. The normal operation of the present sensor is within the exhaust gases from a combustion engine. It is possible to apply this technology to the MACE application with the addition of a separate heating circuit and appropriate hardware

fixtures to allow mounting. It was estimated that this effort will involve one to two man-months of labor to complete.

Development of the Ion Selective Electrodes Test Facility for MACE

A facility for characterization of and experimentation with Ion Selective Electrodes (ISE) was developed during the first year activity using Martin Marietta Capital Equipment funding. This facility was designed to characterize the performance of ion selective electrodes and to measure the kinetics of ionic dissolution from various geochemical regolith samples and analogs. A vendor search was initially conducted to identify commercially available mini-scale electrodes for sensing the ions of interest in aqueous solution. The associated interface electronics was also procured to enable development of a multifuncitional array of sensors. Table E-4 lists the electrodes included in the facility, along with the specific ion sensitivity, sensor size, and supplying vendor.

Table E-4.   Ion Selective Electrodes in the MACE ISE Facility

Ion Selective Electrode (ISE) half cell	Sensor Size (mm)	Specified Sensitivity Range (mM)	Vendor
Chloride (Cl⁻)	1 dia x 4 len	0.0003 - 70	Lazar Scientific
Bromide (Br⁻)	1 dia x 4 len	0.0004 - 80	Lazar Scientific
Nitrate (NO₃⁻)	12 dia x 110 len	.01 - 1000	Orion Scientific
pH (H⁺) (polymer body)	2 dia x 4 len	2 - 12	Lazar Scientific
pH (H⁺) (glass body)	1.2 dia x 2 len	2 - 12	Microelectrodes Inc.
Oxidation Reduction (Eh)	2 dia x 3 len	-300 to+300 mV	Lazar Scientific
Reference Electrode half cells	**Electrode Size (mm)**	**Electrochemical half cell**	**Vendor**
Silver Chloride	12 dia x 200 len	Ag/AgCl	Fisher Scientific
Calomel	12 dia x 200 len	Hg/Hg(l)Cl	Fisher Scientific
Double Junction	3 dia x 180 len	Ag/AgCl	Microelectrodes Inc.

<u>ISE Interface Development</u> -- Figure E-6 shows a schematic diagram of the facility as interfaced through a Macintosh Mac IIci computer with LabVIEW instrument control software for data acquisition functions.
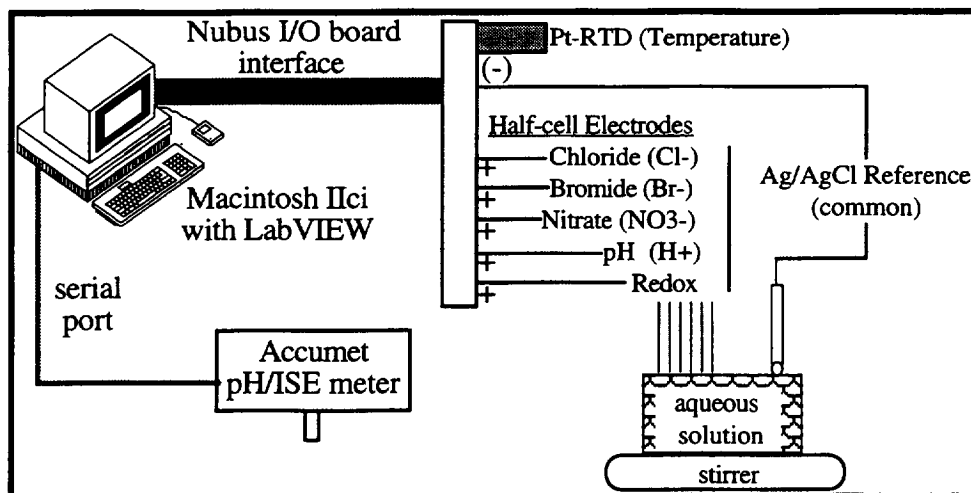

Figure E-6.   MACE ISE Facility Interface Schematic

A separate single channel high impedance electrochemical meter (Fisher Accumet 900) is also shown interfaced to the computer. This meter is not part of the facility, but is used for external verification of single electrode potentials measured through the computer interface electronics. A Resistance Temperature Detector (Platinum RTD) is also interfaced through appropriate electronics to accurately measure the solution temperatures, and to monitor the heats of dissolution associated with various salts.

Software was developed to enable acquisition of electrochemical data from the various electrodes. The LabVIEW instrument control package was used to develop software algorithms to acquire the electrochemical signal from the electrodes and display the data on a screen based strip chart recorder. The method used for calibration of the electrodes was to immerse the electrodes in a series of calibration solutions while monitoring the electrical signals. When the transients had died out, the steady state electrochemical potential was used to construct calibration and interference curves. Figure E-7 shows the front panel of the data acquisition program, where a screen-based strip chart records the voltage (y-axis) of each ISE at user selectable time intervals (x-axis). The program allows data to be acquired and stored to files for further analysis on either a continuous basis for dissolution experiments, or on an intermittent basis for calibration and interference studies.
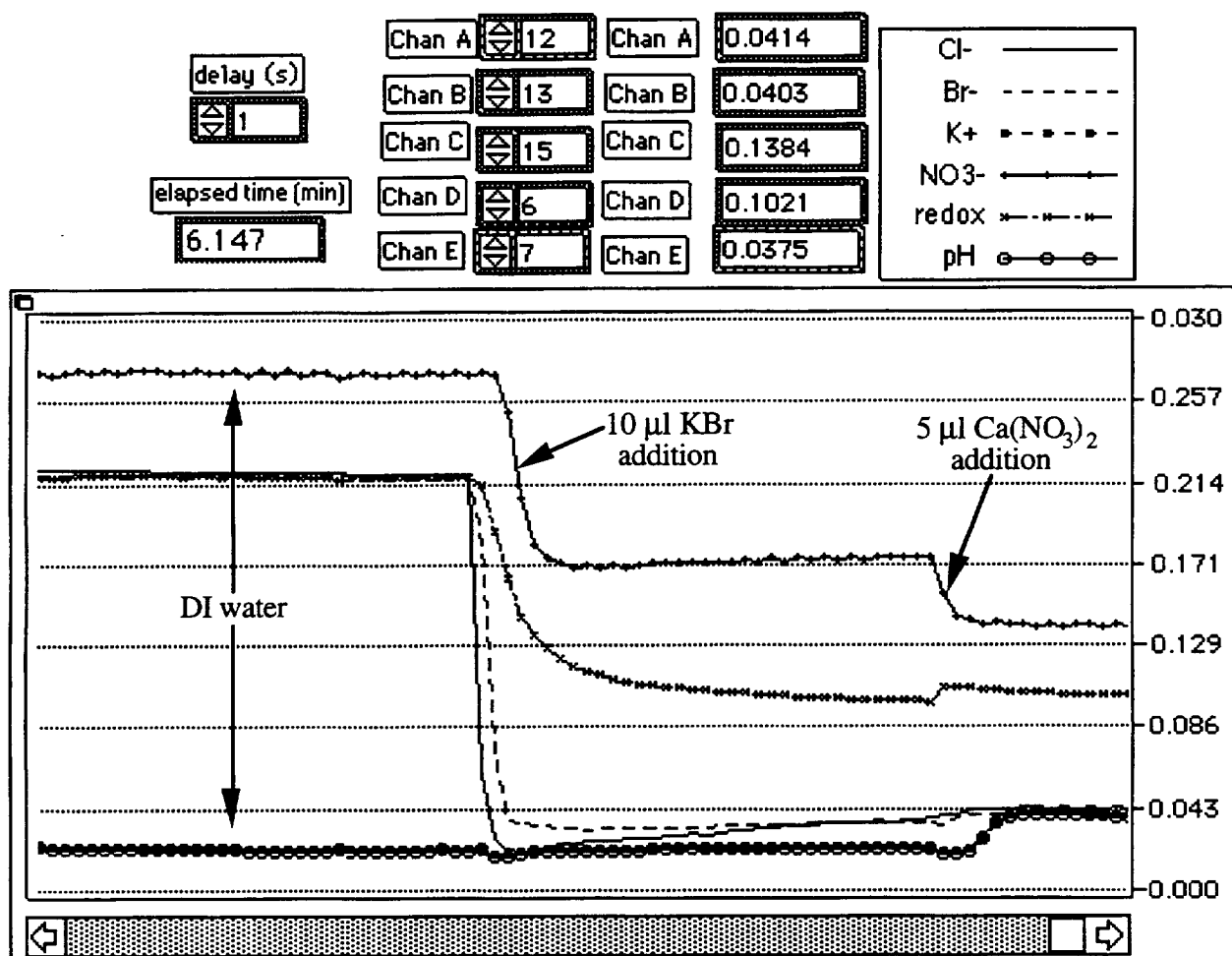

Figure E-7. LabVIEW Front Panel Strip Chart Displaying ISE Transient Data

The data shown on the strip chart represents the voltage transients resulting from addition of 10 μl of 1M KBr (first transient) and 5 μl of 1M $Ca(NO_3)_2$ (second transient) to 10 ml

of deionized water. The response indicates the signal generated for the concentration transient from 0 to 1 mM Br^- and 0 to 1 mM $NO3^-$. The data shown were acquired at one second intervals, showing the typical response where all transients from step changes in concentration settled out within 10 seconds.

The extremely high electrical impedance inherent with these electrochemical cells ($\approx 10^{10}$ Ω) necessitates the use of input electronics having several orders of magnitude greater input impedance ($>10^{12}$ Ω) to accurately measure the developed electrochemical potential. This type of high impedance circuitry is typically employed in analog laboratory meters, such as the Fisher Accumet 900 meter used in the MACE ISE facility to verify the computer acquired data. This type of meter is limited to monitoring a single ISE at a time, however, and each ISE requires a dedicated reference electrode.

The instrumentation amplifier on the nubus I/O board in the Macintosh has an input impedance on the order of 10^9 Ω, too low to be used in an analog mode. A special mode for time-sequenced data acquisition was developed under Martin Marietta internal research to overcome this limitation and allow multiple electrodes to be measured using the single instrumentation amplifier and associated multiplexer circuitry resident on the I/O board. In this mode all non-selected channels are gated to an extremely high input impedance, increasing the impedance seen by the electrodes during non-data acquisition periods. The time averaged, or overall effective input impedance seen by any one electrode is much higher than the nominal instrumentation amplifier input. Data acquired in this manner was very consistent for all electrodes tested, and correlated well with single electrode measurements using the Fisher laboratory ISE meter. The circuitry and driver algorithm developed has the added advantage of requiring only a single reference electrode for all the ISE's interfaced, as opposed to the standard laboratory case where one reference electrode is required for each ISE. The I/O board is configured in the single-ended mode, and has capability for up to 16 separate ISE's to be multiplexed for data acquisition using a single reference electrode.

The offset voltage for each galvanic cell is a function of the type of reference electrode used. Preliminary experiments were performed to characterize the various ISE and reference electrodes, establish calibration coefficients, and to determine selectivity and interference parameters. Initially three reference electrodes (silver - Ag|AgCl, calomel - Hg|HgCl, and an Ag|AgCl double junction gel electrode) were interfaced for data acquisition and tested using the chloride ISE to determine the relative offset voltages. Data was recorded for the potential produced when immersed in two different concentrations of a chloride salt (KCl), as the steady state voltage after the transients had died out. No stirring was used in this preliminary experiment, although the readings changed significantly when stirring was used. Figure E-8 shows a semi-logarithmic plot of the data resulting for each of the three reference electrodes.

The voltage offset (Vo) is shown to be a characteristic of the reference electrode used. The slope of the lines is a function of the ISE half cell, and is consistent among the three traces at about 50 mV/decade of ion concentration. Further experiments were performed using only the Silver (Ag|AgCl) reference electrode because the overall potential developed for all ISE's tested was closest to zero, allowing the highest measurement gain to be used when acquiring the data.
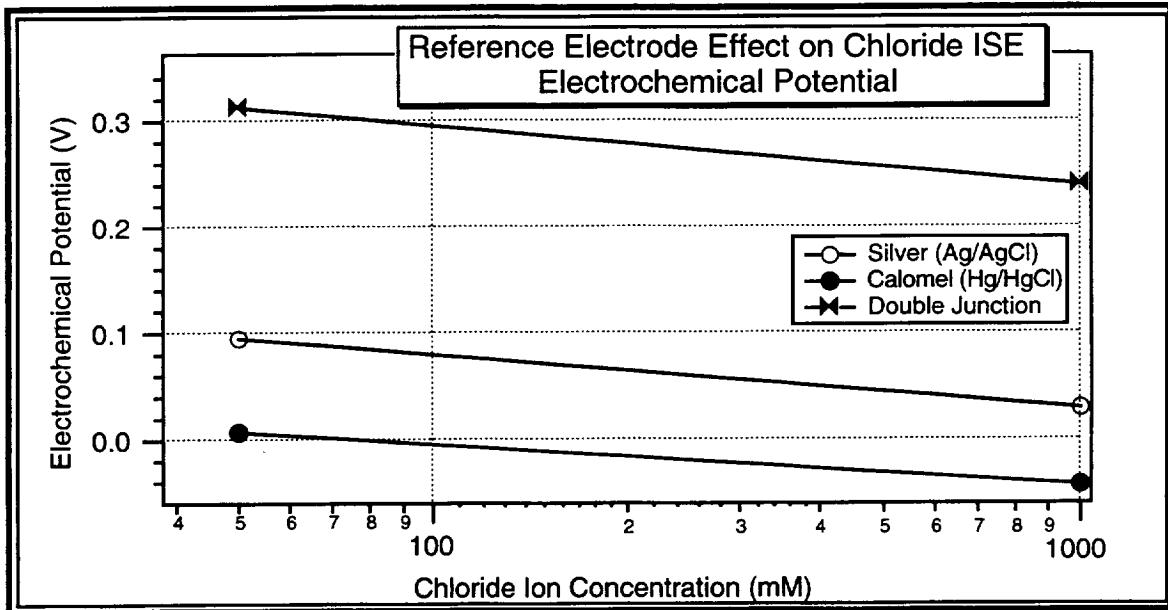
Figure E-8. *Effect of Reference Electrode on Cl⁻ ISE Performance*

ISE Characterizations -- The electrochemical response from the five commercially available
ISE's has been characterized in the MACE ISE test facility, using the data acquisition
software and protocols described in the previous section. The voltage developed by each
galvanic cell was measured during simultaneous exposure to single salt solutions of
varying ionic composition and concentrations ranging from 0.05 millimolar (mM) to 1.0
molar (M). The data obtained from this procedure is shown in Figure E-9. The plot shows
the single ISE concentration dependent voltage response to individual ions in solution,
using the salts: KCl, NaCl, KBr, Ca(NO3)2, and commercial pH buffer solutions.
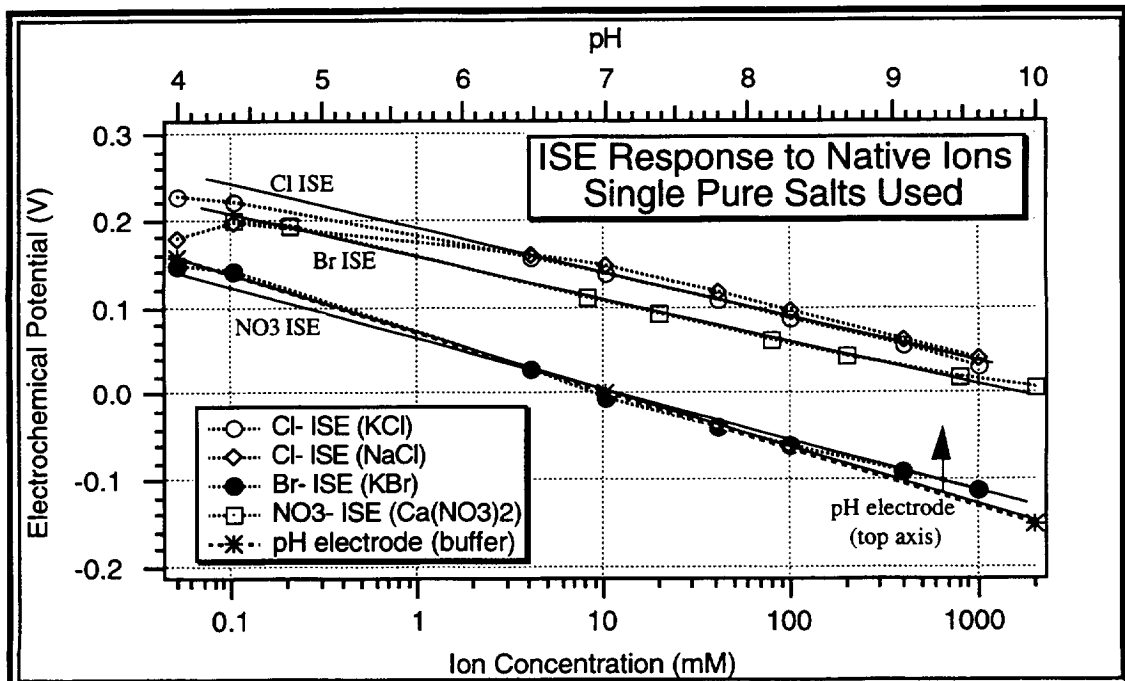
Figure E-9. Single Salt Solution ISE Responses

Calibration equations were developed for each ISE to its native ion (e.g. chloride ISE response to Cl⁻ ions) by performing a least squares regression fit to an equation of the form shown for equation (2). Only data in the linear portion of the resulting calibration curves were used, with the minimum concentration noted where the linear relation holds. Table E-5 summarizes the coefficients obtained in this analysis, and lists the minimum concentration for which the derived linear relation holds.

Table E-5. Regression Fit Coefficients for ISE's and Native Ions

ISE/ion	Vo offset (V)	Slope (V/decade)	Minimum linear Concentration (M)
chloride	0.04166	-0.05151	0.0005
bromide	-0.1200	-0.06281	0.0001
nitrate	0.01402	-0.04738	0.0001
hydrogen	0.3611	0.05125	1.0×10^{-10}

Most of the salts tested had no effect on the pH electrode, as shown in Figure E-10. This is to be expected, because there is very little buffering capacity or hydrogen ion effect associated with pure salt solutions. The exception to this is K_2CO_3, which dissociates into potassium and carbonate ions in aqueous solution, and reacts with water to form carbonic acid (H_2CO_3), an acid that has a definite effect on pH. The pH electrode was calibrated using commercially available pH buffer solution.
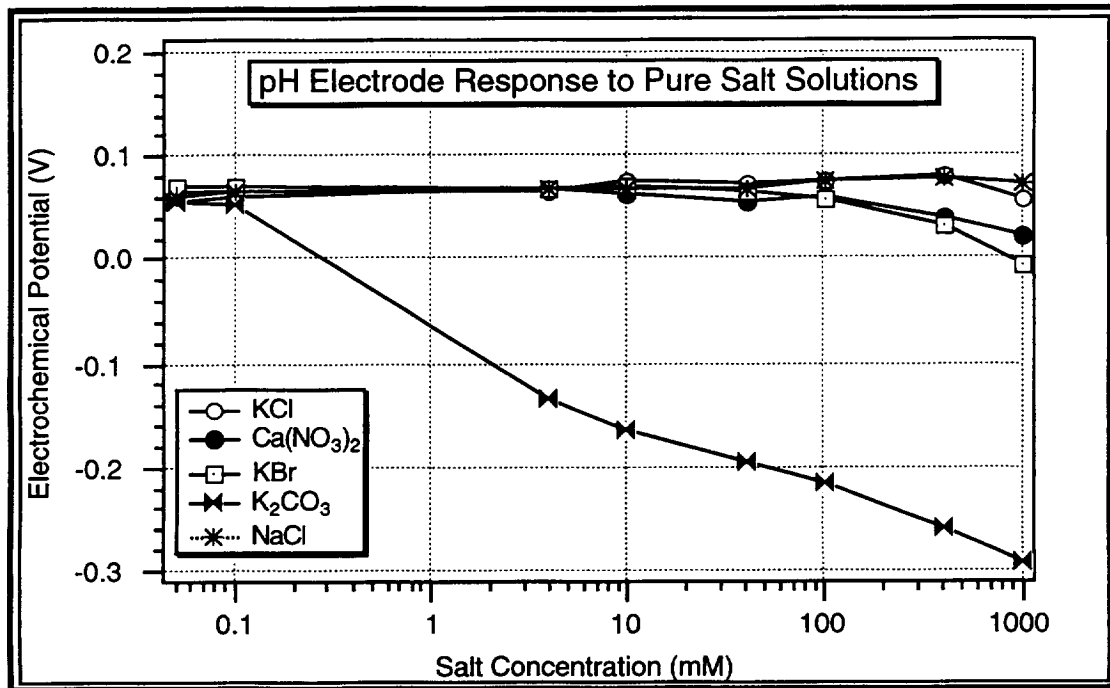

Figure E-10. Single Salt Solution Effect on pH Electrode

ISE Interference Effects -- The transient voltage responses shown previously in the strip chart traces of Figure E-11 indicate the degree of interferences that will be present in a solution containing more than one ion. The addition of Cl⁻ ions caused all ISE's except the pH electrode to change in electrochemical potential, not just the Cl⁻ ISE. This is indicative of a problem in ISE selectivity among ionic species, and is inherent to any ISE design. The name implies this type of response: ion *selective* electrode (not ion *specific* electrode).

E-15

The extent of this problem is apparent in Figure E-11, where the Br ISE response to various salt solutions is shown. A Nernst like response is apparent for all ions tested, but the onset of electrochemical response is very ion specific and concentration dependent. Each of the ISE's tested showed responses similar to this, but each had an apparent selectivity for its native ion (e.g. the Br ISE had a preferential response for Br⁻ ions). It should be possible to construct an iterative algorithm to deconvolve the overall ion concentrations based on the input from each ISE. The approach to this problem is discussed in the next section: Plans for the Coming Year.
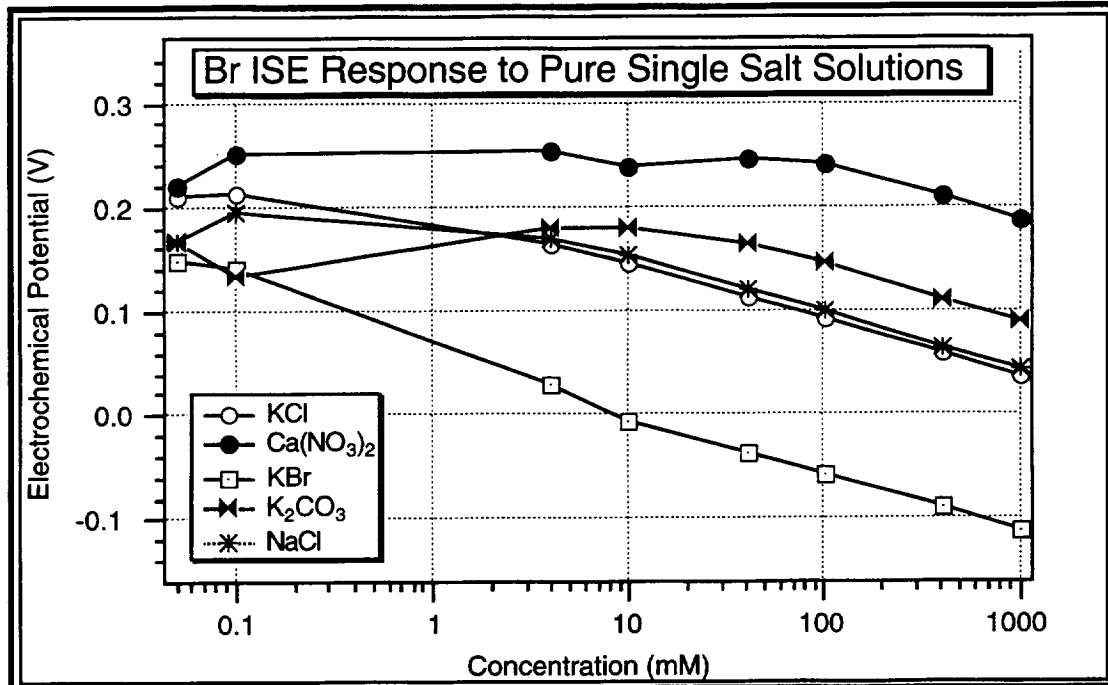
Figure E-11. Br- ISE Response to Various Salt Solutions

Salt Dissolution Kinetics Experiments

Pathfinding experiments were performed to demonstrate measurement of the kinetics of salt dissolution. The sensors used in these experiments included an RTD temperature sensor and seven Ion Selective Electrodes (ISE).

Experimental Procedure -- Four pure salts were used in the experiments to provide a substrate for measurement of dissolution kinetics: {KBr, NaCl, FeCl₂, & Ca(NO₃)₂}. In preparation for the experiments, the electrodes were placed in de-ionized water and allowed to equilibrate. The salts were weighed and enveloped within a single filter paper in preparation for aqueous extraction. The experiment began when the filter paper was immersed in the water, although data was acquired prior to this to establish baseline electrode potentials. The extraction was performed in 15 ml total aqueous solution volume, and stirring was included using a miniature magnetic stir bar measuring 1 mm diam by 5 mm long. The stirring action allowed convective mixing to aid the dissolution process, and minimized the concentration gradients present in the aqueous solution as the salts dissolved. It is apparent that the dissolution of this salt mixture is endothermic, because the temperature decreased by more than two degrees centigrade. Once the dissolution reaction was complete, the temperature began to rise due to heat input from the ambient environment and the stirring apparatus.

The total mass of salt dissolved in the experiment was 4.1 g, split among the four salts to achieve final ion concentrations in 15 ml of solution as follows: 1M NO_3^-, 1.3M Cl^-, 0.3M Br^-, 0.3M K^+, 0.5M Fe^{++}, and 0.5M Ca^{++}.

There are interferences between and cross sensitivities present among the various ISE's. Single and binary solution measurements have shown that these effects are significant, and if not accounted for, may lead to erroneous concentration determinations. The primary interfering action is due to differences in ion activities among the dissolved species, defined as the *effective* ion concentration. This may differ from the *actual* ion concentration by an amount depending on the exact composition of the total solution. In the case of an unknown sample, it is desirable to use an *ionic strength adjustment (ISA)* solution to set the activity of the solution, minimize the interferences between ISE's, and maximize the selectivity of each ISE to its native ion. The optimal composition of the ISA solution has not yet been determined, but will minimize interferences among the specific suite of ISE sensors chosen for use in MACE. No ISA solution was used in these experiments, and the concentration estimates derived from calibration of the ISE's using single salt solutions are not applicable. The steady state electrochemical potentials do correspond to the actual concentration values, however, once the interference and selectivity effects are taken into account. The pH and oxidation/reduction (redox) ISE show the highest selectivity, and function mostly independent of total solution ionic strength. The steady state (final value) electrochemical potential value for pH corresponds to 2.2, and the final oxidation reduction potential is +0.31 V.

These experiments were performed using a commercial macro-scale reference (Ag|AgCl) electrode. The utility of reference cells in a micro-configuration has also been investigated.

The smaller electrodes are also Ag|AgCl cells, but are all solid state and require no liquid electrolyte. These micro-scale reference cells are manufactured for the medical industry as disposable electrodes for *in-vivo* use, and are commercially available at low cost. An initial evaluation in combination with the ISE's used above has shown stable response in very dilute salt solutions, similar to that of the macro-scale reference cell used in the experiments. There is a voltage offset relative to the liquid electrolyte cell, but the offset is constant ($\approx$ -213±5 mV) for all ISE's tested. A constant voltage offset is expected between reference electrodes, as the function is to provide a reference electrochemical half-cell to compliment the sensing ISE and complete the electrical circuit. Separate and independent calibration curves are required for each ISE and reference electrode combination to insure maximum ISE sensitivity, selectivity, and accuracy.

Miniature Mg++ Ion Selective Electrode

A miniaturized Ion Selective Electrode was designed and fabricated by the Stanford Research Institute (SRI) International under Lockheed Martin Internal Research and Development (IRAD) funding. The miniaturized sensor is configured as a coated wire, and has the characteristics and specifications shown in Table E-6.

Table E-6.   Miniature Mg++ ISE Characteristics

Characteristic	Specification
Sensor Type	Coated wire, polymeric ionophore
Mg++ Response Range (Nernst, log-linear)	0.01 - 1000 mM
Response Time (0-90%)	< 800 msec
Recovery Time (100-10%)	< 800 msec
Operational Life (intermittent use)	> 2 years
Shelf Life	> 2 years
Dimensions	wire, 1 mm diam by 3 mm length
Mg++ Selectivity	10:1 wrt Ca^{++}, K^+, Na^+
Precision	±2% wrt Mg++ concentration

Magnesium is an important constituent of the Martian regolith, and the degree to which it is soluble in aqueous solution is indicative of the minerallic composition present. Measurement of the soluble Mg++ ion during acidificaiton of regolith (titration experiment) will provide the buffering capacity and identities of Magnesium bearing minerals. For this reason Magnesium is an important component of the array of ion sensors envisioned for the MACE instrument. No ISE of this type is commercially available. This ion was selected as a demonstration of a miniature solid state sensor of the type appropriate for an aqueous chemistry experiment on an interplanetary lander.

The ISE developed represents an electrochemical half cell, and requires the use of a reference electrode to complete the electrical circuit. ISE devices are inherently very high electrical impedance, and the small size of this custom device makes the impedance even higher. A custom interface circuit was designed to enable the electrochemical potential generated by the ISE to be measured. The interface consists of a dual JFET coupled to a unity gain precision operational amplifier. The circuit includes a trimmer potentiometer adjustment for zeroing the output offset to zero volts when the input is grounded. The output of this interface circuit is coupled to an instrumentation amplifier and analog to digital converter (ADC) for computerized data acquisition. The effective DC input resistance of this front end interface circuit is greater than 10^{12} Ω.

The Mg++ ISE was configured in a circuit with a commercially available Ag/AgCl reference electrode (Fisher Ag/AgCl ceramic junction) and the high impedance interface circuit. A 1.0 Molar solution of $MgSO_4$ was prepared from analytical grade reagent, and serial dilutions performed to yield a series of Mg++ ion concentrations from 0.1 to 1000 mM. The resulting steady state voltage generated by the ISE electrochemical cell was acquired through a computer for analysis. The solution temperatures were all room temperature while the data was acquired (24°C). Figure E-12 shows the results of this calibration response experiment, with the sensor output plotted as a function of Mg++ ion concentration.
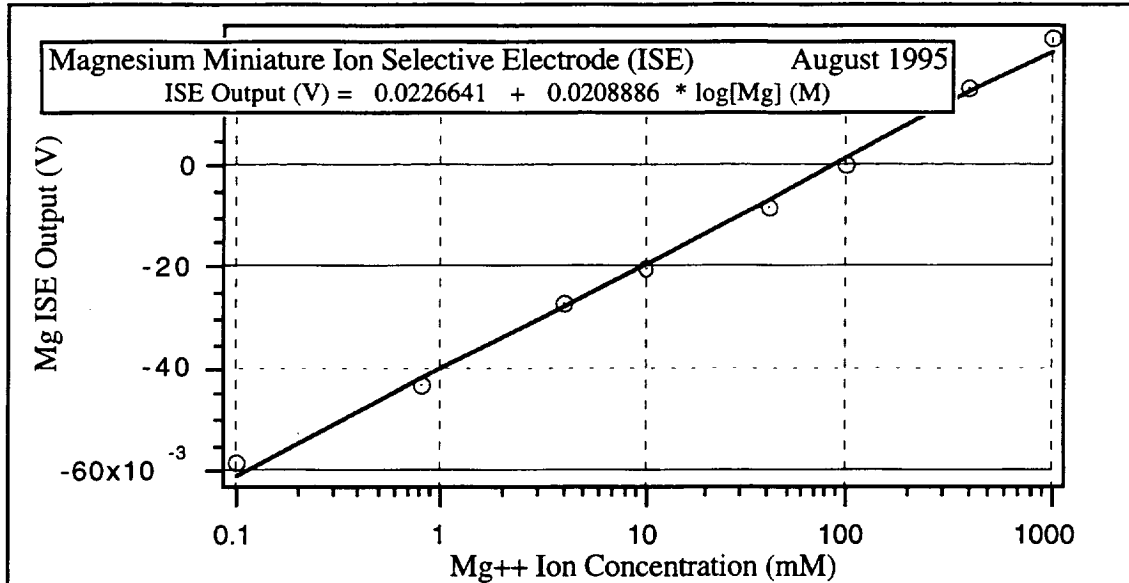
Figure E-12 Calibration Experiment Results suing the Miniature Mg^{++} ISE

The figure shows the data fit to the Nernst equation, the typical log-linear relation that exists between the sensor output and the sensed ion concentration. This relation is expected, and follows the form of Nernst equation shown in Equation 1:

$$E = Eo + S * log[Mg^{++}] \qquad [1]$$

where E = sensor output (V)
      Eo = Nominal offset at 1 M ion concentration
      S = Nernst Slope (V/decade)
      $[Mg^{++}]$ = Magnesium ion concentration (M)

The Nernst slope term (S) is a function of the ion charge (2) and the solution temperature. The slope (ISE sensor response) dependence on temperature important to monitor the solution temperature while measuring ion concentrations, especially during dissolution operations when the solution temperature may be changing due to energy from heat of solution being released concurrently with ions.

The utility of these Ion Selective Electrodes is most apparent when used in a titration analysis. An analysis if this type was performed using Magnesium Carbonate $(MgCO_3)$ and titrating with 5.0 Molar hydrochloric acid (HCl). In this analysis, 100 mg of $MgCO_3$ was added to 15 ml of deionized water, and the solution monitored using a pH electrode and the miniature Mg^{++} ISE while continually stirring. Hydrocholric acid was used as the titrating reagent, and added in microliter amounts during the course of the experiment. Figure E-13 shows the HCL addition, pH electrode, and Mg^{++} ISE time profiles that were recorded during this experiment. The oscillating trace represents the solution pH, a parameter that changes as a function of the amount of acid that has been added and the buffering capacity of the solution. The solid line indicates the total amount of acid (in units of milliequivalents) that has been added, and the dotted line is the concentration of magnesium ions in solution.
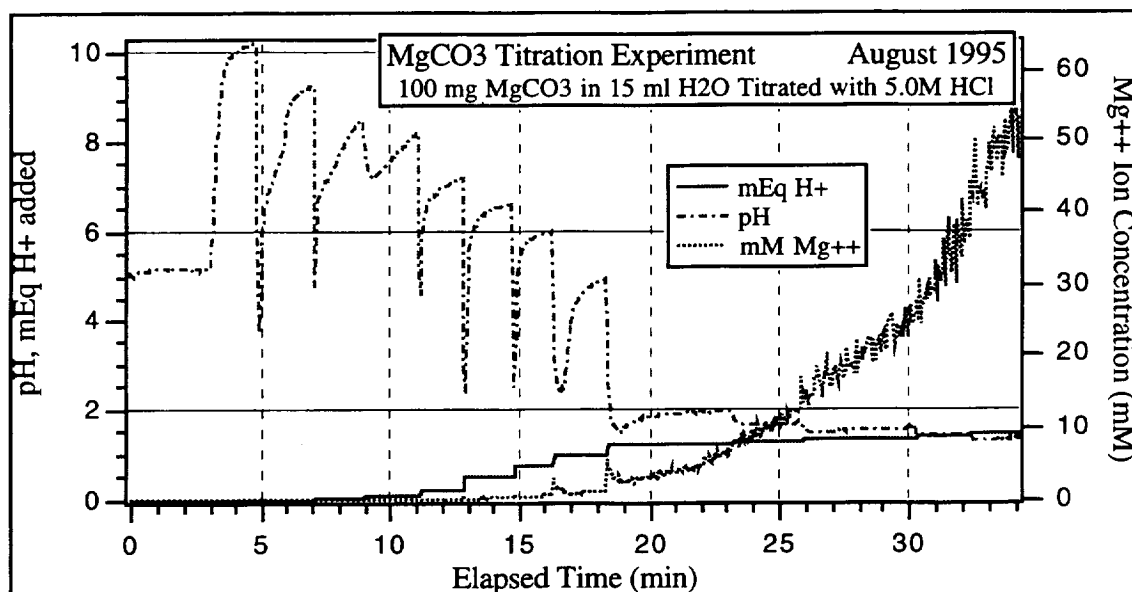
Figure E-13. MgCO₃ Titration Experiment Time Profiles

Visual observation showed that the solution was cloudy up to about 17 minutes elapsed time, at which point the solution cleared and began to bubble and fizz. This presumably is related to the dissolution of carbonate material and evolution of CO_2 gas. This is verified by the trace that shows the concentration of Mg^{++} ions in solution, which increases rapidly at the same time the solution cleared and bubbles appeared.

The data was further analyzed by plotting the "steady state" value for pH as a function of the total amount of titrating acid that had been added. Figure E-14 shows the results of this analysis where the inflection point indicates the equivalence point for the dissociation of MgCO3. The equivalence point occurs at 1.18 mEq H+, a number that correlates very well with the total amount of material used in the experiment (100 mg MgCO3 = 1.19 millimoles). The total concentration of Mg^{++} ions in solution should theoretically level off at 80 mM (100 mg $MgCO_3$ in 15 ml H_2O). Data was not taken past 35 minutes elapsed time, but the concentration of Mg++ ions is approaching the theoretical 80 mM limit.
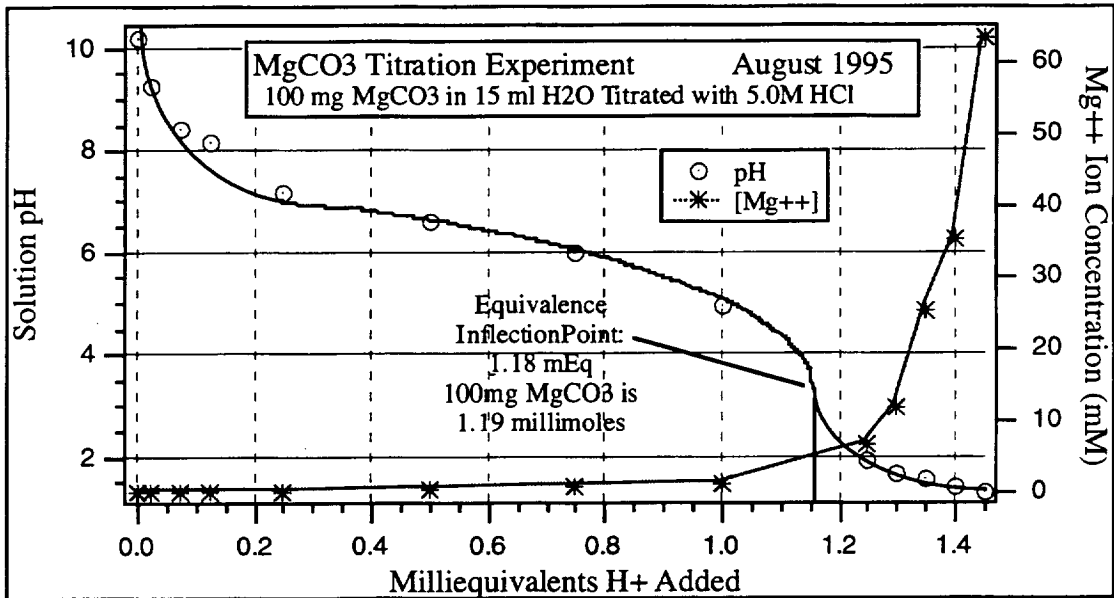
Figure E-14.   Plot of MgCO₃ Titration Equivalence Point

This analysis technique is applicable for determining the minerallic composition of unknown regolith samples. The use of multiple ISE's and gas sensors in conjunction with acid and base titration analyses can unambiguously determine the anions, cations, and gas evolution chemical species. This analysis is particularly appropriate for carbonate rich minerals as the above experiment demonstrates.

Optical Sensing of Suspended Particles

One or more of the ten test cells in MACE is planned to be equipped with instrumentation to measure the kinetics of particle settling using optical techniques. This haws been termed the Particle Settling Experiment (PSE), and will yield information relating to particle size and distribution of the insoluble portion of the Martian regolith. The settling rate of particles suspended in solution is known to be proportional to the particle size distribution, and measurement of a regolith sample on Mars should provide an *in situ* estimate of the size distribution of insoluble particles. A test system is currently being designed to investigate how light transmission and scattering can be used to perform this measurement. This includes various light sources (LED, laser diodes, laboratory lasers) and detectors (single and arrays of photodiodes). The detector and cell geometries are being developed to enable the use of both forward and side scattering to maximize the measurement sensitivity. During the initial portion of the experiment, when particles have just been suspended via the stirring mechanism, forward scattering (or transmission) will provide the highest sensitivity to particle settling. Small changes in the optical density of the suspended solution will be manifest as large differences in optical transmission, providing a high signal to noise ratio on the measurement. Conversely, at the end of the experiment when particles have settled out, scattered light will be highly sensitive to suspended particles.

There are many variables to consider in the development of this analysis, including: reduced gravity effects, irregularly shaped particles, anisotropic light scattering, and optical cell geometries. The initial effort is directed toward proving the measurement concept. Once a system has been developed, measurements will be performed using a variety of mono- and poly-disperse particle size distributions. The fidelity of the measurements acquired will determine the efficacy of this type of experiment. The amount of scattering depends upon the number of suspended particles, their size, shape, and composition. For

E-21

a suspension of identical spherical particles of diameter D and index of refraction η, Mie scattering theory predicts that the ratio of the optical power scattered into a detector at angle φ and θ to the power in the incident beam is given by equation (1):

$$\frac{\Phi(\theta,\phi)}{\Phi_0} = \frac{nL}{k^2} \{[\int i_p(x,\theta,\eta)\cos^2\phi d\Omega]^2 + [\int i_s(x,\theta,\eta)\sin^2\phi d\Omega]^2\}^{1/2} \quad (1)$$

where:

$\Phi(\theta,\phi)$= power scattered into detector in direction (θ,ϕ) [W];

Φ_0= power in incident beam [W];

$d\Omega$= solid angle subtended by detector at scattering center= $\sin\theta d\theta d\phi$ [sr];

n= number density of suspended particles [cm^{-3}];

L= length of the scattering volume [cm];

k= magnitude of incident light wavevector =$2\pi/\lambda$ [cm^{-1}];

$i_p(x,\theta,\eta)$= parallel component of the Mie scattering function [sr^{-1}];

$i_s(x,\theta,\eta)$= perpendicular component of the Mie scattering function [sr^{-1}];

x=particle size parameter=$2\pi D/\lambda$ [dimensionless].

Figure E-15 shows the geometry of the scattering measurement. This equation assumes single scattering only. If the particle cloud is dense enough to produce multiple scatter, the situation is far more complex.
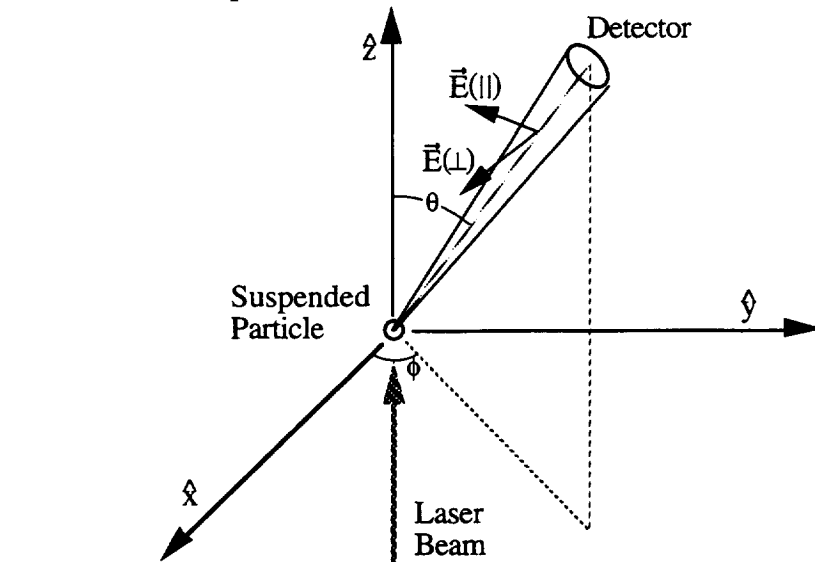

Figure E-15.   Geometry of the Suspended Particle Light Scattering Experiment

Equation (1) can be used to solve for the particle number density, n, if the particle size and index of refraction, η, are known from a single detector measurement of the scattered power. In a realistic experiment there will be particles of different sizes, shapes, and compositions. The total scatter will be a combination of the right hand side of equation (1) for many particle species. The accuracy with which n can be determined, if at all, will depend on the number of scattering angles which are taken as well as *a priori* knowledge of the nature and types of particles in the soil sample.

A proof of concept experiment has been performed to investigate the efficacy of making such measurements over a period of time which allows the particles to settle. A laser beam is directed into a water filled optical cuvette (1 cm path length) and a soil sample introduced. Small detectors such as silicon photodiodes and phototransistors were placed around the test cell to enable measurement of the scattered light resulting from the suspended particles in the water. The rectangular optical cell was constructed using a plastic cuvette, blackened on its interior surfaces to reduce internal reflections from the walls. A Helium Neon (HeNe) laser operating at 630 nm was used to provide the incident beam. Available sensors were used (a Newport silicon diode sensor and a Hamamatsu lateral effects sensor), and set up to monitor transmitted (straight through position) and scattered light (at a right angle to the incident beam). Photodiodes and phototransistors with matching preamplifiers are planned to replace these larger detectors in later versions of this experiment. The smaller the detector, the more refined the angular location for the scattered light measurement.

The straight through position is essentially an optical transmission measurement. The more particles in suspension, the more light is scattered, and the less light transmitted. The scattering measurement at a right angle to the incident beam varies in the opposite way: the more particles, the more laser light scattered into the detector. As the particles settle out with time, the transmission detector registers more and more light while the scattered registers less and less. Pure water (*i.e.*, no suspended particles) provided the calibration reference point for both measurements. The initial experiments were performed using sand (SiO_2) particles that had been sieved through 230 mesh screen, resulting in a particle distribution having diameters less than 63 μm.

The results of the initial proof of concept experiments show that multiple scattering occurs within the suspended particles during the first hours of settling. The narrow incident laser beam blossoms into a cloud of radiance which nearly fills the cell, and results in multiple scattering. Later, as more particles settled out, fewer particles (the smaller ones and the ones with large settling times) remained in suspension in the laser optical path, and single scattering dominated. The experiments were successful in demonstrating the light scattering concept, and showed that this technique will be useful for measurement of particle settling times in the MACE instrument. Further experiments are required to determine how the detected scattered and transmitted light profiles can be used to measure the particle size distribution, and in turn used to calculate the number density as a function of particle size. It also remains to be determined how the reduced gravity of Mars will affect the settling time on known particle size distributions.

F. INSTRUMENT CONCEPT

As the design concept of the future Mars mission spacecraft matured during this development effort, the interface between the MACE instrument and the spacecraft also evolved. The updated concept is for sample to be delivered to the science instruments for analysis, which simplifies the original MACE sample acquisition concept, where a drive tube was used to acquire regolith for analysis. Figure 1 shows our current concept, termed the MACE carousel. Designed for analysis of multiple independent regolith samples using cones of filter paper to contain the regolith during aqueous humidification, dissolution, and analysis.
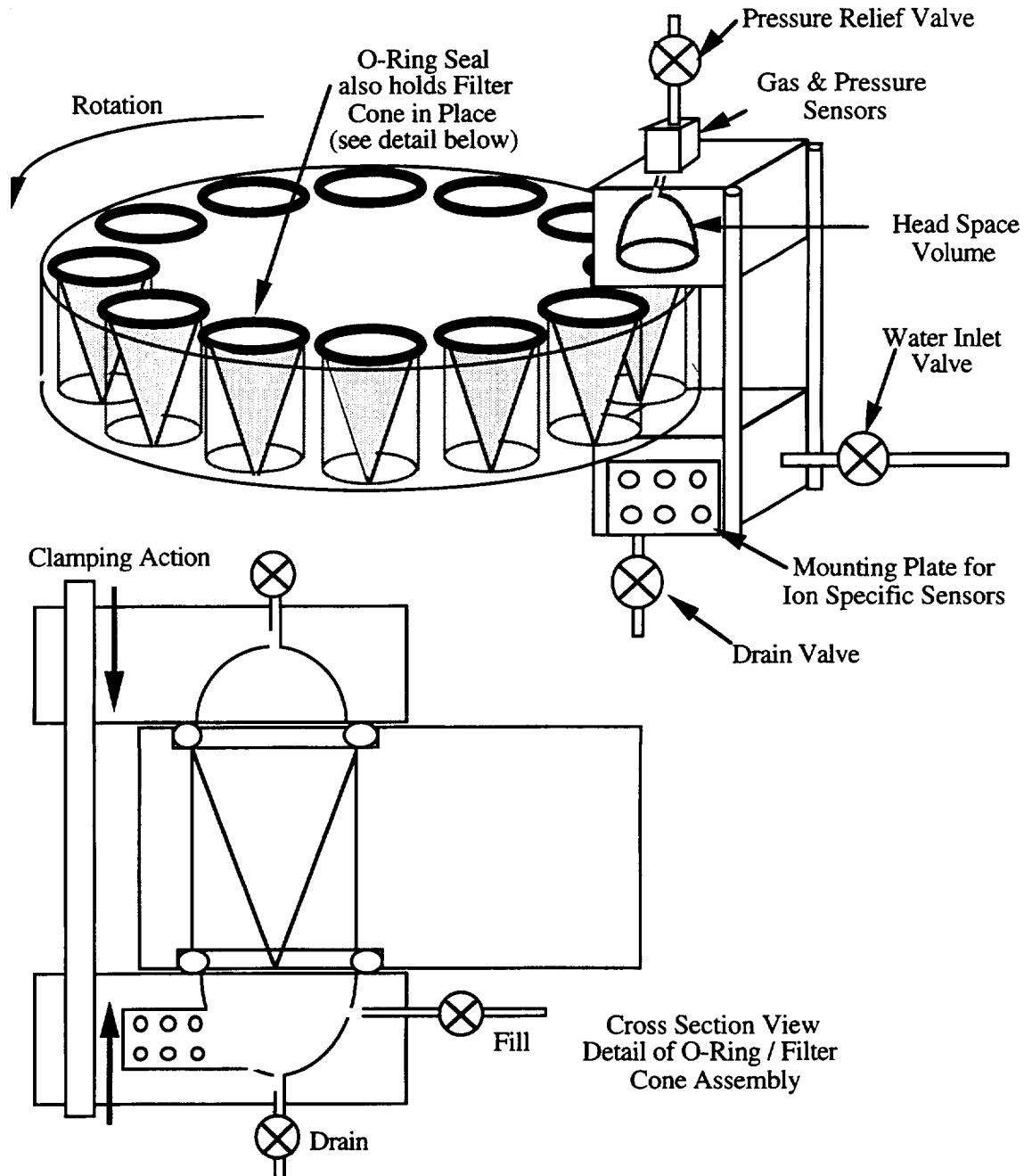
Figure 1 MACE Carousel Concept

Table 1 summarizes the capabilities and functionality of the MACE baseline concept. The estimates and capabilities listed are derived from detailed analysis of existing systems, and predicted from the mechanisms detailed in the following sections.

Table 1   MACE Baseline Concept Summary

MACE Instrument Parameter	Baseline Concept Specification	Comments
Total Instrument Mass	2.66 kg	Based on detailed estimates for over 250 individual line items
Total Instrument Dimensions	14.93x13.97x13.86 cm	Cube shaped
Total Instrument Volume	2.9 liters	Instrument bulk density ~ 0.9 g/cc
Analysis Capability (Sample Cells)	10 individual cells, 0.3 cc sample each	Mounted on carousel for random access to sample loading and analysis stations
Transport Mechanisms	Shaped Memory Alloy (SMA) driven, 1 Carousel Motor	•High reliability, low power, simple mechanisms, reduced electronics. •Motor used for random access capability
Analysis Water Reservoir	80 cc	6 cc per analysis + 2 cc for rinse
Liquid Analysis Reagents	5 liquid reservoirs	Micropump used to meter liquid reagents
Powdered Analysis Reagents	2 Porous Wheel Particle Dispensers (PWPD)	PWPD's used to meter powdered reagents into test cell for a variety of analyses
Thermal Control	Electrical Heater Units Shaped Memory Alloy (SMA) thermal switches	Configuration maintains internal instrument temperature above freezing, even in 150K ambient conditions
and Mechanisms	(ISE) array Redox potential temperature conductivity titration & decomposition analyses particle size distribution solution stirring	•12 distinct ions measured in solution •Oxidation reduction electrochemical pot. •heats of solution measurement •solution total ionic strength •metered reagent addition using micropumps and powder dispensers •light scattering from insoluble particles •required to suspend particles, mix ions
Evolved Gas Sensors	chamber pressure Gas Selective Electrodes	•gas evolution events measurement •Partial pressure of specific evolved gases
XRF interface	Kapton window in MACE sump	Interface for x-ray fluorescence measurement of elemental composition of soluble regolith components

The sequence for a MACE aqueous dissolution analysis has been defined. The scenarios for sample acquisition and fluid management refer to Figures 1 and 2, showing detailed drawings of the MACE baseline instrument concept from the top view. Figure 2 shows the analysis chamber from the side view. The figures show the instrument concept and analysis chamber at full scale, with all mechanisms and actuators having full functionality.

Sample Acquisition and Preparation
A stationary Sample Inlet Cone covered by a Coarse Screen is accessible from the outside of the instrument housing. Soil samples to be analyzed by MACE are delivered to the Sample Inlet Cone of the instrument by a robotic arm, or perhaps a small rover. The Coarse Screen prevents oversize particles from entering the instrument while the 45° mounting angle serves to deflect the larger particles away from the Sample Inlet Cone. Soil sample particles small enough to pass through the Coarse Screen and fill the cavity within the Sample Volume Control plate. This volume essentially defines the sample volume: about 0.3 cubic centimeters (cc).

A Shape Memory Alloy (SMA) activated mechanism moves the Sample Volume Control plate from the position directly beneath the Sample Inlet Cone to the Fill Position aligning with the inlet to the Sample Test Cells. The inlet to the Sample Test Cell is kept free of sample particles that could degrade or prevent proper sealing by use of a stationary O-Ring Guard located directly above the Sample Test Cell fill position. When in the position to fill the Sample Test Cells, the Sample Volume Control plate also allows excess sample material to be discarded through the Excess Sample Exit in preparation for a receiving a new sample. Immediately after the sample material has been deposited into the Sample Test Cell, the Sample Volume Control plate is returned to the original position beneath the Sample Inlet Cone. This scenario results in minimal cross contamination between samples.

To rotate the carousel to another position, the SMA Clamping System of the Analysis Chambers must first be energized. Applying power to the SMA Clamping System causes the Analysis Chambers to move away from the Sample Test Cell, and frees the carousel to rotate to the next position via random access. The SMA mechanism of the Clamping System must be activated to release the Sample Test Cell any time the carousel rotates. When power to the SMA mechanism of the Clamping System is removed, the conventional compression springs apply sufficient force to the upper and lower O-Ring Seals of the Sample Test Cells to create a gas tight seal around the Analysis Chamber.
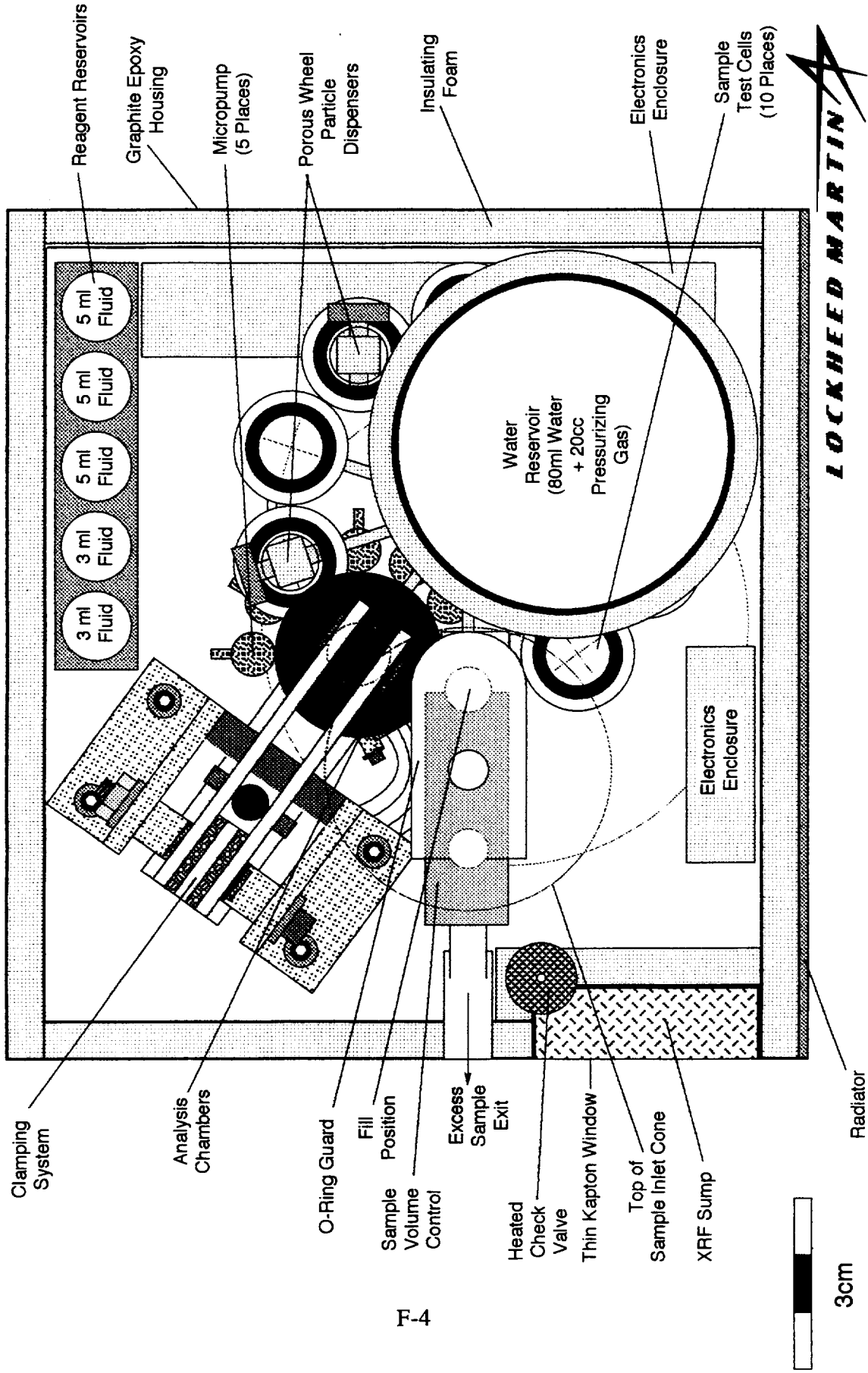
After the sample material has been deposited into the Sample Test Cell, the random access carousel supporting the 10 individual Sample Test Cells can be rotated. The rotation may move the test cell directly to the Analysis Chamber, or alternately position the test cell to align with the outlet of either Porous Wheel Particle Dispenser (PWPD). The PWPD is used to dispense a metered quantity of powdered reagent into the test cell. The PWPD is driven by a SMA mechanism that rotates the PWPD central shaft to deliver a metered quantity of powder for the analysis. After the desired quantity of powder has been added, the carousel is rotated to the Analysis Chamber position.

Fluid Management

Water used within the analysis chamber must be de-gassed to prevent outgassing when exposed to the low pressure ambient environment present within the analysis chamber. Degassed water needed for the aqueous experiments to be conducted is supplied by a 100 ml reservoir filled with 80 ml of water. The water is stored within a collapsible bladder to prevent gas from being absorbed. The remaining volume within the reservoir is used to provide pressurization of the bladder containing the water and allows filling of the lower portion of the analysis chamber and the lower portion of the sample test cell.

F-3

MACE

Top View Of MACE Concept

Reagent Reservoirs

Graphite Epoxy Housing

Micropump (5 Places)

Porous Wheel Particle Dispensers

Insulating Foam

Electronics Enclosure

Sample Test Cells (10 Places)

Water Reservoir (80ml Water + 20cc Pressurizing Gas)

Electronics Enclosure

Clamping System

Analysis Chambers

O-Ring Guard

Fill Position

Sample Volume Control

Excess Sample Exit

Heated Check Valve

Thin Kapton Window

Top of Sample Inlet Cone

XRF Sump

Radiator

LOCKHEED MARTIN

Filename = MACE 8/95 TV Concept 8/29/95 MGT

Figure 1 MACE concept top view

Scale = 1:1   Enclosure = 14.93cm Length X 13.97cm Wide X13.86cm Height   Volume = 2890.81cc

3cm

MACE

Analysis Chamber With Stirring Bar

Side View

Scale: 1mm = 1mm

Upper Clamping Arms

Confor C-47 Urethane Foam
with Gold Coated Kapton

Shape Memory Alloy Wire

Clamping System Mount

Lower Portion of
Reaction Chamber

Magnetic Stirring Bar

Stirring Motor
(with Magnet)

Upper Portion of Reaction Chamber

Sample Test Cell
(10 Places)

Micropump

Microvalve

LOCKHEED MARTIN
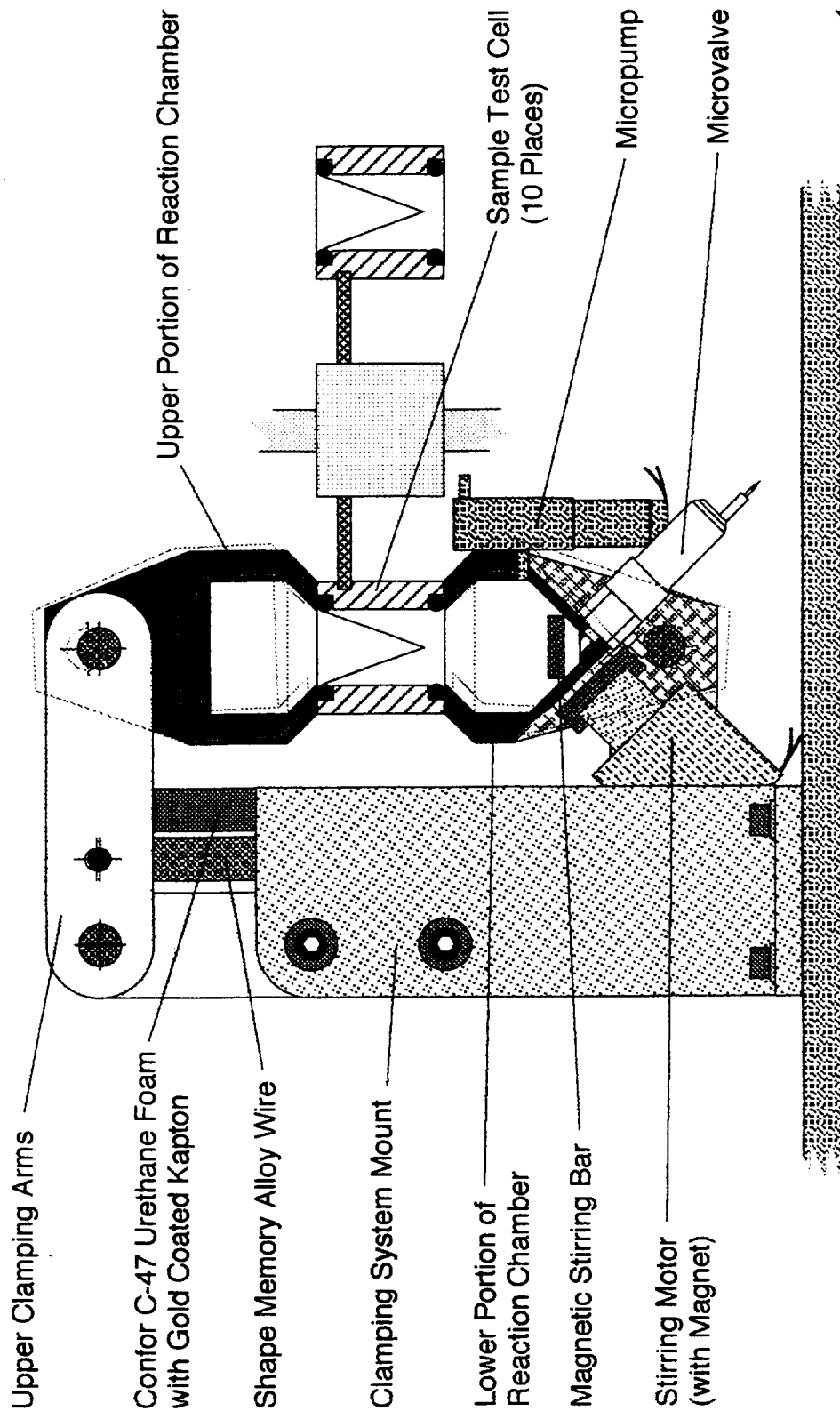
Filename = Front View + Stir Bar   12/21/95   MGT

Figure 2 MACE analysis chamber side view

The reservoir contains enough water to conduct experiments on 10 different soil samples, with adequate reserve to allow rinsing of the lower Analysis Chamber between analyses. If a titration or decomposition analysis is to be performed, liquid reagents are added to the water within the lower portion of the Analysis Chamber by first opening the appropriate Microvalve and activating a Micropump. The micropump is an implantable miniaturized solenoid activated pump developed for *in vivo* insulin addition in diabetic patients. The reagent may be added to the analysis chamber in precise increments of 0.5 μl, enabling titration and controlled decomposition analysis scenarios to be performed. Our baseline concept includes three separate Reagent Reservoirs having 5 ml fluid capacity each, and two additional Reagent Reservoirs with 3.2 ml fluid capacity. Each Reagent Reservoir has its own Microvalve and Micropump for independent operation. The choice of chemical reagents (liquid and powder) to be used within these reservoirs is TBD, but will likely include acid, alkaline, and surfactant reagents.

When the analysis of a sample is completed, all fluids are drained into the XRF Sump. A heated valve and vent tube connected to the upper portion of the Analysis Chamber is opened and the liquid remaining in the soil sample is allowed to sublimate to the low pressure ambient environment of Mars. This is done before opening the Analysis Chamber to avoid a build up of water vapor on the inside of the instrument enclosure that could degrade the emissive nature of the thermal surfaces and affect the stability of the instrument. A Heated Check Valve and vent tube attached to the XRF Sump performs a similar function to remove the liquid from the waste received from the Analysis Chamber. After the liquid portion of the waste has evaporated, the residue deposited on the Thin Kapton Window of the XRF Sump can be analyzed by an external X-Ray Fluorescence (XRF) spectrometer to qualitatively and quantitatively identify elements leached from the soil sample. This will reveal the water soluble elements contained in the Martian soils. Table 2 summarizes the MACE operational modes and analytical measurement capabilities.

Table 2 MACE Instrument Modes of Operation

Mode	Physical Operations	Analytical Measurements
Sample Loading, & Transport	receive regolith sample transport sample to reaction chamber seal sample chamber (hermetic)	bulk volume used to meter sample
Sensor Calibration	seal chamber (hermetic) meter cal sol'n(s) to sensor chmbr flow cal gas past gas sensors chamber rinse & unseal	ISE calibration gas sensor calibration temperature sensor calibration
Humidification	meter water into sensor chmbr so only vapor contacts sample	evolved gases comp. (superoxides) ΔP from gas evolution ΔH of humidification sample bulk conductivity
Aqueous Dissolution	meter water into sample chamber to wet sample	ionic dissolution species/kinetics sol'n calorimetry, ΔH of hydration freezing point depression evolved gases composition/kinetics ΔP from gas evol. & decomposition solution conductivity/kinetics oxidation reduction potential
Acidification	addition of acid reagent(s)	acid soluble species sol'n calorimetry, sample bulk Cp evolved gas ΔP, composition
Post Analysis Activities	neutralization of analysis water transport of anal. water to sump sensor chamber cleanup spent sample transport	pH titration/buffering capacity particle size/settling kinetics
Water Evaporation	water evaporation to ambient atmosphere	freezing point depression XRF of soluble sample fraction

MACE Instrument Thermal Model

The thermal model of the MACE instrument was developed using Systems Improved Numerical Differencing Analyzer (SINDA), which analyzes resistor-capacitor network representations of thermal systems. Figures 3 and 4 show drawings of the MACE instrument with numbers identifying the locations of the thermal nodes. Conduction, radiation, and electrical heater units (EHU) heating thermal transport modes were modeled within the instrument enclosure. The current analysis does not include heating from the electronics assemblies.

Thermal Model Description

The thermal interactions of the MACE instrument enclosure with the Mars environment include: solar heating, free convection, radiation to the environment, and conductive and radiant exchange with the spacecraft baseplate. The solar heating is modeled as a solar constant (dependent on the Mars location) multiplied by the solar absorptance of the instrument enclosure and a factor to account for sun angle. The solar absorptance used in the thermal model is 0.85, based on the Viking thermal model. Lower solar absorptance than this was assumed to be unobtainable due to the frequent dust storms on Mars, which would degrade the emissive nature of any optical coating. Three Mars locations were modeled to evaluate the range of heating conditions. These cases are identified as hot, nominal and cold. The hot case is representative of -30° latitude, the nominal case +30° latitude, and the cold case +60° latitude, each taken at the latitude specified while Mars is at perihelion. The thermal

design for the MACE instrument was optimized for each of these cases based on the temperatures achieved during the daily solar cycling. Table 3 summarizes the thermal design and environmental conditions for each case.

Table 3   MACE Thermal Design and Environmental Conditions

Environment Case	Latitude at perihelion	Solar Constant	Temperature Range	Thermal Design features
Nominal	+30°	550 W/m^2	155 - 220 K	2 EHU's Internal emissivity: 0.05 Baseplate emissivity: 0.03 Reservoir emissivity: 0.2 Polyurethane foam: 0.25"
Cold	+60°	0 W/m^2	150 K	2 EHU's Internal emissivity: 0.03 Baseplate emissivity: 0.02 Reservoir emissivity: 0.2 Polyurethane foam: 0.25"
Hot	-30°	700 W/m^2	188 - 293 K	2 EHU's Internal emissivity: 0.05 Baseplate emissivity: 0.05 Reservoir emissivity: 0.2 Polyurethane foam: 0.25"

The MACE design incorporates 2 EHU's (each generating 1W) for heating the instrument enclosure. 0.1 W from one EHU is conductivly coupled to the water reservoir, and the remaining 1.9 W is radiated to the enclosure interior. Both EHU's include variations of a specially developed Martin Marietta Shape Memory Alloy (SMA) actuated Thermal Switch mechanism to allow for the heat to be routed to the instrument radiator from either EHU, and also for the water reservoir EHU to break thermal contact with the reservoir in the event of high ambient temperature.

Foam insulation (Confor polyurethane foam) is used around the inside of the instrument enclosure, sump sample inlet and the spacecraft baseplate to provide thermal isolation from the Mars environment. The insulating foam isolates the instrument interior from the ambient environment and acts to stabilize the interior temperature. Low emissivity surfaces are provided by single or possibly multiple layers of coated Kapton films. The specific coating used on the Kapton is dependent on what emissivity is required to stabilize the enclosure temperature, and is dependent on the ambient conditions. Higher values for the emissivity provide a more flexible design which is better able to withstand the effects from contamination. The contamination will be minimized within the enclosure by venting the enclosure to the exterior environment following each analysis.

Temperatures on Mars vary as a function of latitude, season, and time of day. The ambient temperature profiles used in the thermal model are based on the 1972 JPL Mars Environment Model by Kieffer, which was derived from Mars planetary temperature data. The thermal model was run for three ambient temperature cases: Nominal, Hot, and Cold, representing the hot and cold extremes, and an average. The MACE instrument enclosure radiation is modeled as a cube that radiates to a constant 100K thermal sink (Mars sky) through the upper surface, and radiates to a sink at the planet temperature through the sides of the enclosure. For free convection calculations, the air temperature was set equal to the planet temperature. This approach is consistent with previous Viking thermal analyses.

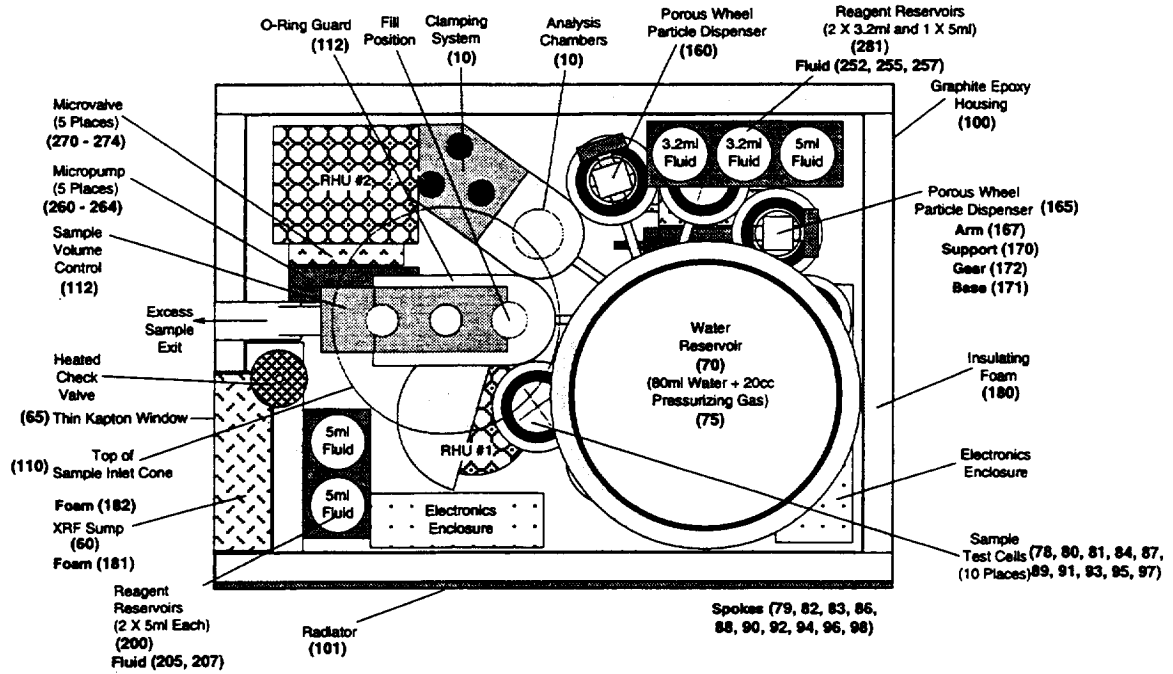**Note: Boldface type identifies thermal node numbers**

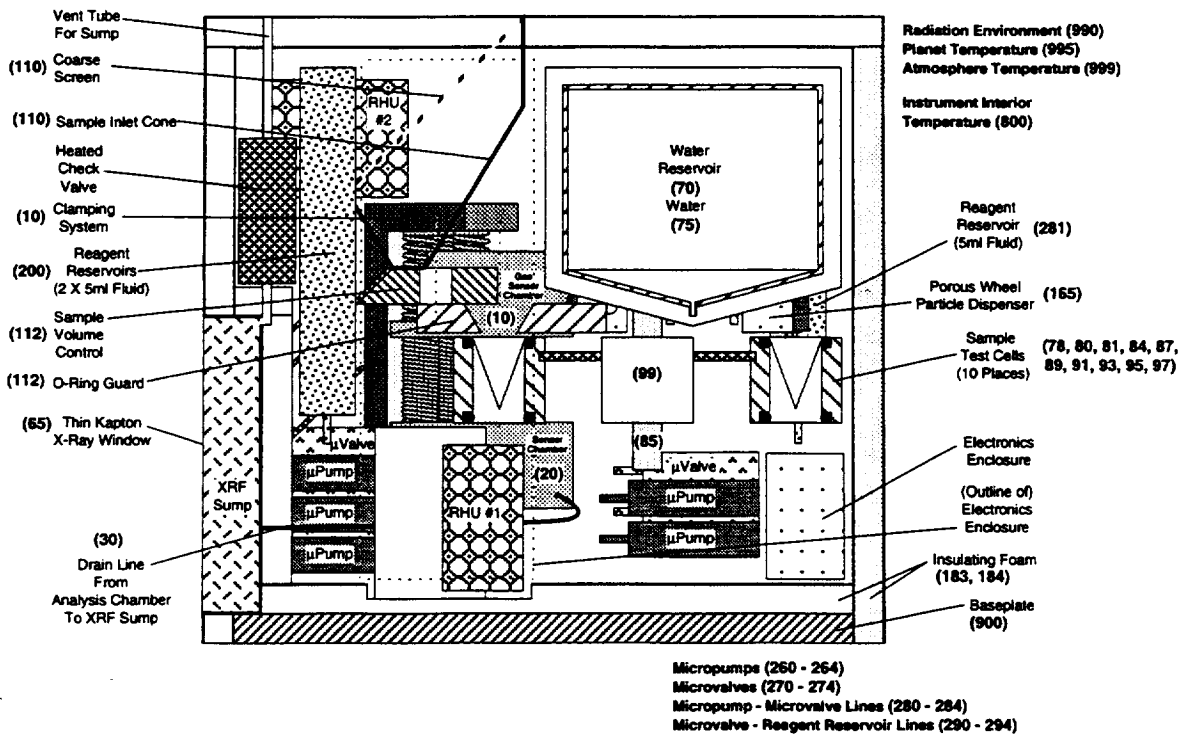Figure 3   Top View of MACE Thermal Model

Figure 4   Side View of MACE Thermal Model

Thermal Model Results

Figures 5 through 7 show plots of the sump, water reservoir, enclosure, and environment temperatures over two days of solar cycling. For each case the water reservoir was thermally isolated from the instrument enclosure to maintain the reservoir temperature stable to within ±0.5 K. In every case (nominal, cold, & hot) the instrument enclosure remains above 278 K (+5°C) to prevent freezing of the analysis water. In the event that the enclosure temperature rises above an acceptable nominal temperature (from solar input or high ambient temperature), the SMA thermal switch shunt is actuated to thermally connect the EHU's to the instrument radiator plate, reducing the heat load within the enclosure.
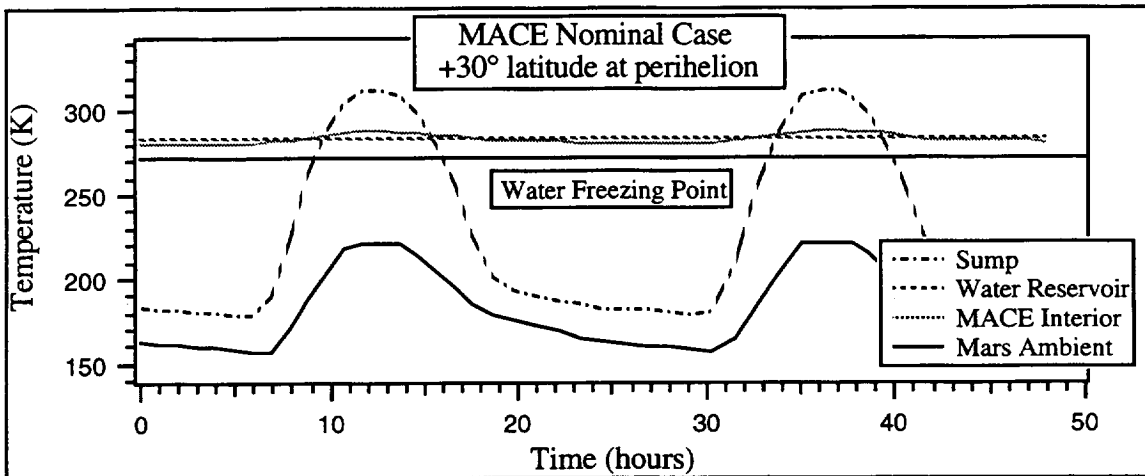
Figure 5   Thermal Model Nominal Case Temperature Profiles
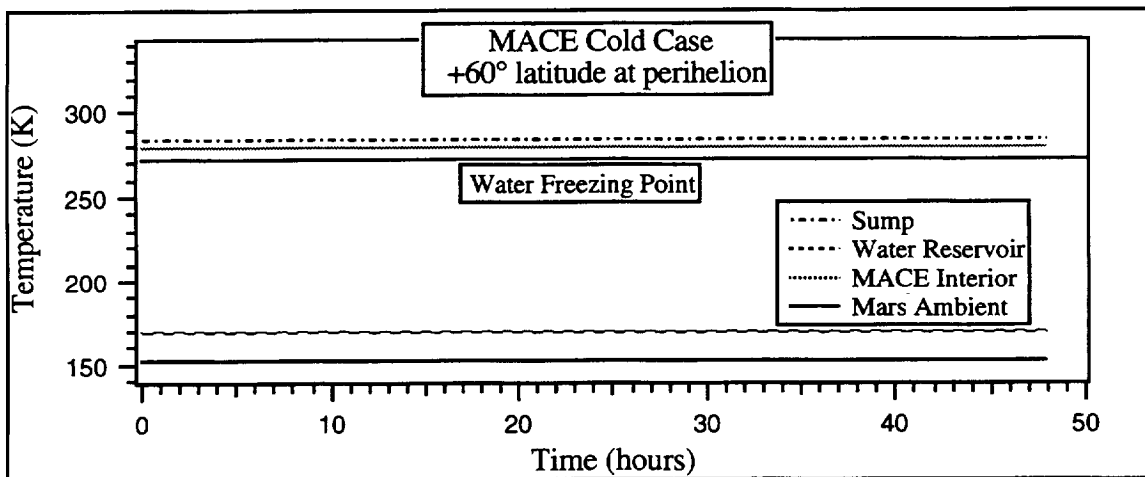
Figure 6   Thermal Model Cold Case Temperature Profiles
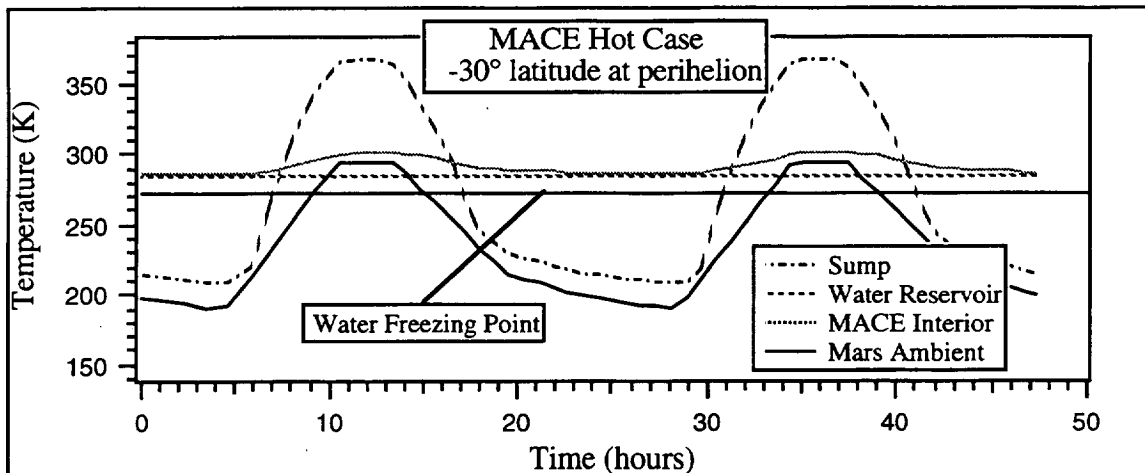
Figure 7 Thermal Model Hot Case Temperature Profiles

Analysis Chamber Clamping System

A detailed design for a flight instrument analysis chamber and clamping system has been developed based on the use of Shape Memory Alloy (SMA) wire. For a flight instrument, a 0.035" diameter nickel-titanium SMA wire will be used to develop the required sealing force to assure sample containment during an analysis. The SMA wire will be and will require dual condition training to allow both opening and closing of the analysis chamber to be performed. The SMA wire for the analysis chamber is designed with a memory strain of 1%. Memory strains of up to 8% can be used if only a few actuations are needed. As the percentage of memory strain decreases, the number of actuations and the long term motion repeatability improve. Typical memory strain values are 3% to 4% when reliability over thousands to tens of thousands of actuations is required. Although larger dimensional changes could be achieved, the 1% memory strain was selected to provide maximum reliability. With a 1% memory strain, the repeatability of the opening and closing force is excellent. A total change of less than 0.5% in the opening/closing force and stroke is expected after millions of actuations. A minimum of 40°C between the upper and lower SMA wire transition temperatures must be maintained to assure that the full dimensional change of the SMA wire is achieved. The motion produced by heating or cooling the SMA wire is mechanically amplified by a factor of 3 to achieve a minimum analysis chamber clearance of 1.2mm both above and below the test cell. A side view of the analysis chamber clamping system is shown in Figure 2.

As power is applied to the SMA wire, it begins to heat up. When the upper transition temperature is achieved, the length of the wire increases, thereby opening the analysis chamber. When power to the SMA wire is turned off, the wire begins to cool. As the SMA wire temperature drops below the lower transition temperature, the wire returns to the starting length and the analysis chamber is closed. Power to the SMA wire is required only when changing test cells to minimize the total power required. The amount of time required for the SMA wire to open the analysis chamber is directly related to the amount of electrical current applied, with larger diameter wires of SMA requiring more current.

The lower transition temperature for the SMA wire must be higher than the maximum ambient temperature environment within the MACE instrument. The transition temperature range for nickel titanium shape memory alloys can be adjusted over a wide range from
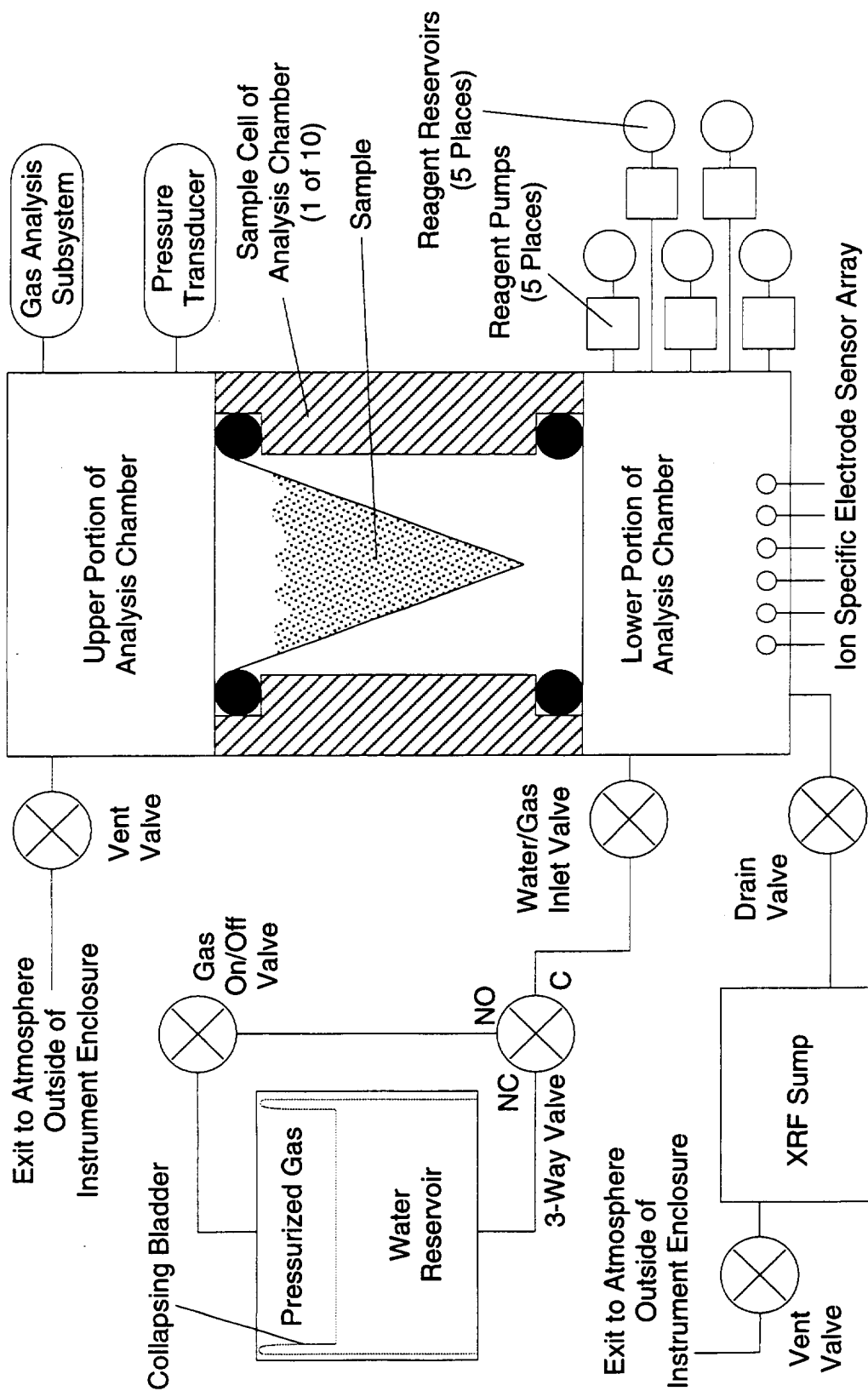
cryogenic temperatures up to about 110°C. Transition temperature is controlled by variations in the percentages of the nickel and titanium components of the alloy.

In the anticipated test, operating, and pre-launch environments that a MACE instrument might encounter, an upper transition temperature of not less than 60°C should provide adequate margin to prevent inadvertent opening of the analysis chamber. Since the transition temperature can be reached in about one second and change out between test cells will take only a few seconds, the potential for sample heating prior to analysis is minimized. To further minimize sample exposure to the heat of the SMA wire during sample change out, a 6mm thick piece of Confor C-47 urethane foam covered with a layer of gold coated kapton is positioned between the SMA wire and the analysis chamber. The SMA wire itself should also be enclosed within a layer of gold coated kapton and Confor C-47 foam. This will help to minimize the amount of power required to open the analysis chamber and will also assure that the analysis chamber is closed slowly on the test cell to avoid packing or dislodging sample from within the sample cone.

An alternative approach to having a single SMA wire trained for two different temperature transitions, would be to add a second SMA wire at an equal distance away from the pivot points of the analysis chamber clamping system, but located on the opposite side of the pivot points. This alternative to the baseline design presented would require a separate signal to the controlling SMA wire to open or close the analysis chamber. There is a potential advantage in that the analysis chamber could be left in either the open or closed position without power to maintain that position. The disadvantage would be increased mass and size of the clamping system, and increased power since both SMA wires would need to be heated to the transition temperature.

For the tests conducted with the MACE Prototype #5 analysis chamber, a manually operated threaded rod was used in place of the SMA wire design of the clamping system for a flight instrument. Manual rotation of the threaded rod controlled the sealing force against the o-rings of the test cell.

Plumbing Schematic

MACE

Gas Analysis Subsystem

Pressure Transducer

Sample Cell of Analysis Chamber (1 of 10)

Sample

Reagent Reservoirs (5 Places)

Reagent Pumps (5 Places)

Upper Portion of Analysis Chamber

Lower Portion of Analysis Chamber

Ion Specific Electrode Sensor Array

Exit to Atmosphere Outside of Instrument Enclosure

Vent Valve

Gas On/Off Valve

Water/Gas Inlet Valve

Drain Valve

Collapsing Bladder

Pressurized Gas

Water Reservoir

NO

C

NC

3-Way Valve

Exit to Atmosphere Outside of Instrument Enclosure

XRF Sump

Vent Valve

LOCKHEED MARTIN

Filename = MACE Rev B Plumbing Schematic 9/12/95 MGT

Figure 8   MACE Plumbing Schematic

Table 4   MACE Mass Properties Summary

MACE Mass Properties Summary

Rev C   12/21/95

Intrument Mass =   2.66   **Kilograms**

		Revision	Mass Each (Grams)	Subsystem Mass (Grams)
A.	**Instrument Case And Structure**			668.59
	1. Instrument Enclosure	A	155.32	
	2. Support Structure	A	60.39	
	3. Insulation/Thermal Control	C	85.26	
	4. Baseplate	A	142.52	
	5. Mounting Legs to Lander	A	19.52	
	6. Internal Wiring Harness	A	19.14	
	7. Spacecraft And Test Connectors	A	186.43	
B.	**Sample Manipulation Subsystem**			1152.04
	1. Sample Inlet System	A	43.80	
	2. Sample Volume Quantitation	A	107.46	
	3. Sample Cone Carousel	A	184.68	
	4. Water Reservoir	C	288.66	
	5. Interconnect Tubing, And Fittings	A	26.36	
	6. Analysis Chamber & Clamping System	C	278.41	
	7. Porous Wheel Particle Dispensers	A	18.15	
	8. Liquid Additive Systems	A	145.52	
	9. XRF Sump System	A	58.99	
C.	**Thermal Control Subsystem**			217.24
	1. EHU #1 Thermal Control	C	81.74	
	2. EHU #2 Thermal Control	C	66.25	
	3. Radiator Thermal Interface	C	59.14	
	4. Electrical Heaters (with Wiring)	A	10.11	
D.	**Electronics Subsystem**			618.33
	1. Sensor Electronics	C	55.00	
	2. Sample Manipulation Control	A	26.00	
	3. Thermal Control Electronics	A	12.03	
	4. Central Electronics Assembly	A	525.31	

Summary of Final Reference Concept

Our final concept includes the following design features and capabilities:

- Provides 10 individual sample test cells mounted on a random access carousel;

- Analysis chamber has all sensors, valves, and micropumps mounted in either the upper or lower portions with a total internal volume of 11cc;

- Clamping system for sealing the analysis chamber to the test cell is automated using shape memory alloy wires;

- Includes a water reservoir with 80ml of water for use in experiments;

- Allows selection of 5 different liquid reagents to be added to the sample in precise quantities;

- Thermal control for the instrument is provided by electric heater units (EHU), a passive radiator and thermal switches;

- Provides 2 porous wheel particle dispensers (PWPD) to allow precise quantities of powders to be added to the sample;

- Random access to liquid and powdered reagents allows experiments with each sample test cell to be customized to take advantage of results from previous analyses;

- Includes sensors to perform the following analyses and measurements, specific gases, temperature, ion specific electrodes, particle sizing, conductivity, pH, and gas quantity/pressure;

- Includes a stirring mechanism for continuous mixing of fluids within the analysis chamber;

- Provides the required interface for analysis of sample fluid residues by an external x-ray fluorescence (XRF) spectrometer,

- To save on mass, instrument volume, and control electronics, only the stirring mechanism and the carousel to rotate the sample test cells use motors, but all other motions are achieved using mechanisms driven by shape memory alloys (SMA).

G. EXPERIMENTS WITH THE PROTOTYPE

Titration Experiments Performed in Atmospheric Pressure (820 mb)

A series of titration experiments was performed using a micro-reaction chamber having a fluid volume of 2 cc. The chamber was configured with commercially available sensors for measuring a variety of solution parameters. The specific sensors included in this suite are listed in Table G-1.

Table G-1. Sensors and Data Acquisition Capabilities in Micro-Reaction Chamber

Reaction Chamber Sensor	Sensor Type	Measurement Range
pH	Solid State micro pH (Model PHM-146, Lazar Research Laboratories)	0 - 14
Chlorine Ion	Solid State Micro Cl⁻ Ion Selective Electrode (Model ISM-146, Lazar Research Laboratories)	2 mM - 2 M Nernst response
Oxidation - Reduction Potential (Redox)	Solid State Micro Redox Electrode (Model ORP-146, Lazar Research Laboratories)	-5000 to + 5000 mV with respect to Reference Electrode
Reference Electrode	Micro Ag/AgCl Reference Electrode (Model MI-402, Microelectrodes Inc)	Reference electrode required for pH, Cl-, and redox electrodes
Electrical Conductivity (EC)	Pt Electrodes in Coaxial configuration, conductivity measured using 10kHz signal	100 - 20,000 μS/cm
Solution Temperature	Pt Resistance Temperature Detector (Pt RTD) (Model 1 Pt 100, Omega Engineering Inc.)	0 - 100°C

The reference electrode used was a commercially available Ag/AgCl electrode manufactured by Microelectrodes Inc. of Londonderry, NH (603) 668-0692. It consists of a small Pt wire that terminates in a silver element. This element is enclosed in 1.9 mm diameter PVC tubing that is filled with 3M KCl electrolyte solution, and terminates with a ceramic frit junction that contacts the solution to be measured. This is necessary for any potentiometric electrode to complete the electrical circuit. It represents one half of the electrochemical cell (a half-cell), with the other half represented by the specific electrode for the desired measurement.

Stirring of the solution was provided by a micro size stir bar (1.5 mm diam x 3 mm length) that was actuated using a laboratory magnetic stirrer. The reaction chamber was positioned on top of this bench model stirrer, and used over the course of each titration experiment.

Titration experiments were performed using a Wilson Greatbatch micro-solenoid pump (Model P650007C) that precisely dispenses a fluid volume of 5.5 μl with each pulse. The pump unit was designed as an implantable medical device for delivering precise quantities of insulin to diabetic patients. It is configured as a cylinder 8 mm diameter by 29 mm length, with inlet and outlet ports in axial and radial directions. The materials that are exposed to the fluid path include Titanium and Titanium alloys, a Cr-Mo Iron alloy, and silicone rubber. These materials were taken into consideration when selecting an acid for use in the titration experiments. It was found that titanium is fairly resistant to oxidizing

acids such as Nitric acid (HNO_3) and Perchloric acid ($HClO_4$). All experimental titrations were performed using 10.0 Molar HNO_3 as the titration reagent.

Interface circuitry was developed for all sensors listed above, as well as a circuit to allow the titration pump to be actuated under computer control for calibration and titration functions. The sensors all require a slightly different interface, but some share common characteristics. The potentiometric ion sensors (pH, Cl⁻, redox) all require a very high impedance amplifier to measure the voltage signal generated. This high impedance is characteristic of this type of sensor, but the small physical size of the sensors increases the characteristic impedance even higher. A dual JFET/Operational Amplifier circuit was designed to provide an input impedance of greater than $10^{14} \Omega$ to accurately measure the potentiometric signal generated by this type of sensor.

The temperature sensor changes in electrical resistance with temperature, and is measured by reading the voltage produced by a constant current through the sensor. A commercial module that produces a voltage proportional to the sensor resistance was used to perform this measurement.

The aqueous conductivity measurement was performed using a custom built circuit that operates by generating a 10kHz signal on the inner electrode of the coaxial sensor element, then receives the signal on the outer element. The received signal is amplified and rectified to produce an analog voltage that is related to the conductivity of the aqueous solution. The sensor was found to respond over three decades in solution conductivity, as measured using standard KCl solutions.

Each of the sensors was calibrated using standard solutions and analytical grade reagents. The conductivity sensor was calibrated using dilutions of a standard 2.0M KCl solution, with the conductivity value derived from tables in the Chemical Rubber Company (CRC) handbook. The pH sensor was calibrated using 3 standard laboratory solutions (pH 4, 7, and 10), and generating a linear regression fit to the resulting sensor output data.

Software was written using LabVIEW, a graphical instrument control application, to acquire data and control instrument functions. Figure G-1 shows the main control panel used to perform titration experiments. The upper portion shows all the user selectable file disposition options and displays current sensor readings in numerical format. The controls allow sensor data to be acquired at user defined intervals and enable the titration pump for performing the analyses. The lower portion of the is a strip chart to display trends in the acquired data, in this case showing the pH and conductivity sensor outputs.
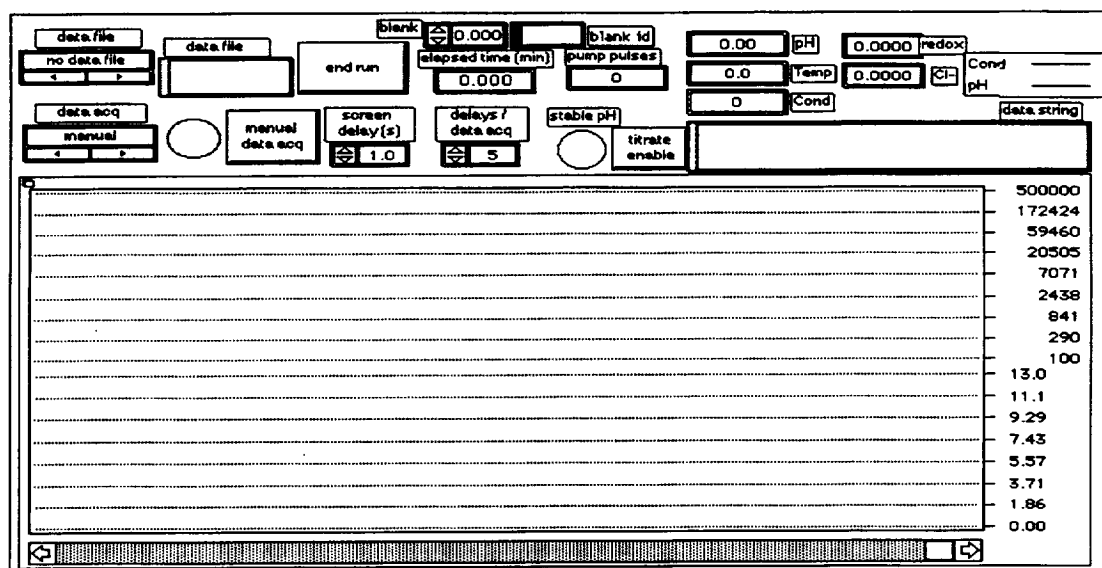
Figure G-1.   Titration Experiment Control Panel

Routines were written to acquire data from the sensors in terms of raw voltages, and incorporate calibration factors to produce data in units appropriate for each sensor. This data is recorded in a data file for each titration experiment for later analysis and presentation.

Software algorithms routines were also written to control and document the titration pump activity. The "enable titration" control button on the front panel allows execution of the program segment that controls the titration pump. The algorithm that drives the pump is "smart" in the sense that prior data is taken into account to determine how many pump pulses to command for the current titration reagent addition event. The prior pH data is compared with the current pH level, and the difference between the two is used to calculate the titration reagent addition amount. This closed loop algorithm has a user settable gain as an input value, allowing the titration analysis to be optimized using various samples. The titration algorithm also includes a module for computing the moving average of the time-varying pH. This moving average is used to lock out the addition of more titration reagent during the transient period after an amount of acid has been added, until steady state conditions in terms of pH have been reestablished.

A series of titration experiments were performed using analytical grade carbonate reagents to determine the titration characteristics of the MACE instrument. This set of experiments were all carried out in ambient pressure (~820 mbar) with no capability to sense the evolved gas. The micro reaction chamber and aqueous sensors described above were used in conjunction with the solenoid driven micropump to add the titration reagent (10 molar Nitric acid) to stirred solutions containing the carbonate materials. The amount of material was measured using a volumetric aliquot equivalent to that anticipated in the MACE instrument. This sample volume is a cylinder of 7 mm diameter by 8 mm length (~0.3 cc). The powdered carbonate material was measured using this volume with no tamping or shaking to settle the granules. This measured volume of material was then put into the micro reaction chamber and stirred using the micro stir bar setup described above. The transients associated with dissolution of the sample material were measured using the sensors in the chamber (temperature, conductivity, and pH), allowed to reach a steady state value, and then the titration reagent addition was enabled. The titration was allowed to proceed until the pH reached a value of about 2.0, at which time the experiment was ended.

G-3

The algorithm that controls the titration addition amount was optimized in terms of the data acquisition rate, the gain associated with the change in pH relative to the titration reagent (acid) addition, and the size of the moving average used to determine when the pH had reached a steady state level. The optimal data acquisition rate was one time per second, the acid addition gain was 20 relative to the change in pH from the prior steady state value to compute the number of pump pulses commanded for the current addition. The moving average size used was 30 to determine when steady state conditions existed. When the current pH value was within 1% of the moving average value, steady state was assumed and the titration algorithm was used to compute next acid addition amount.

Figure G-2 shows a typical titration analysis for $MgCO_3$, where the data is shown as a function of time for the solution pH and the amount of titration reagent added via the titration micropump.
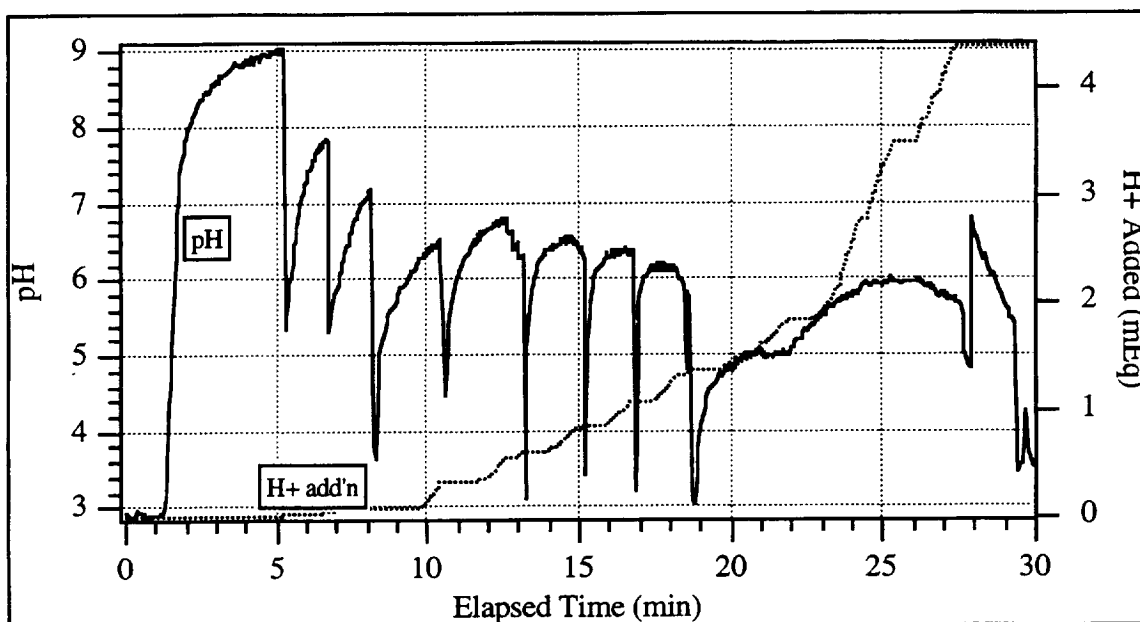
Figure G-2 Titration Experiment for 100 mg $MgCO_3$ Titrated with 10 M HNO_3 Showing pH and Acid Addition Profiles as a Function of Time.

The oscillating behavior of the pH signal is due to mixing effects of the acid as it is added to the reaction chamber. There is some time required to effectively mix the acid and allow the reaction to proceed. In this case the reaction evolved carbon dioxide gas, and fizzing of the aqueous solution was observed in each of the periods of pH oscillation. In this titration, the solution remained cloudy until about 18 minutes elapsed time, at which time the solution cleared and looked remarkably like seltzer water. After this point there were no more large pH transients with acid addition, and no more significant gas evolution.

The other sensors present in the reaction chamber were also monitored during the titration, and are shown as a function of time in Figure G-3.
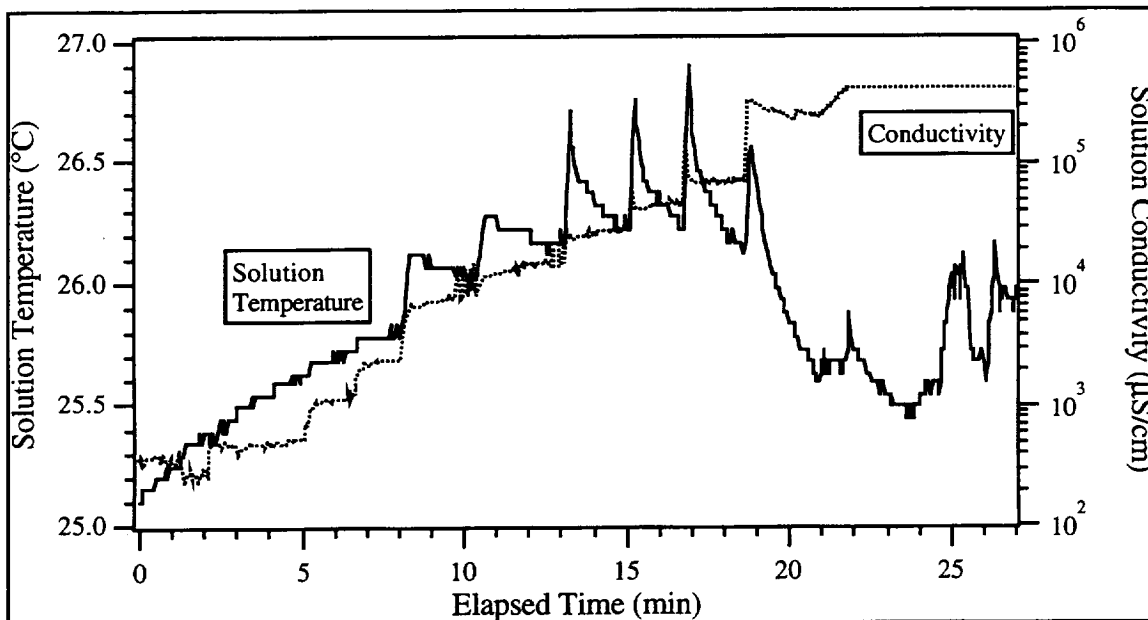
Figure G-3   Time Profiles of Solution Temperature and Electrical Conductivity during 100 mg $MgCO_3$ Titration with 10 M HNO_3.

The temperature transients seen in this figure correspond to acid addition events in the titration. The temperature change is caused by the heat of dissolution of the acid in water. The increasing solution conductivity is caused by Mg^{++} ions dissolving into solution as a result of the acid hydrolysis of the carbonate salt. The carbonate is dissolved in solution until saturation occurs, then is converted to carbon dioxide gas that bubbles out as evolved gas. If this experiment had utilized a sealed reaction chamber volume and associated gas pressure transducer, as will be done in the flight experiment, the pressure data would follow the conductivity trace.

The amount of carbonate material present in the sample volume of this magnesium salt (100 mg) is 1.19 mEq, and should require a corresponding mEq of acid to decompose all the carbonate into carbonate ions in solution, and eventually as evolved CO_2 gas. This forms the basis of the titration analysis technique, that is, the amount of acid required to produce an inflection point in the pH sensor is equal to the amount of material being titrated. The concentration (mEq/ml) of the titrating acid is known very well, and a volumetric measure of the acid introduced into the reaction chamber (pump pulses) to produce a pH inflection in conjunction with the known acid concentration gives measure of the amount of material in the sample being titrated. In the MACE instrument, the sample mass is known to ±30%, but the ionic equivalents will be measured to a much higher accuracy.

Figure G-4 shows the same data from the MgCO3 titration experiment, but plotted as a function of mEq of acid added to the reaction chamber. The plot shows the data from the pH electrode and conductivity cell as a function of added acid. The large spikes seen at various intervals correspond to an acid addition event, where the solution pH goes through a wide swing as the acid reacts with the sample material. This behavior is typical of titration analyses, and the instrument software is designed to wait until a pH stasis has been attained after an acid addition event.
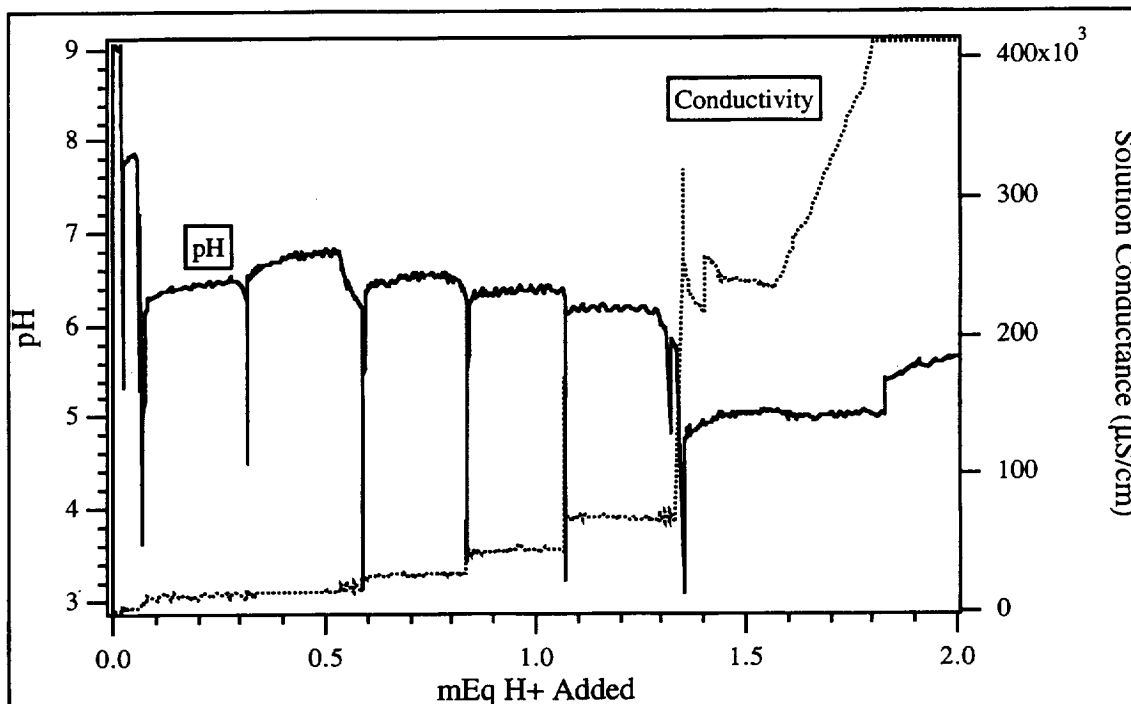
Figure G-4.   Acid Addition Profile of 100 mg $MgCO_3$ Titrated with 10 M HNO_3.

The titration endpoint is seen at an acid addition of ~1.35 mEq, when the pH undergoes an abrupt change, and the solution conductivity increases dramatically. This corresponds to all the sample material being decomposed into constituent ions, with the carbonate released as evolved CO2, and the Mg++ ions dissolving in solution, increasing the solution electrical conductivity.

Figure G-5 exhibits data from the other sensors in the reaction chamber, showing the oxidation - reduction potential and solution temperature as a function of acid addition. The spikes on the temperature trace show the heat of solution of the Nitric acid as it is added, and the oxidation - reduction potential clearly shows the titration end point. This change in redox potential corresponds to a net reduction of the solution components, going from a more oxidized state initially to a more reduced state after acid decomposition.
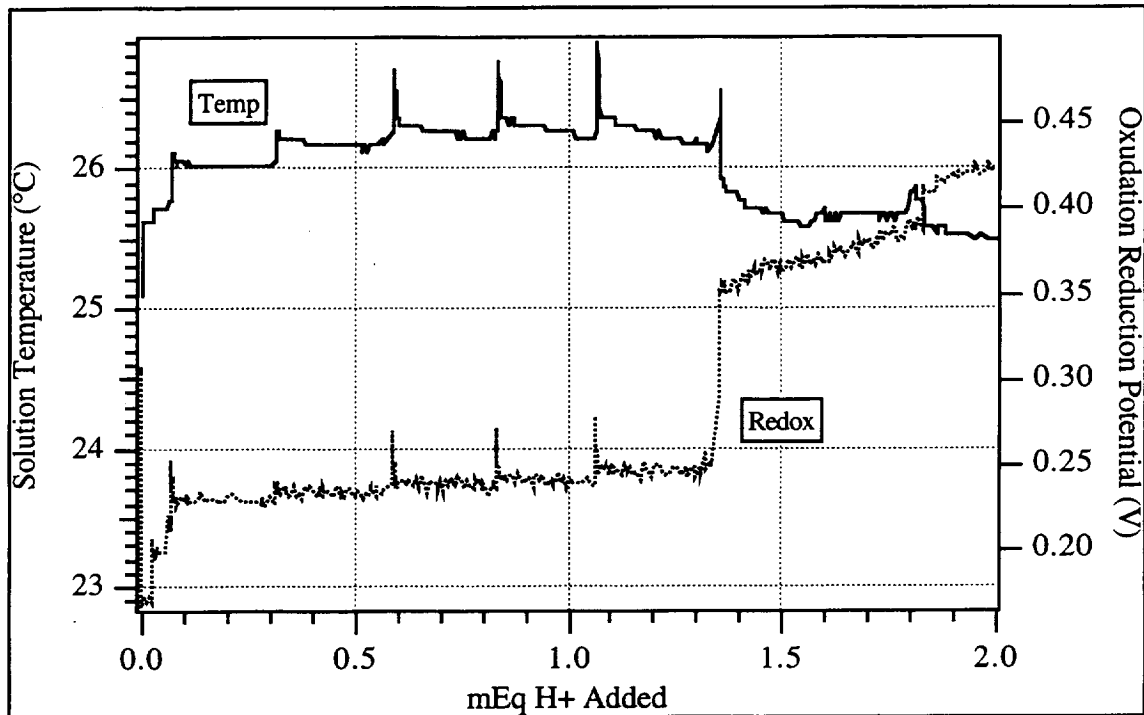
Figure G-5.   Acid Addition Profile for 100 mg $MgCO_3$, in Terms of Oxidation-Reduction Potential and Solution Temperature

A series of carbonate materials (analytical reagents and regolith simulations) were subjected to titration analysis using this reaction chamber and associated sensors. The data from these experiments is shown in the following figures, and summarized in Table G-2.

Table G-2.   MACE (1 Atm) Titration Experiments Summary

Sample	Mass (mg)	Actual mEq	Titration mEq	Inflection pH
K_2CO_3	420	3.04	4.2	6.8
Na_2CO_3	380	3.59	5.4	7.8
$CaCO_3$	170	1.7	2.4	6.4
K_2CO_3	110	0.8	2.0	6.6
+ $MgCO_3$	100	1.2	1.25	9.5
Travertine	130	?	1.78	6.0

On pages G-8 through G-15 which follow, are included selected examples of additional data taken during these experiments.
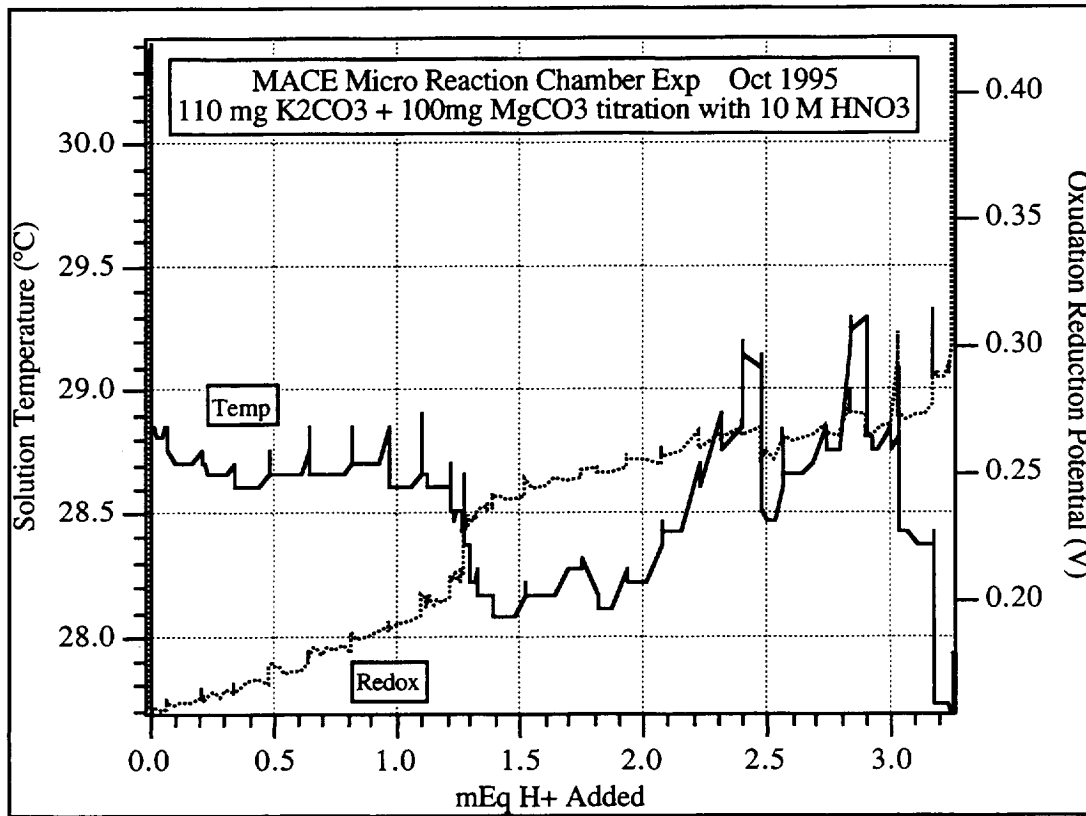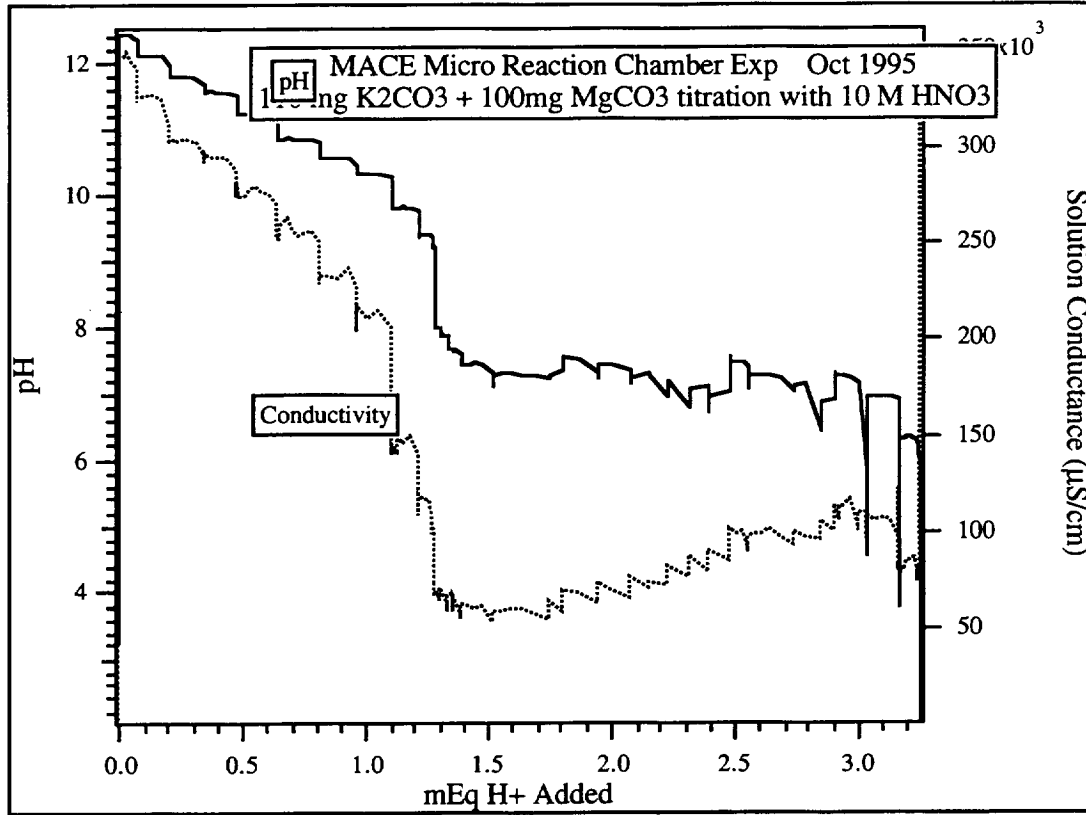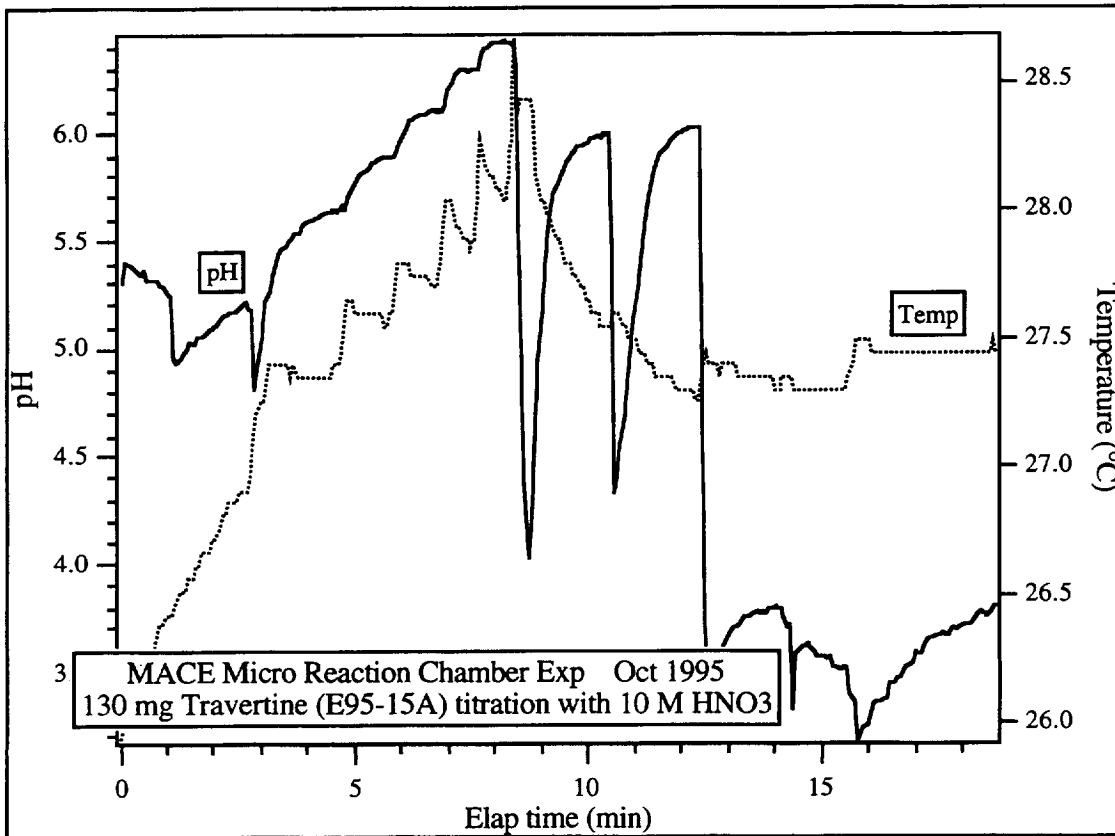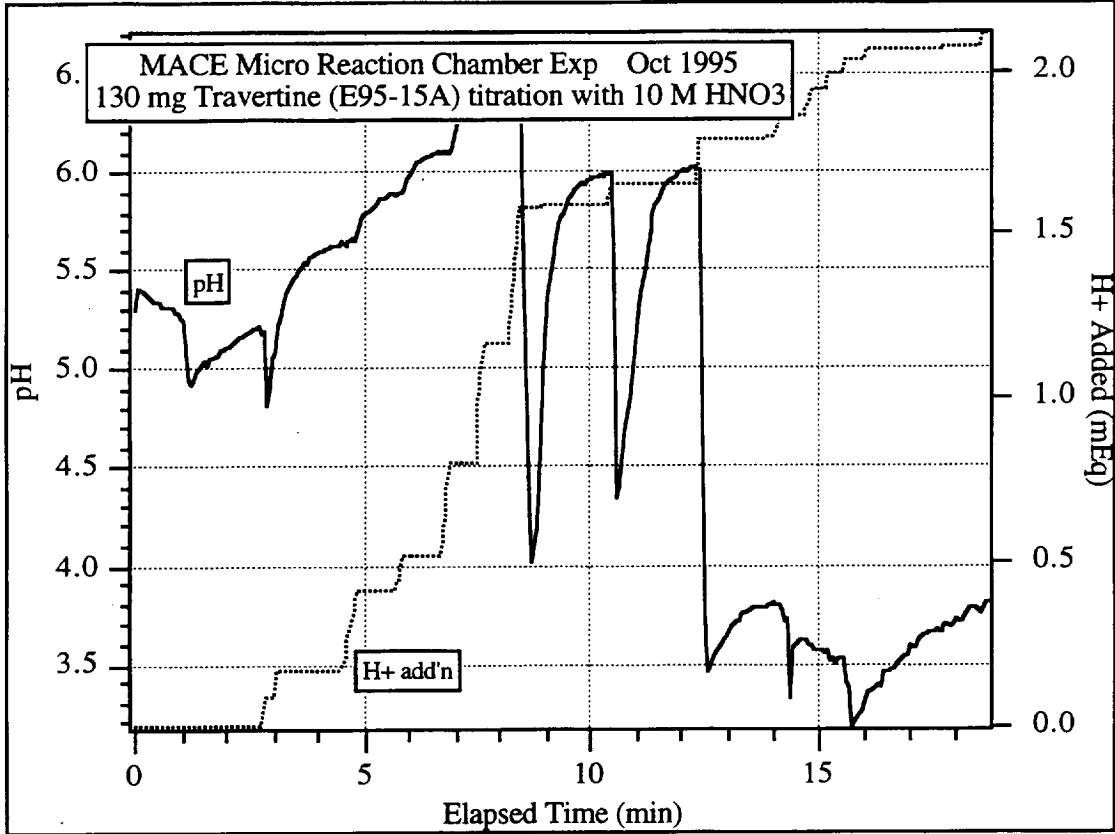
MACE Micro Reaction Chamber Exp   Oct 1995
420 mg K2CO3 titration with 10 M HNO3

pH

H+ add'n

H+ Added (mEq)

Elapsed Time (min)

MACE Micro Reaction Chamber Exp   Oct 1995
420 mg K2CO3 titration with 10 M HNO3

pH

Temp

pH

Temperature (°C)

Elap time (min)

MACE Micro Reaction Chamber Exp   Oct 1995
420 mg K2CO3 titration with 10 M HNO3

MACE Micro Reaction Chamber Exp   Oct 1995
420 mg K2CO3 titration with 10 M HNO3

MACE Micro Reaction Chamber Exp   Oct 1995
380 mg Na2CO3 titration with 10 M HNO3

MACE Micro Reaction Chamber Exp   Oct 1995
380 mg Na2CO3 titration with 10 M HNO3

MACE Micro Reaction Chamber Exp   Oct 1995
380 mg Na2CO3 titration with 10 M HNO3

MACE Micro Reaction Chamber Exp   Oct 1995
380 mg Na2CO3 titration with 10 M HNO3

G-11

MACE Micro Reaction Chamber Exp   Oct 1995
110 mg K2CO3 + 100mg MgCO3 titration with 10 M HNO3

MACE Micro Reaction Chamber Exp   Oct 1995
110 mg K2CO3 + 100mg MgCO3 titration with 10 M HNO3

MACE Micro Reaction Chamber Exp   Oct 1995
110 mg K2CO3 + 100mg MgCO3 titration with 10 M HNO3

MACE Micro Reaction Chamber Exp   Oct 1995
110 mg K2CO3 + 100mg MgCO3 titration with 10 M HNO3

G-13

MACE Micro Reaction Chamber Exp   Oct 1995
130 mg Travertine (E95-15A) titration with 10 M HNO3

pH

H+ add'n

Elapsed Time (min)

MACE Micro Reaction Chamber Exp   Oct 1995
130 mg Travertine (E95-15A) titration with 10 M HNO3

pH

Temp

Elap time (min)

MACE Micro Reaction Chamber Exp   Oct 1995
130 mg Travertine (E95-15A) titration with 10 M HNO3

MACE Micro Reaction Chamber Exp   Oct 1995
130 mg Travertine (E95-15A) titration with 10 M HNO3

Reduced Pressure Titration Experiments

The next generation of MACE was designed and fabricated, termed MACE Prototype 5. The apparatus is designed to perform titrations in reduced the pressure environment on Mars. The prototype has a micro-reaction chamber that is complete with electrical conductivity sensors (EC), a pH and Mg^{++} ISE with a specially designed miniature reference electrode, a gas pressure sensor, a thermistor to measure solution temperature, and a stirring motor for the solution. The reaction chamber volume is ~2 cc, and measures 1.5 inches diameter. It includes valving for the analysis water inlet, sump outlet, gas headspace volume outlet, and the acid micropump to enable titration. Figure G-6 shows a picture of the polycarbonate reaction chamber alone, with the various sensors and valves attached around the periphery.
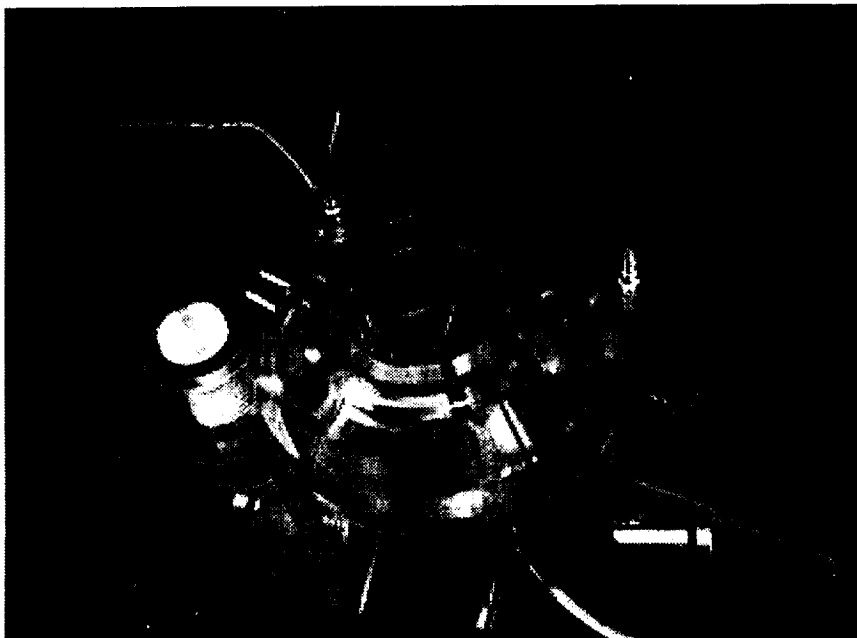
Figure G-6.   MACE Prototype 5 Miniature Reaction Chamber and Associated Sensors

The sensors shown are (from 12:00 position clockwise):

        (2 o'clock) Analysis water inlet valve from water reservoir
        (3 o'clock) Miniature pH electrode
        (5 o'clock) Magnesium Ion Selective Electrode (ISE)
        (6 o'clock) Reaction chamber drain tube to sump
        (9 o'clock) Reference electrode for pH and Mg ISE
        (10 o'clock) Acid addition micropump

The reaction chamber is common to all analyses performed in MACE. The upper surface of the reaction chamber seals to each of the individual sample cells during an analysis. Each sample cell includes a filter cone that keeps the insoluble particulates out of the reaction chamber to avoid cross contamination between sample analyses, and allows only soluble compounds to enter the sump.

The reaction chamber is mounted within MACE to enable analysis of multiple samples. The sample manipulation is performed by a carousel that rotates each sample cell into position. The MACE Prototype 5 has two sample cells, and is shown in Figure G-7.
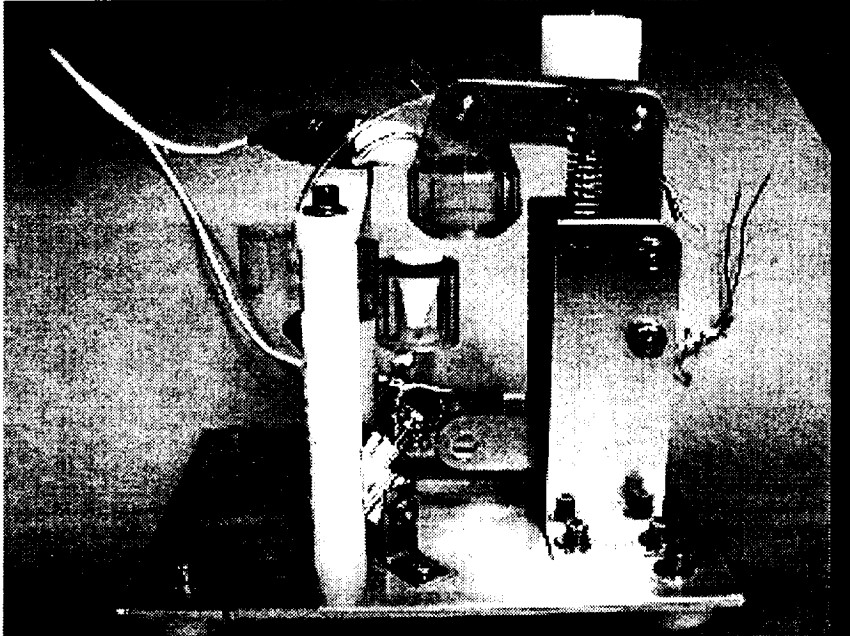
Figure G-7. MACE Prototype 5 without Reaction Chamber

The clamping mechanism shown is used to seal the reaction chamber to a sample cell to perform analysis. O-rings are used between the upper and lower sealing surfaces of the sample cell to provide a hermetic seal. The figure shows the miniature gas pressure sensor (top) and stirring motor (lower left) used to mix the solution during an analysis.

A worst case analysis was calculated to determine the magnitude of gas pressure that could build up in the gas headspace for several different volumes. The worst case assumed was a pure carbonate sample that evolves quantitatively and very rapidly. Table G-3 shows the magnitude of the pressure for a series of headspace volumes.

Table G-3. Worst Case Gas Evolution Pressures
(Sample = 0.95 g, 11.2 mEq 100% $MgCO_3$ Carbonate Rock)

Volume (cc)	Max Pressure (bar)
1	9.30
5	1.87
10	0.929
20	0.472
50	0.193
75	0.131
90	0.110
100	0.100

A gas handling system was designed to monitor the gas evolved from acid hydrolysis of the regolith sample. The system includes valving to exhaust the evolved gas if the pressure gets too high. Figure G-8 shows the schematic diagram for this system. All of these valves are under manual control in the MACE Prototype 5 system.
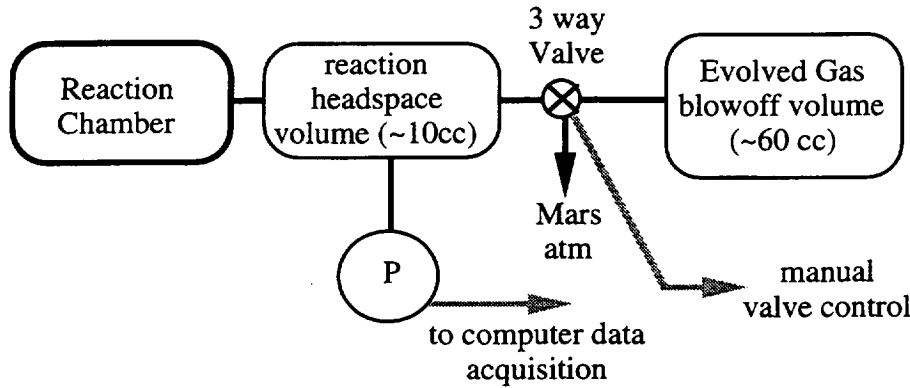
Figure G-8.   MACE Prototype 5 Gas Handling System

The MACE Prototype 5 instrument was used to perform experiments in the reduced pressure environment of a vacuum chamber, pumped down to Mars atmospheric pressure (~7 mbar). These experiments were performed to conceptually prove the MACE instrument concept in a reduced pressure environment. The regolith sample was manually loaded and sealed into the sample cell. All other instrument functions were performed remotely from outside the vacuum chamber, or automatically under computer control. Each experiment consisted of a complete end-to-end analysis in reduced pressure, including transfer of water from the reservoir to the reaction chamber, stirring of the analysis solution, data acquisition from all included sensors, and automatic titration. The regolith samples used for these experiments were metered into the sample cell using the MACE volumetric sample measure (a cylinder 7 mm diameter x 8 mm length), then weighed using an analytical balance. The titration reagent used was 10M Nitric acid (HNO_3).

The titration and pressure data from a reduced pressure experiment that analyzed a 1% carbonate rock sample is shown in Figure G-9. The regolith sample defined by the MACE metering volume (without packing) weighed 270 mg. The experiment shown used a sample of simulated regolith material that contained by weight:

       1% carbonate rock (Travertine tufa, mostly $CaCO_3$),
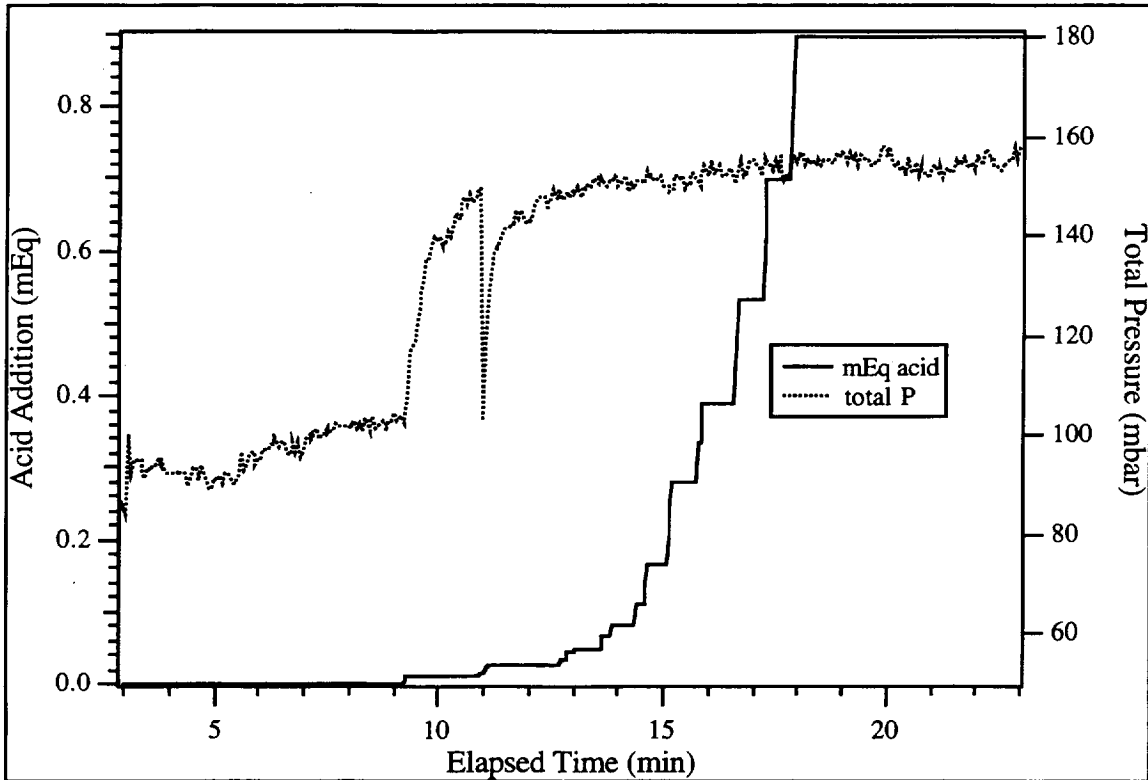   0.5% NaCl (analytical reagent)
       98.5% ground sand.

Figure G-9. Titration and Evolved Gas Pressure Data from 1% Carbonate Rock Reduced Pressure Analysis, Titrated with 10.0 M Nitric Acid

The Travertine rock in this sample is nearly pure calcium carbonate, as seen in Figure G-10, an x-ray fluorescence emission spectrum taking in our laboratory. This represents 0.03 mEq of carbonate material, or 0.03 millimoles of carbon dioxide evolved upon decomposition. This correlates fairly well with the titration data shown in the figure, where after the initial acid addition of ~0.02 mEq, no further change in the headspace pressure is seen. The change in reaction chamber headspace pressure (from 100 to 150 mbar) reflects the fact that the CO_2 evolved from the carbonate decomposition (acid hydrolysis), and is a measure of the total amount of carbonate material present. The transient spike seen after the initial pressure rise is from manually venting the reaction chamber headspace into the blowoff volume. Assuming a volume of 10 cc for the headspace volume, room temperature, and a pressure change of 50 mbar, the ideal gas equation can be used to solve for the original amount of carbonate material:
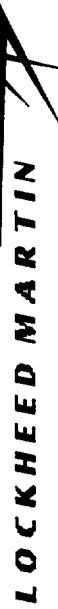
$$n = PV/RT$$

where P = the change in pressure upon decomposition (mbar)
         V = headspace volume (cc)
         n = number of moles of carbonate material (or molar equivalents, Eq)

IBJ XRF

IBJ080 E95-15A Travertine
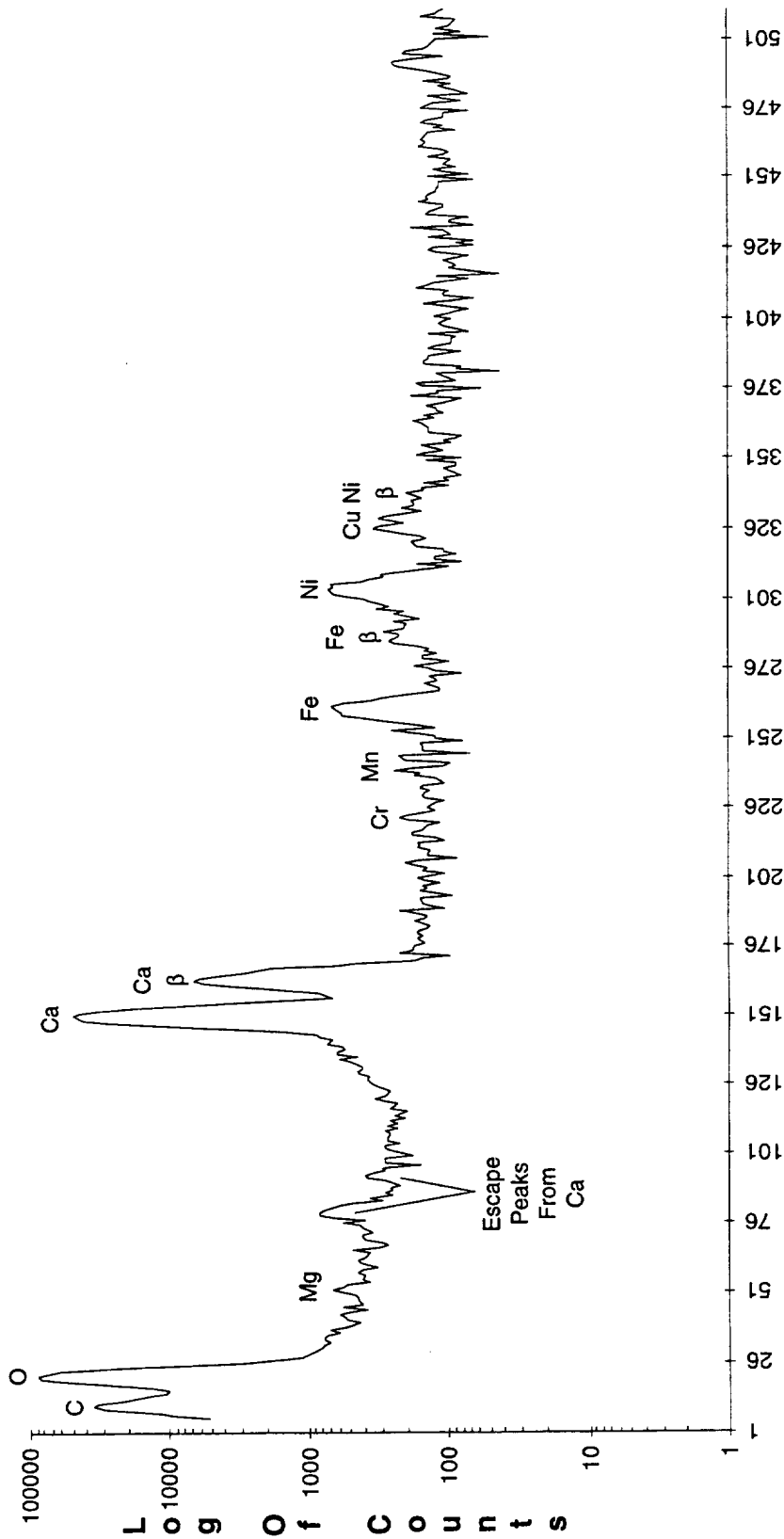
Spectrum shows 0 to 12.59 keV = 24.59 eV per Channel

Channel Number

LOCKHEED MARTIN

Excitation Source = 244Cm 1.8mCi Radioisotope Source
Live Time =7,200 Seconds Total Counts = 142,440
Spectral data has been normalized to 1 million counts

Filename = Draw IBJ080 E95-15A Travertine 6/29/95 MGT

Figure G-10. X-Ray Fluorescence Spectrum of Travertine Sample

R = ideal gas constant (mbar•cc/gmol•K)
T = temperature (K)

Solving this equation, the number of moles of carbonate is 0.02 millimoles, in very good agreement with the acid titration data, and reasonable agreement with the sample composition.

The titration sensitivity could be increased by lowering the concentration of the titrating acid. This has the effect of decreasing the milli-equivalents of acid per pulse of the titration pump, requiring more pulses for a given titration. Increasing the pulses required for a titration increases the resolution of the addition, but more volume of titration reagent must be used, and carried along with the instrument.

Table G-4 shows a parametric listing of the acid titration requirements for the worst case scenario of 100% MgCO3 carbonate rock. The analysis is assumed to proceed past the titration end point, and the total volume of acid required for the titration is 120% of the number of mEq present in the sample. The effective titration resolution is shown in the right hand column, where the mEq of acid per pump pulse is listed. The titrations shown here used 10 M Nitric acid as the stock solution.

Table G-4. Worst Case Titration Parametrics
(Sample = 0.95 g, 11.2 mEq 100% MgCO$_3$ Carbonate Rock)

Nitric Acid stock sol'n (M) or (mEq/ml)	ml for 120% of sample mEq	# of 0.5 µl pump pulses	mEq H+ per pulse
2	6.705	12190	0.0011
3	4.470	8127	0.0017
4	3.352	6095	0.0022
5	2.682	4876	0.0028
6	2.235	4063	0.0033
7	1.916	3483	0.0039
8	1.676	3048	0.0044
9	1.490	2709	0.0050
10	1.341	2438	0.0055
11	1.219	2216	0.0061
12	1.117	2032	0.0066
13	1.031	1875	0.0072
14	0.958	1741	0.0077
15	0.894	1625	0.0083
15.9	0.843	1533	0.0087

Data acquired from the electrical conductivity and solution temperature sensors during the initial dissolution and acid addition in this analysis is shown in Figure G-11. Both sensors clearly detected the carbonate dissolution/decompostion process.
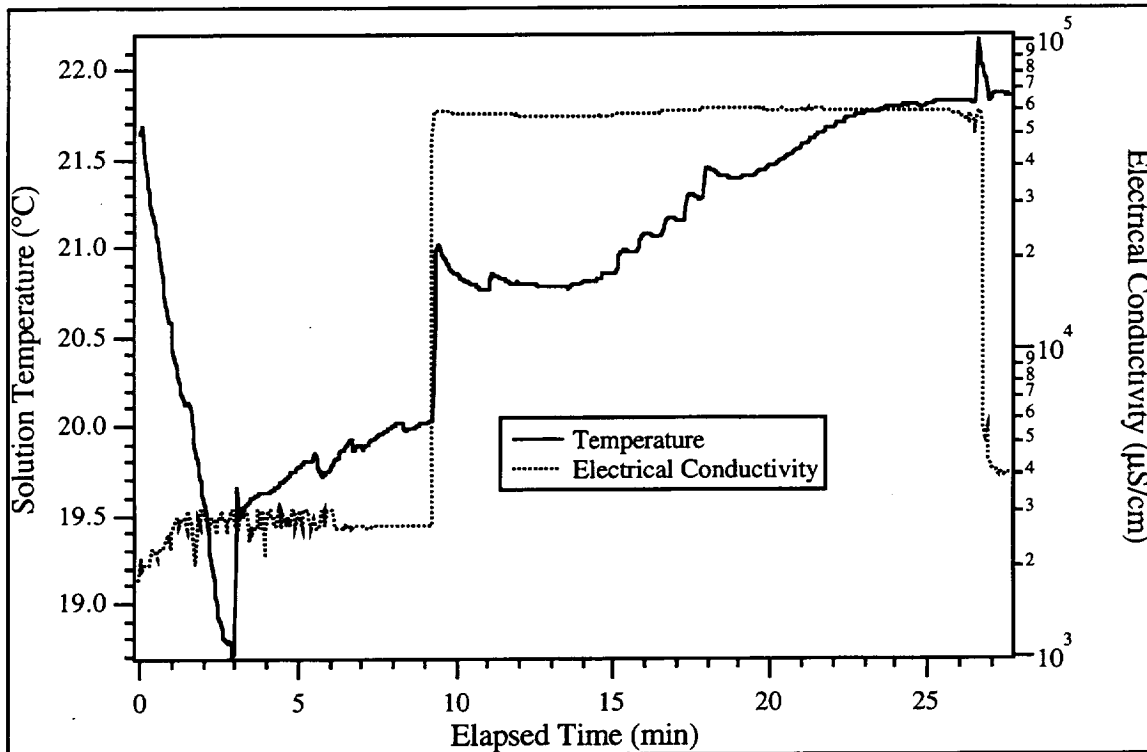

Figure G-11. Electrical Conductivity and Solution Temperature Data From 1% Carbonate Rock Titration in Reduced Pressure

The enthalpy change associated with the regolith heat of solution is clearly evident, and the heat of solution from the acid addition events are also seen. The large transient that occurs at elapsed time of 10 minutes is associated with the titration end point, and the associated carbonate decomposition/gas evolution. The electrical conductivity data also clearly show the titration end point. The calcium ions dissolving into solution increase the conductivity at the same time as the carbonate evolves as CO_2.

A regolith sample consisting of 240 mg of 20% Potassium carbonate (K_2CO_3) and 80% ground sand was also analyzed under reduced pressure conditions. In contrast to calcium carbonate, potassium carbonate is fully soluble in water before any acid is added. The titration curve and headspace pressure data for this analysis are shown in Figure G-12.
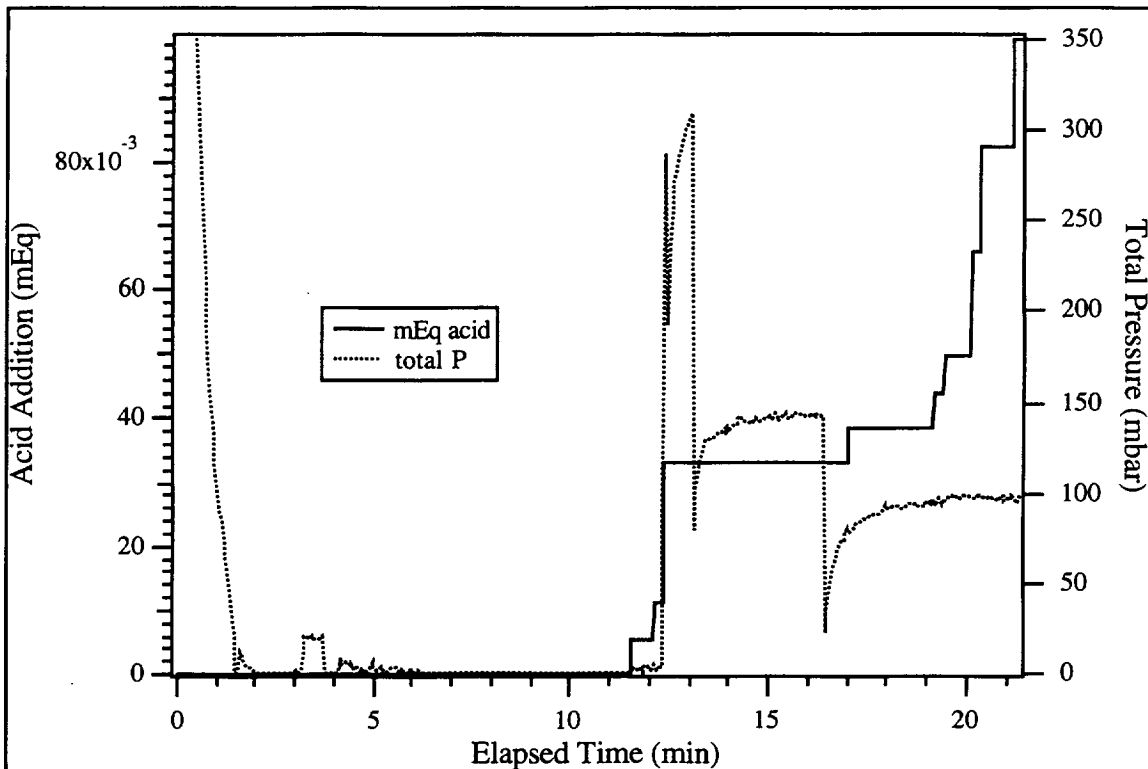
Figure G-12.   Reduced Pressure Titration Analysis Data for 20% Potassium Carbonate + 80% Ground Sand

The initial pressure decrease shown before 2 minutes elapsed time is the chamber pumpdown with dry regolith sample in the sample cell. The analysis water was added at about 3 minutes elapsed time. The small pressure peaks at this time are probably associated with dissolved carbonate ions decomposing to carbon dioxide and evolving as gas under the reduced pressure environment. The acid addition begins at 11.5 minutes, with the titration endpoint reached at the large gas evolution event at ~12.3 minutes. The titration endpoint of this analysis is about 11 mEq; after this point additional acid has no effect on gas evolution. The pressure decrease transients are due to manually actuating the gas evolution valve and venting the evolved gas into the blowoff volume and to atmosphere to protect the instrument from possible damage. This large pressure inside the reaction chamber had the effect of forcing open the reaction chamber drain valve, and venting some of the analysis solution to the inside of the vacuum chamber. For this reason the results shown here are not quantitative; the titration end point does not represent the quantity of carbonate material present in the sample. The instrument designed to analyze samples on the Martian surface will include a robust design that insures that large gas evolution pressure transients do not adversely affect the performance of the instrument.

Particle Settling Experiments

The final experiment planned for the MACE instrument is a unique cell that is specially configured to monitor the settling kinetics of insoluble particles to determine the particle size distribution. This final experimental cell is different from all others in that it does not have a filter, and is configured with a small laser to provide incident light, and a photodetector positioned at 90° from the incident light to monitor the scattered light as a function of time. Figure G-13 shows a schematic diagram of the experimental cell.

TOP VIEW   SIDE VIEW
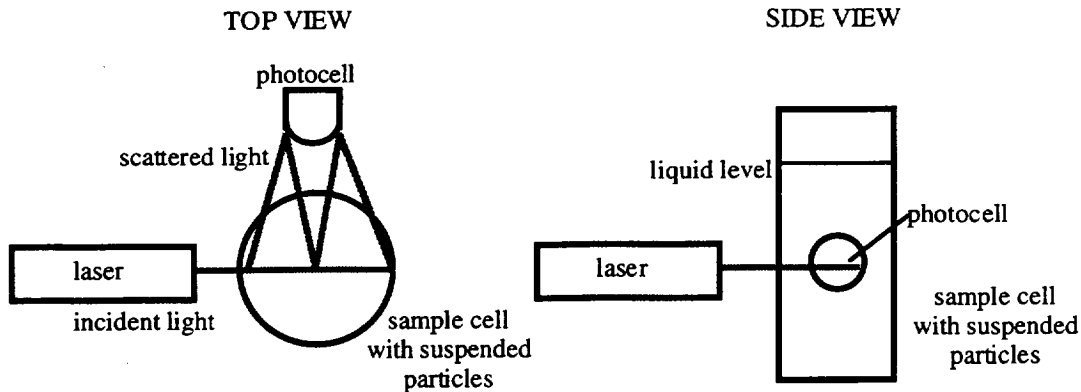
Figure G-13.   Schematic Diagram of the MACE Particle Settling Cell

An experimental setup of this type was developed to perform experiments and gather data from the particle light scattering setup. A polycarbonate optical cuvette was modified with a mask to minimize external light effects, and fitted to a laboratory stirrer. Two silicon photodiodes were interfaced to the controlling computer through an operational amplifier circuit to provide a voltage signal (0 to -5 volts) proportional to the light incident on the photodiodes. Software was written to acquire the signal data from the sensors, and to measure the time intervals and temperature during the course of each particle settling experiment. The settling kinetics of various particles with differing size distributions were measured using this setup.

A protocol was developed for consistency in experimental data taking and results. Before a sample was placed onto the cuvette for analysis, it was weighed and the density determined using volumetric displacement in a volumetric flask. This step was not performed if the density of a sample was known from literature or from vendor provided information. An amount of sample for use in the experiments was weighed out using an analytical balance and transferred to the cuvette for analysis. Deionized water (the settling fluid) was added to the cuvette until it was about 2/3 full (about 2 ml), and a micro-sized stir bar added to enable stirring. Parafilm was used to seal the cuvette top to insure that no water evaporated during the course of an experiment. The cuvette was placed on top of the stirrer and positioned so that the laser and photodiodes were in the appropriate geometry shown above. Precise dimensional measurements were then taken to record the position of the laser beam with respect to the cuvette position and internal fluid level. These data were used in developing the analytical model to reconstruct the size distribution from the light scattering data.

To initiate an experiment, the computer was first enabled to collect data, then a box was placed over the experiment to eliminate interference from stray light. A small hole in the side allowed the laser light to enter. The photodiode signals that correspond to the zero suspended particles condition were recorded. The box was then removed and the stirrer was turned on until the particles formed a homogeneous suspension within the DI water. When the stirrer began spinning, the particles initially formed a small cloud around the stir

bar. The cloud grew until it reached the laser beam, and scattered laser light filled the cuvette. After a few minutes the particles formed a homogenous suspension within the fluid. The box was replaced and the stirrer turned off, with the experiment elapsed shutoff time recorded. Data was collected until the photodiode signal was equivalent to that before the stirrer was turned on. Multiple experiments of this type were performed on each sample to determine the experimental repeatability and variance associated with this technique.

The initial proof of concept experiments were performed using "ground sand" from the geological samples collection in the Planetary Sciences Lab. It represents sand that has an unknown size distribution typical of that found on earth. Figure G-14 shows the raw data collected in this experiment. The large transient at the beginning of the experiment is where the stirring bar was actuated and the transmitted light slewed from 100% transmission to maximum occlusion, and the scattered light transitioned from 0% scattering to its maximum value. This is the value where the interface circuit saturated, maximum signal. As expected, the scattered light intensity is lower than the transmitted light intensity.
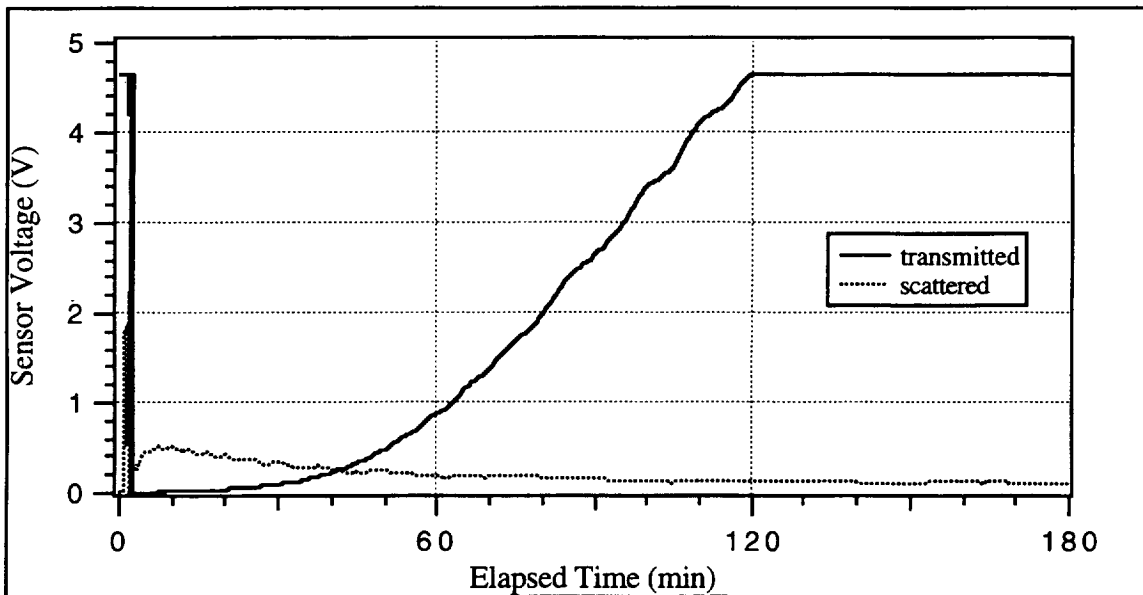
Figure G-14. Raw light scattering data from 100 mg "ground sand" in 2 ml H2O

The two photocells used in these experiments measured scattered light at 90° and transmitted light at 180°. The transmitted light reached maximum value after about 2 hours, and provided relatively little information about the particle settling dynamics. Data from the scattered light sensor , however, showed more structure and dynamic composition during the settling process. The scattering data showed signal well after 5 hours of experiment elapsed time. This is illustrated in Figure G-15, where the ratio of the scattered and transmitted light normalized to the zero particle value is plotted.
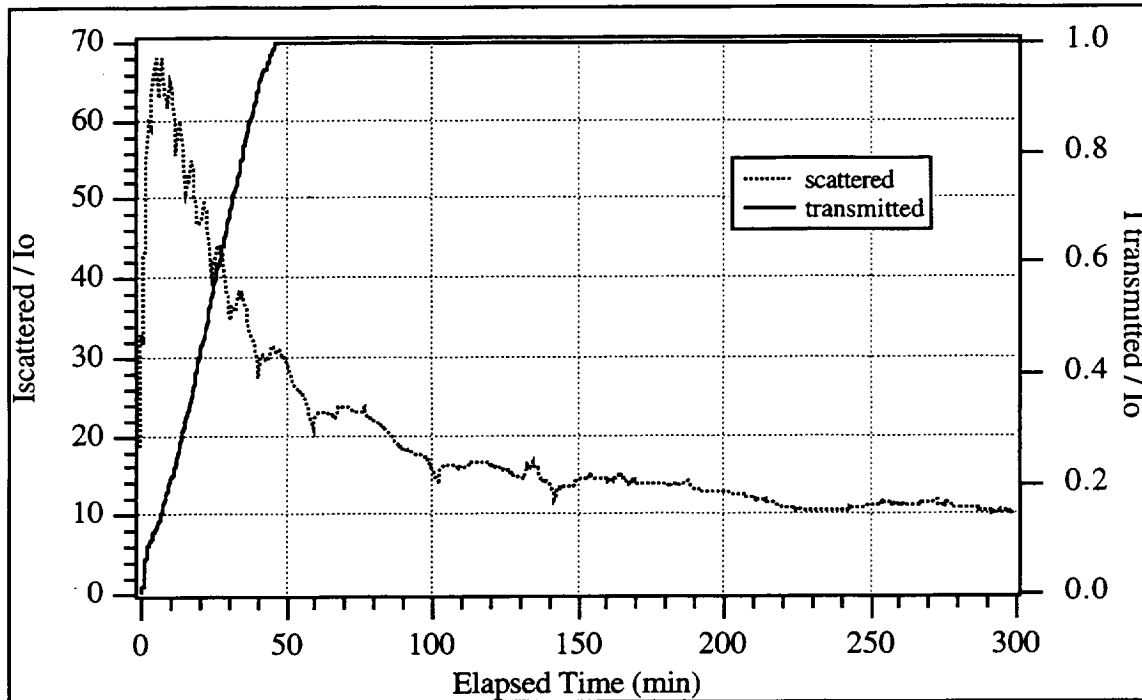
Figure G-15.   Kinetic Profiles of Light Intensity Ratios, (Iscat and Itrans) Normalized to Zero

This method of measuring particle size distribution has some inherent biases. The overall method sensitivity is limited by the total number of particles suspended, the time they are suspended for, and the extent to which multiple scattering occurs. The transmitted light has highest sensitivity to large particles, but large particles settle out faster. The experiment is initiated by turning off the stirring mechanism, but some momentum from the swirling action continues for some minutes after the stirring action stops. This has the effect of keeping the larger particles suspended for longer time periods than would otherwise occur, biasing the results. The faster settling time for larger particles limits the number of data points that can be acquired during the settling time. Alternatively, the scattered light shows highest sensitivity for smaller particles because of higher total particle numbers. Smaller particles also remain suspended for longer periods of time, increasing the total number of associated data points, and sensitivity. The data show that the data from the scattered light sensor is of higher fidelity than the transmitted light.

For these reasons the sensitivity of this method is highest for smaller particles. This will be especially true in a reduced gravity environment, where the magnitude of the settling forces is lower, and the associated settling times are greater. For these reasons the MACE instrument particle size distribution cell need have only one photodiode to measure the particle settling profile.

The initial results showed that the method had promise, so additional experiments were performed to further characterize the technique. Glass microspheres having a known size distribution were procured and subjected to analysis using this method. Three different size distributions were tested: <20 μm, 45-54 μm, and 90-106 μm. Each experiment was performed multiple times to determine the repeatability and variability. Figure G-16 shows the raw data typical of these experiments.
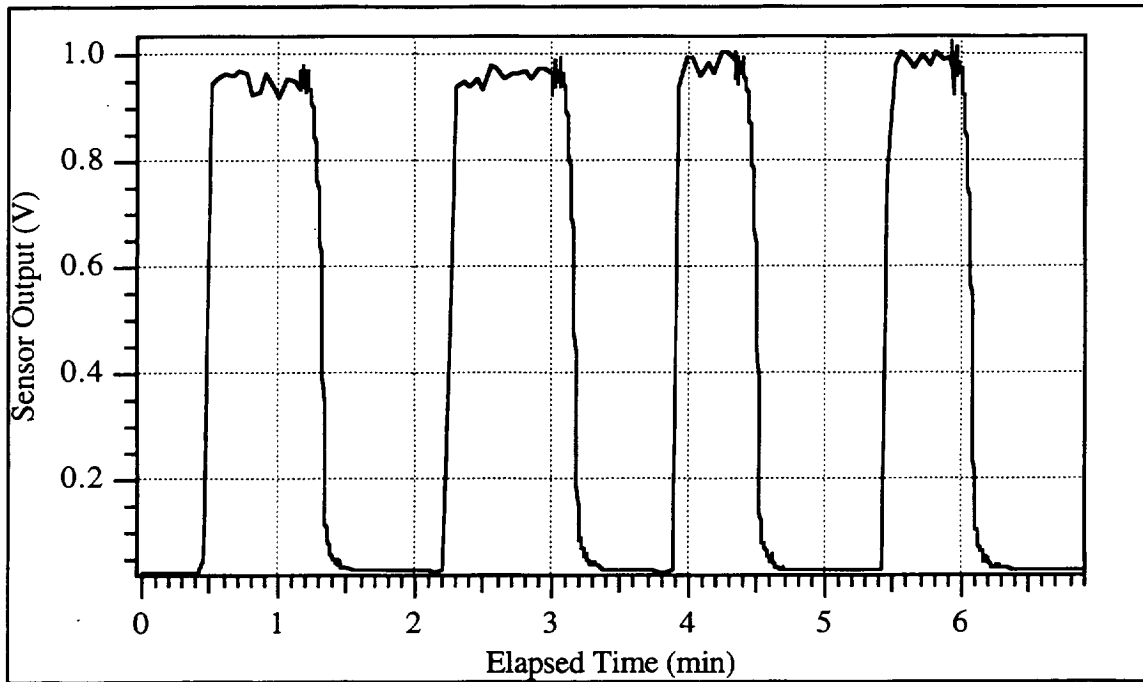

Figure G-16. Raw Data From 46-54 μm Glass Microsphere Settling Experiments, Repeated 4 times

The experiment shown here was repeated four times, shown by the four peaks on the figure. Stirring was performed for about one minute in each case shown by the width of the peaks. The variability seen while stirring is indicative of the stochastic nature of the stirring and light scattering events. The decay transient contains the particle settling information. Figure G-17 shows the normalized scattering data for these four settling experiments plotted on a log scale.
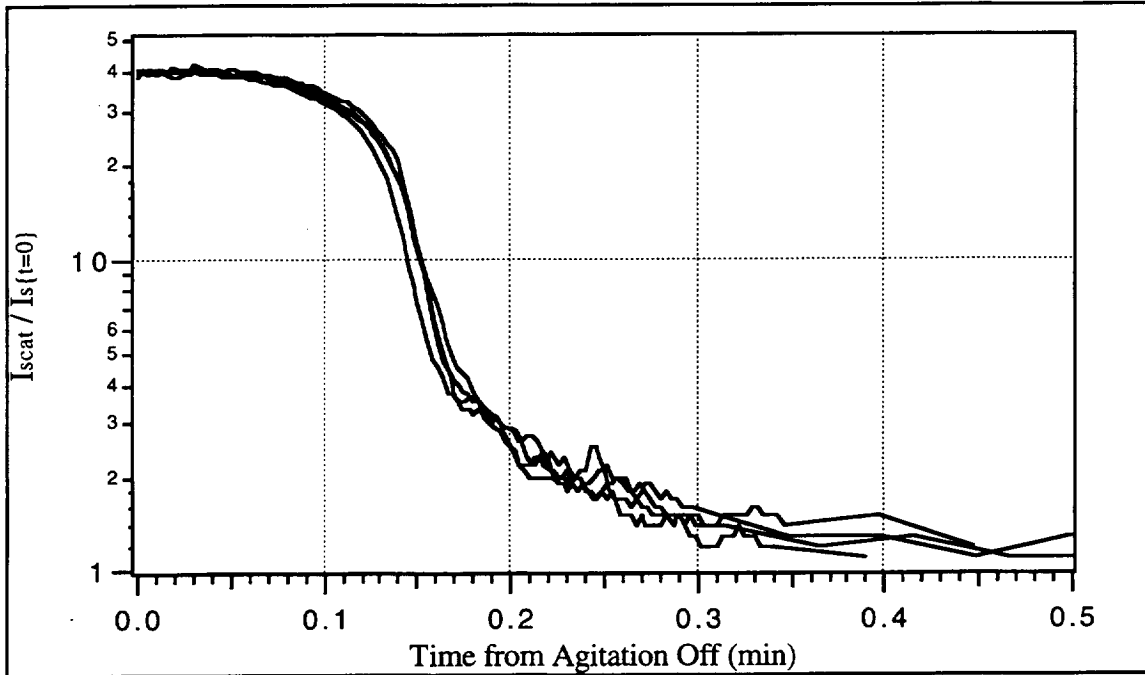
Figure G-17. Normalized Data from 46-54 μm Glass Microsphere Settling Experiments

Each trace on the figure shows the settling decay transient normalized to the zero suspended particle condition and to the stop stirring event. The data show that repeatability is not an issue, and that the variability between runs shows similar structure. The data from the <20 μm glass microsphere experiments is shown in Figure G-18.
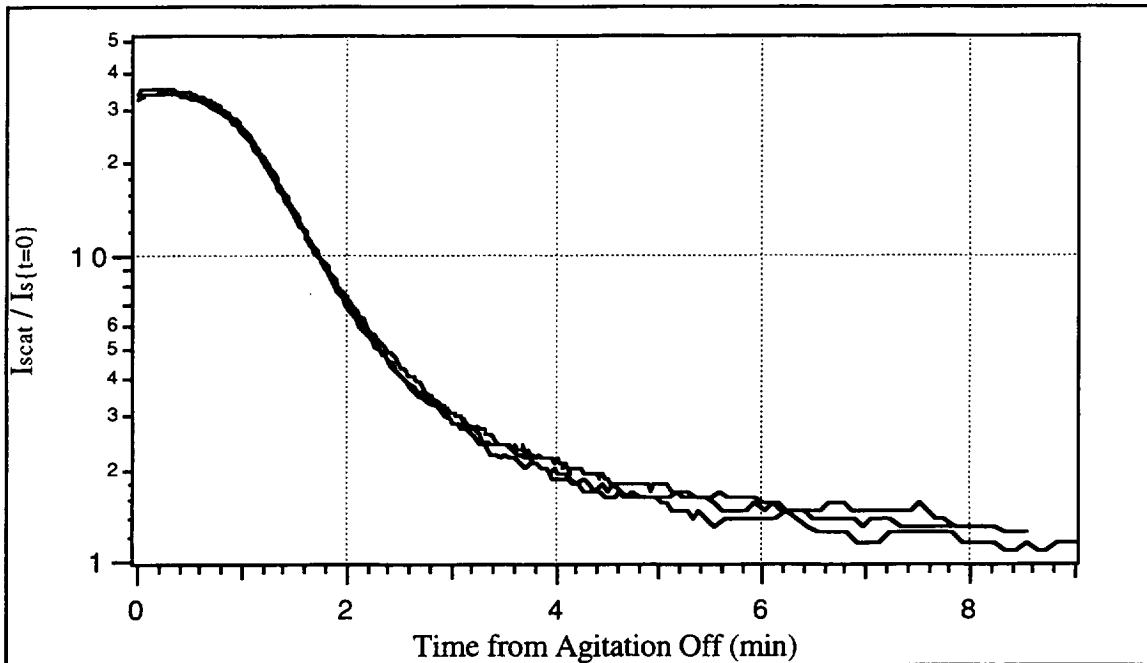
Figure G-18. Normalized Data from <20 μm Glass Microsphere Settling Experiments

The higher sensitivity to smaller particles is illustrated in this figure. These normalized decay transients have a much longer duration than the 46-54 μm particles, and the variability is significantly lower than for the larger particles. This is due to minimal effects from the stirring-swirling, and larger total time to acquire data.

Concurrently with the particle settling experiments, an analytical model was developed to reconstruct the particle size distribution using experimental data and empirical fluid dynamic relations. The model uses data from the 90° scattered light photodiode to reconstruct the particle size distribution. The model can predict settling times for defined particles and solutions, or reconstruct a particle size distribution based on settling data. It includes terms for the geometrical dimensions and layout of the cell, particle and fluid characteristics (density, sphericity), and gravity. Figure G-19 shows the configuration of the model cell setup and the characteristic dimensions required for reconstruction of the particle size distribution.
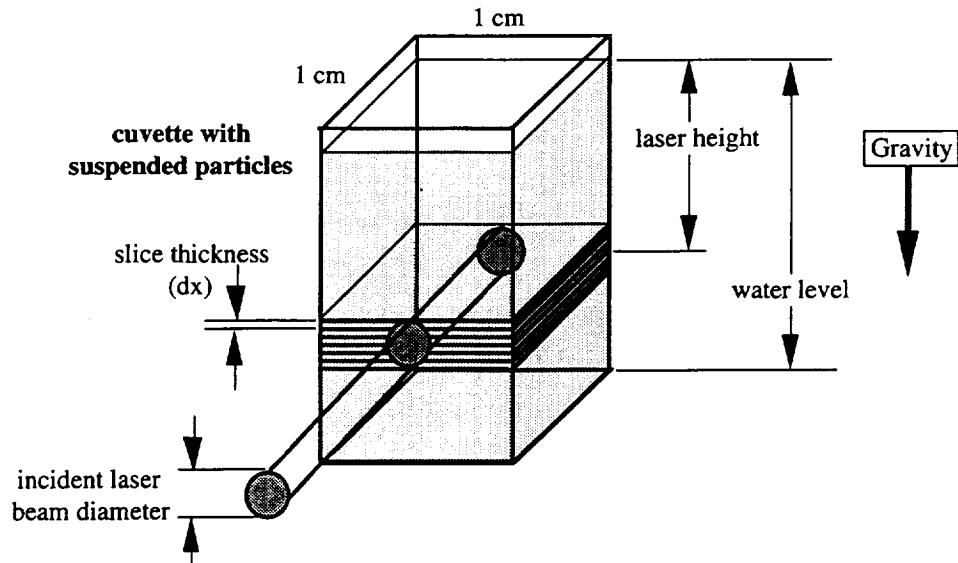
Figure G-19. Dimensions in the Particle Size Distribution Reconstruction Model

The model works by computing the particle settling velocity based on the fluid characteristics (viscosity, density relative to the particle, and temperature). These parameters are used to compute the settling time as a function of particle diameter. The most important parameter in this geometry is the distance from the laser beam (center) to the top of the fluid (laser height). This dimension determines the longest settling distance and sets the associated settling time. As the experiment elapsed time proceeds, particle diameters associated with this maximum settling distance can no longer be present within the laser beam to scatter light. Only particles smaller than the diameter set by this distance and the elapsed time can be present to scatter light into the photodiode. The scattered light signal essentially represents an integrated size distribution. Analytically differentiating the scattered light signal with respect to time gives a curve that represents the relative size distribution as a function of settling time, which is then correlated to the particle diameter based on fluid dynamic calculations. Figure G-20 shows a schematic diagram of a single particle settling through a fluid, and the fluid and particle characteristics utilized by the model.
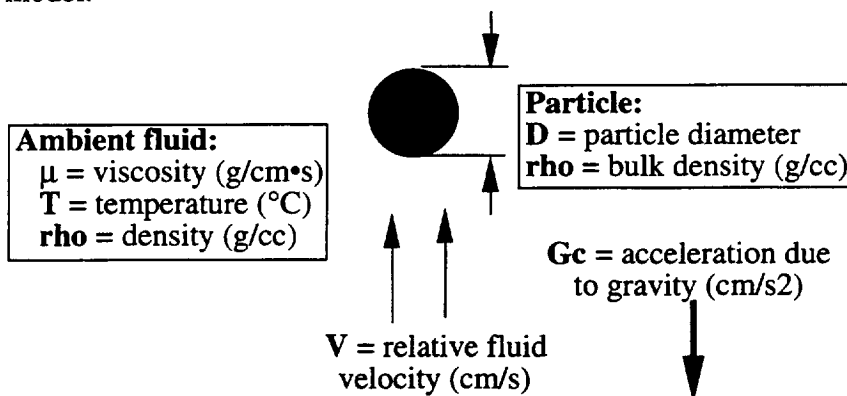

Figure G-20. Fluid Dynamic Characteristics Used to Reconstruct Particle Size Distributions

The forces acting on the particle cause it to accelerate to a terminal settling velocity until it reaches the bottom of the cuvette. These forces are directly related to the difference in density between the fluid and the particle, as well as the acceleration due to gravity. The

G-30

terminal velocity is limited by the volume, cross sectional area, and mass of the particle, and the viscosity of the fluid (a function of temperature). The Reynolds number is used to determine the flow regime around the particle, and an associated fluid drag coefficient computed based on the flow regime. Correlations were developed to predict the drag coefficient (Cd) as a function of Reynolds number for spherical particles. Most of the settling occurs in the creeping flow and vortex flow regimes. This will also be true on Mars where the reduced gravity will result in lower Reynolds numbers for the same size particles. The correlations used in the model are summarized in Table G-5. Additionally, the viscosity of water (the settling fluid) as a function of temperature was fit to a polynomial for use in the model.

<u>**Reynolds Number (Re) & Drag Coef (Cd):**</u>

$$Re = \frac{(rho)(V)(D)}{(\mu)}$$

<u>Flow Regime</u>	<u>Re</u>	<u>C_D</u>
creeping flow	Re < 0.765	$\frac{24}{Re}$
vortex flow	0.765 < Re < 20k	
Cd=10^(1.40422-0.792723*log(Re)+.0126024* log(Re)^2+.0182319**log(Re)^3)		
turbulent flow	Re > 20k	0.47

Table G-5. Reynolds Number and Drag Coefficient Correlation Used to Predict Terminal Settling Velocities

The simplest case is the creeping flow regime where the terminal velocity is a simple function of Reynolds number. The following equations show the derivation of velocity in the creeping flow regime.

$$\vec{\frac{F}{A}} = \frac{(\Delta rho)(G_c)(vol)(\vec{e_y})}{(S)\,(A)} = \frac{(24)(rho)(V^2)}{(Re)(2)} = \frac{12\,\mu\,V}{D}$$

$$V_y = \frac{(\Delta\,rho)\,G_c\,4\,\pi\,r^3}{18\,\pi\,\mu\,D}$$

$$\boxed{V_y = \frac{(1\text{-}rho_p)\,G_c\,4\,r^2}{18\,\mu}}$$
Assuming all creeping flow (Stokes Drag)

Variables with an arrow above them represent vectors with respect to the gravity direction. The variables are defined as follows:

F = force acting in y direction (vector)
A = particle cross sectional area
Δrho = difference in density between the bulk particle and the fluid
Gc = Gravitational acceleration constant
vol = particle volume
ey = unit vector in +y direction (opposite the gravity direction)
S = sphericity factor, ratio of actual cross sectional area to that of a sphere
Re = Reynolds number (dimensionless)

μ = fluid viscosity
D = particle diameter
r = particle radius

Particle characteristics that fall in the vortex flow regime require that the drag coefficient be explicitly calculated at each stage in the computation. A fourth order polynomial was fit to the empirical data available for drag coefficients as a function of Reynolds number for spherical particles. The equations below are used in conjunction with this correlation to compute the velocities in the vortex flow regime. The variables are defined as before.

$$\frac{F}{A} = \frac{\Delta rho \cdot G \cdot vol}{A} = C_D \frac{rhof \cdot V^2}{2}$$

$$V^2 = \frac{8 \cdot \Delta rho \cdot G \cdot r}{3 \cdot C_D}$$

$$V = \sqrt{\frac{8 \cdot \Delta rho \cdot G \cdot r}{3 \cdot C_D}} \qquad \text{where } C_D = f\{Re\}$$

For a test case, this model was used to predict the settling velocities of sand (rho=2.25) and quartz (rho=2.25) on Earth (Gc=980 cm/s2) and Mars (Gc=372.5 cm/s2), for particle sizes ranging from 0.01 μm to 1 mm. Figure G-21 shows the results of this analysis.
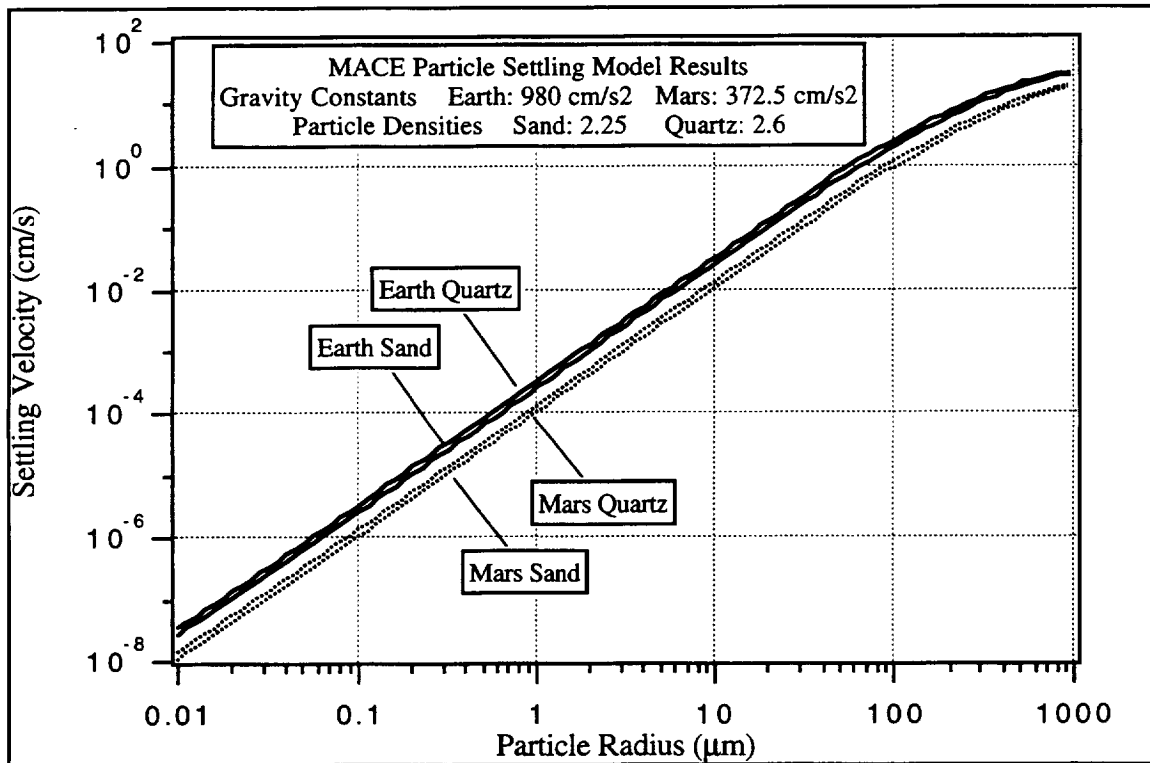

Figure G-21.   Model Settling Velocity Predictions for Sand and Quartz on Earth and Mars

The figure shows that the model predicted settling velocities are a well defined function of particle size if all else is constant. The effect of the reduced gravity on Mars will be slower settling velocities, allowing larger particles to be measured with this method than is possible on Earth. The one variable remaining is the particle shape. This is accounted for in the sphericity factor as the ratio of the particle projected area (cross sectional) to that of a

sphere. A larger cross section will distribute the forces over a larger area and slow the settling velocity. This will mimic the settling of a smaller particle, and result in an error in the prediction of particle size distribution If the particle is extremely non-spherical (i.e. needle shaped or flakes) the settling velocity cannot be predicted using this method. A parametric analysis of this variable was performed, and the results are shown in Figure G-22. These results show that to a first order the sphericity of the particle does not affect the settling velocity.
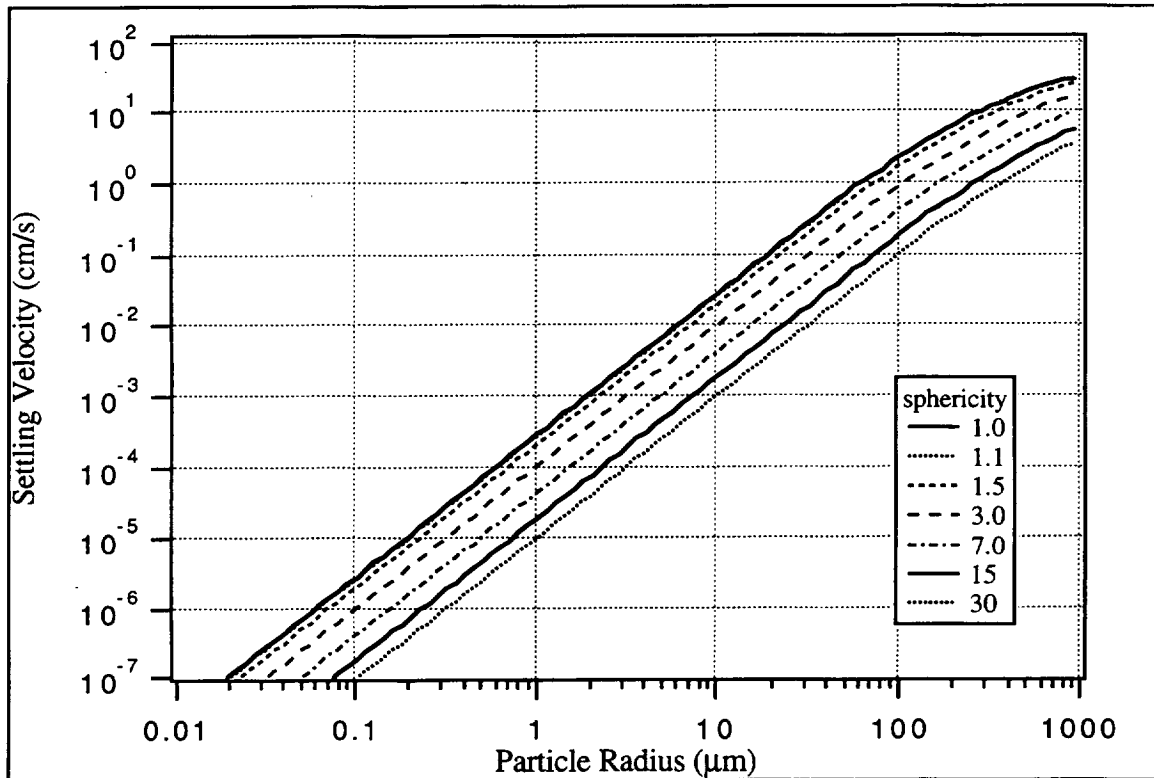
Figure G-22. Effects of Particle Sphericity on Settling Velocity. The particles here all have density: Rho(particle) =2.25 g/cc and gravity=980 cm/s2.

The model was used to reconstruct the particle size distributions of the glass microspheres described earlier. The normalized signal from scattered light photodiode was used in the reconstruction of the distribution with no additional processing. This makes the assumption that all particles scatter light equally, which may or may not be true, depending on the optical characteristics of the particular particles under analysis. This assumption is true for the homogeneous glass microspheres, but is may not be true for a heterogeneous regolith sample.

A computer algorithm was developed to read in the raw data from the experiments, perform normalizing and timing corrections, and predict the settling velocities associated with particle size. The settling velocities were then converted into experiment elapsed times in relation to the settling cell and laser geometries, and the cell dimensions. The scattered light signal was differentiated with respect to time, and the relative intensity plotted as a function of particle size for the course of the experiment. Figures G-23 through G-25 show the results of this analysis for each of the glass microsphere size ranges tested.
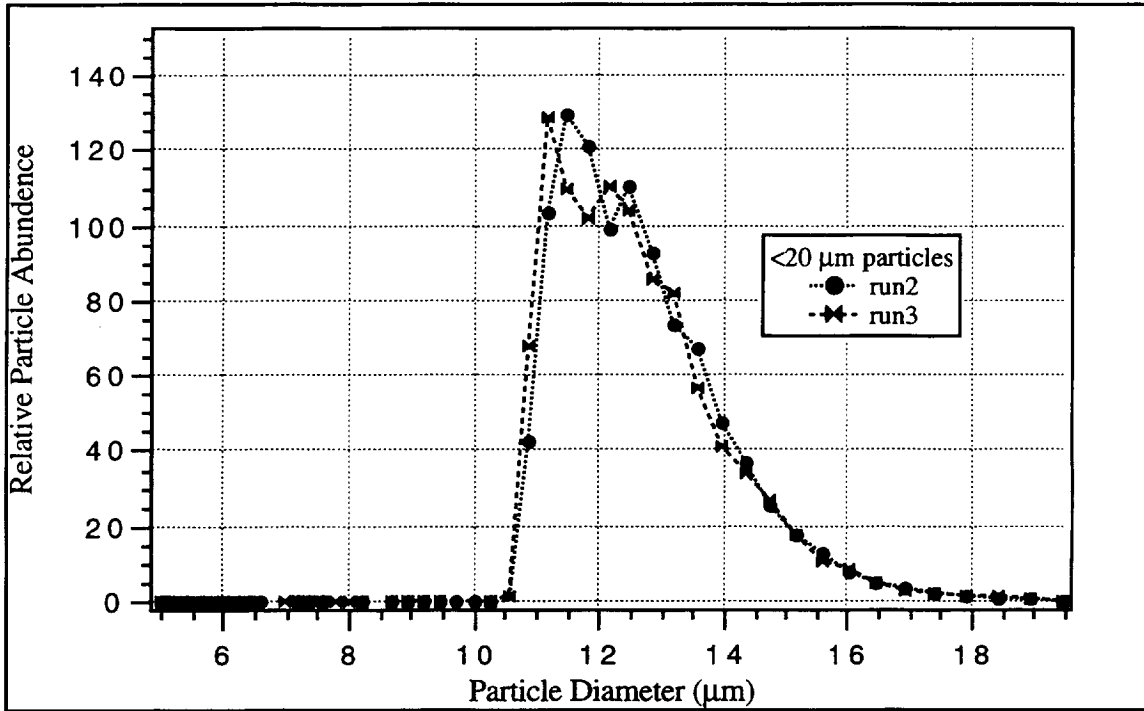
G-33

Figure G-23.   MACE Particle Settling Experiments Reconstituted Particle Size
Distribution
Glass Microspheres <20 μm, Gc: 980   Rho(particle): 2.3 Temp: 24.85°C Sph:1.0
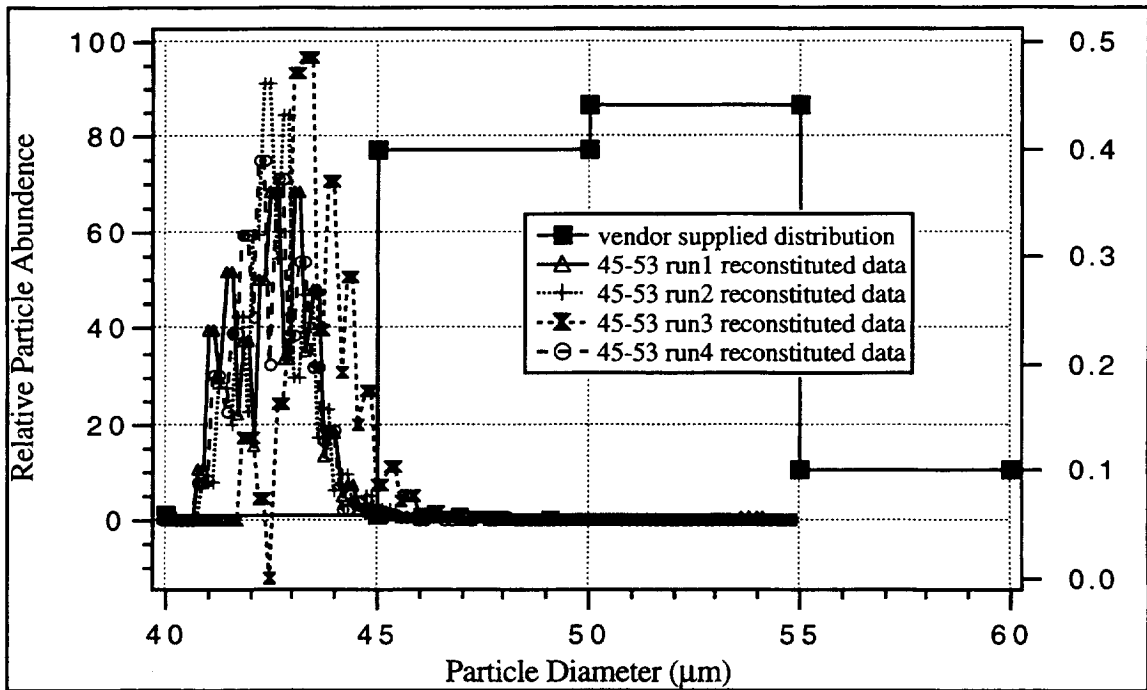Laser: 1.43

Figure G-24.   MACE Particle Settling Experiments Reconstituted Particle Size Distribution
Glass Microspheres 45-53 μm, Gc: 980   Rho(particle): 2.3 Temp: 24.85°C Sph:1.0
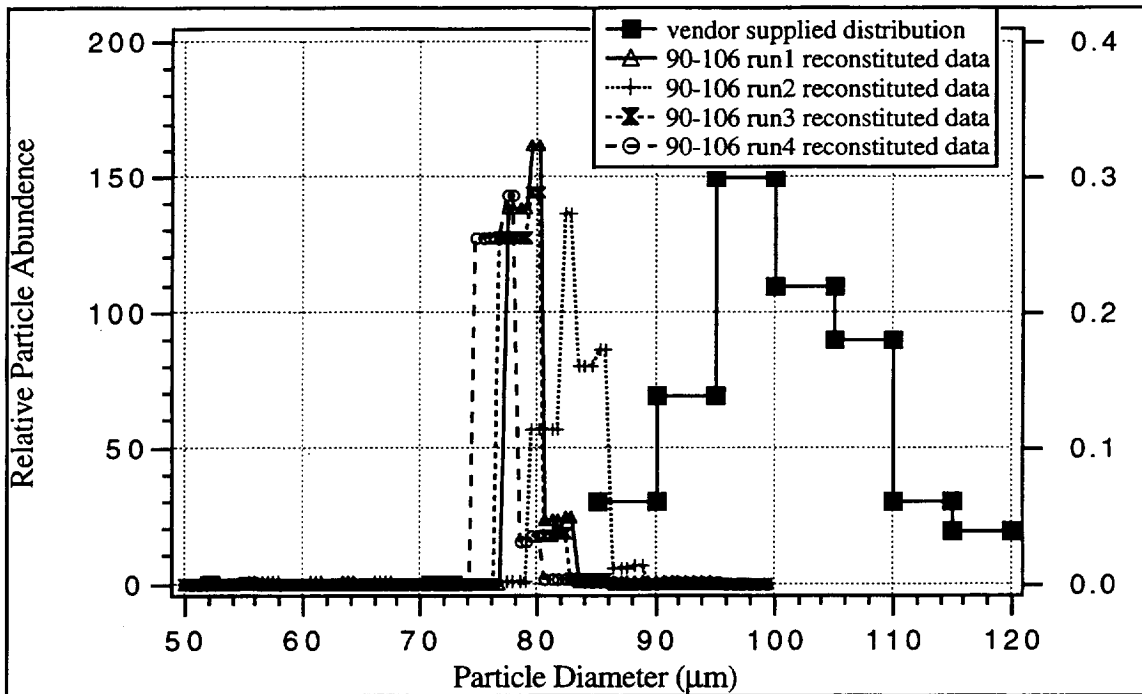Laser: 1.43

Figure G-25. MACE Particle Settling Experiments Reconstituted Particle Size Distribution
Glass Microspheres 90-106 μm, Gc: 980 Rho(particle): 2.3 Temp: 24.85°C Sph:1.0 Laser: 1.43

These results show errors in the reconstituted size distributions that increase with increasing particle size, as predicted. It is possible to calibrate these effects out, but the main utility of this method remains in the smaller particle range. The longer the settling time, the less influence residual swirling from the stirring affects the results. The swirling effects are also diminished as a fraction of the time that data is taken.

The initial sample that was run, labeled "ground sand" was analyzed using these algorithms, and the results are shown in Figure G-26. The reconstituted size distribution shows a bimodal histogram, with the peak around 2 µm. This is reasonable based on visual observations of the particles under a microscope.
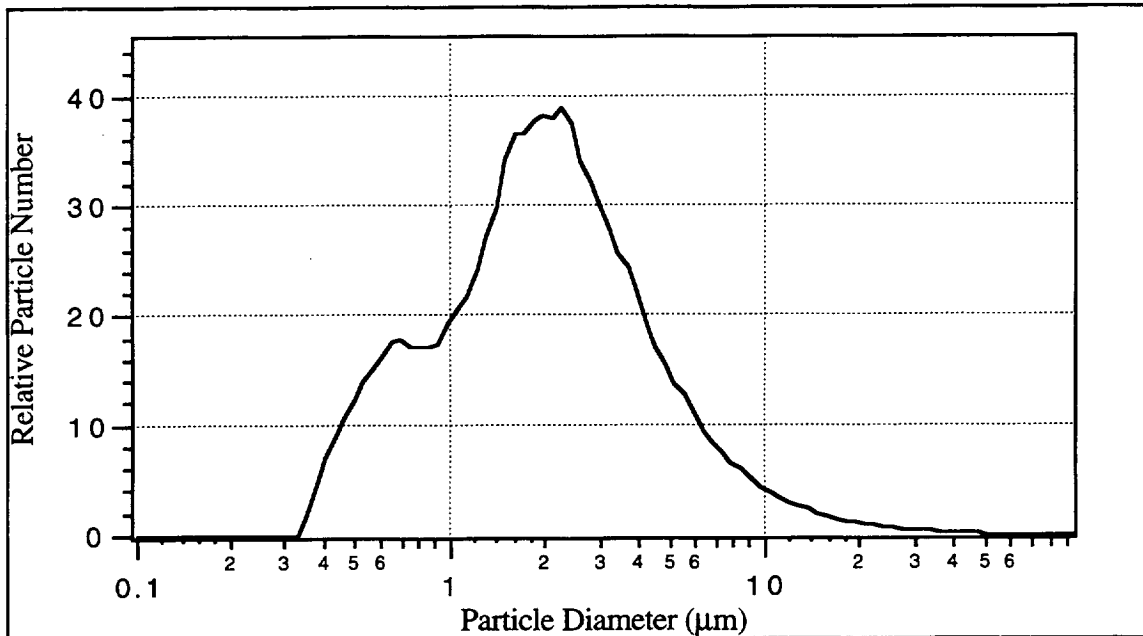

Figure G-26. MACE Particle Settling Experiments Reconstituted Particle Size Distribution. "ground sand" sample, Gc: 980 Rho(particle): 2.25 Sph:1.0 Laser: 1.0

There are several parameters in the model that must be defined to predict a size distribution based on the scattering data. These include the number of size bins the reconstituted distribution is divided into, the expected range of sizes, and the density of the particles. If Martian regolith is analyzed with this procedure, a number for bulk density will be required to predict the associated size distribution. If the regolith is heterogeneous in terms of optical properties or density, the results of this analysis will be in error. It is possible to determine the particle density directly if similar regolith samples can be analyzed in two different fluids, or more specifically, two fluids having different densities and viscosities. The light scattering curves obtained in the two fluids can be compared, and the relative differences in settling velocity determined. This can in turn be used to calculate the particle density; it "falls out" of the calculations so to speak.

The limitations of flight instrumentation may not allow two analyses of this type to occur, but if it is possible there are several candidate fluids that may be useful. Figure G-27 shows the parametric space defined by fluid dynamic viscosity and fluid density for a variety of fluids.
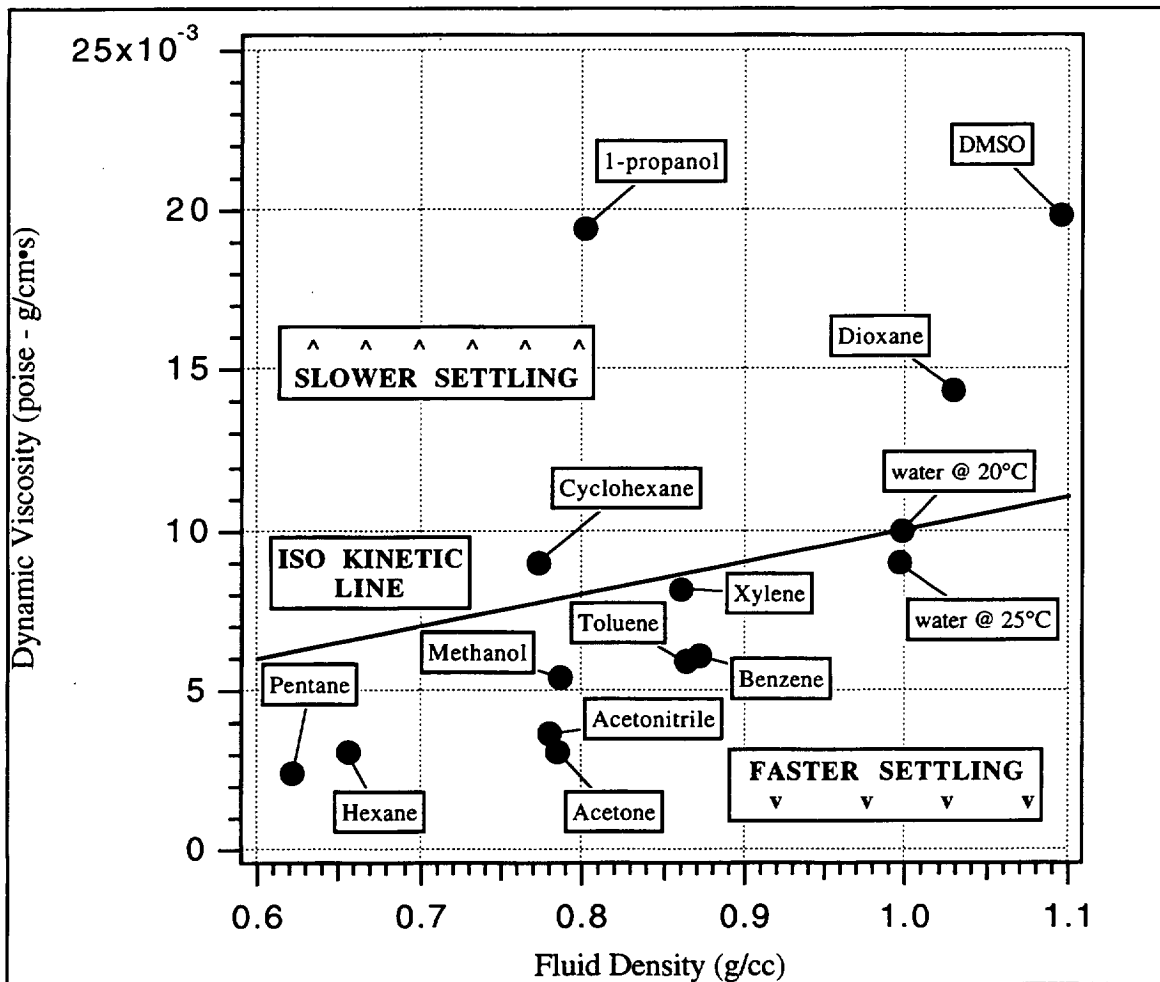

Figure G-27. Settling Properties of Various Fluids at 20 - 25°C

The figure is split in half by the isokinetic line that runs in the horizontal direction. Any fluid that falls on this line will have characteristics similar to water at 25°C, and will not be useful for the density determination analysis. Fluids that fall above the line will exhibit slower settling velocities (longer times) than water, and the fluids below the line will show faster settling velocities (shorter times). The most accurate density determination will occur where the fluid characteristics are the most different from water. The method inherently favors longer settling times, so the logical choices for alternate fluids are above the isokinetic line (slower settling), either 1-propanol or dimethylsulfoxide (DMSO).

H. CONCLUSIONS AND RECOMMENDATIONS

The concept of an aqueous-based chemical analyzer for Martian surface materials has been demonstrated to be feasible. During the processes of analysis, design, breadboarding, and most importantly, testing, it has become quite apparent that there are many challenges in implementing such a system. Nonetheless, excellent progress has been made and a number of problems which arose have been solved.

The ability to conduct this work under a development environment which is separate and which precedes the project-level development has allowed us to find solutions to these implementation realities at low cost. If the instrument had been selected for a mission without this laboratory pre-project work, the costs of implementation would be much higher.

In the four areas covered in Sections D, E, F, and G of this Final Report, outstanding progress has been made. There still remains the task of flight-qualifying certain of the components. This is traditionally done under the aegis of a Flight Project, but just as the concept development can be done at much lower cost when kept small and focused, so could the qualification program of critical parts benefit. We recommend, therefore, that NASA consider means of such qualifications and brass-boarding, in advance of final flight development. This is a generic recommendation, but hardware such as MACE and other similarly-new concepts are particularly applicable.

MACE now has wide versatility, in being able to reliably dispense both liquids and solids as chemical reagents to an entire suite of samples. The hardware and the experiment is much simpler than was developed for the Viking Biology instrument, yet can accomplish all the inorganic chemical measurements that it was capable of. In addition, it is much more flexible and versatile to new experiment protocols (and reagents) than the Viking design ever could have been.

MACE opens up the opportunity for many different scientific disciplines to design sub-experiments and to benefit from the investigations that can be conducted. In this sense, it will have the value of a facility, although our recommendation would be that it be under the stewardship of a single lead investigator to insure that conflicting requirements not compromise the straight-forward design that have been achieved.

MACE is an excellent candidate for upcoming Mars missions, including the Mars Surveyor Program (MSP) lander missions in 2001 and 2003. In addition, it could be used for any mission to the surface of any other planet or planetary body (including small bodies). An important next step is to encourage various investigators to propose specific uses for this experiment that specifically address their major scientific objectives for upcoming missions.